
Editorial Office of *Earth's Cryosphere (Kriosfera Zemli)*
Institute of Geography, Russian Academy of Sciences
37 Vavilov str., office 22, Moscow, 117312, Russia
Editorial staff: *N.V. Arutyunyan, N.G. Belova, O.V. Levochkina, O.M. Lisitsyna, G.E. Oblogov*
Phone: 8(985) 957-10-01, e-mail: kriozem@gmail.com

Journal promoted by
Russian Academy of Sciences, Siberian Branch, Novosibirsk
Earth's Cryosphere Institute, Tyumen Scientific Centre SB RAS, Tyumen
Melnikov Permafrost Institute, SB RAS, Yakutsk

Editorial Manager *M.A. Trashkeeva*
Designed by *N.F. Suranova*
Typeset by *N.M. Raizvikh*

English text by *M.A. Korkka, V.A. Krutikova, V.V. Kuzovkin, N.N. Mzhelskaya*

RUSSIAN ACADEMY OF SCIENCES
SIBERIAN BRANCH
EARTH'S CRYOSPHERE INSTITUTE, TYUMEN SCIENTIFIC CENTRE

EARTH'S CRYOSPHERE
SCIENTIFIC JOURNAL

Founded in January 1997	6 issues per year	Vol. XXV, No. 2	March–April 2021

CONTENTS

NOVOSIBIRSK
SIBERIAN BRANCH OF THE RUSSIAN ACADEMY OF SCIENCES

EARTH'S CRYOSPHERE
SCIENTIFIC JOURNAL

Kriosfera Zemli, 2021, vol. XXV, No. 2, pp. 3–12

GEOLOGICAL CRYOGENIC PROCESSES AND FORMATIONS

RECONSTRUCTION OF THE FORMATION HISTORY OF THE PEAT PLATEAU IN THE LOWER REACHES OF THE NADYM RIVER

O.S. Sizov[1], A.A. Yurtaev[2], A.V. Soromotin[2], E.M. Koptseva[3], A.O. Volvakh[4], E.V. Abakumov[3], N.M. Berdnikov[5], N.V. Prikhodko[2], D.S. Guryev[6]

[1] *Institute of Oil and Gas Problems, Russian Academy of Sciences, Gubkina str. 3, Moscow, 119333, Russia; kabanin@yandex.ru*
[2] *Tyumen State University, Volodarsky str. 6, Tyumen, 625003, Russia*
[3] *St. Petersburg State University, 16th Line V.O. 29, St. Petersburg, 199178, Russia*
[4] *Sobolev Institute of Geology and Mineralogy, Siberian Branch of the Russian Academy of Sciences, Akademika Koptyuga ave. 3, Novosibirsk, 630090, Russia*
[5] *Earth Cryosphere Institute, Tyumen Scientific Centre, Siberian Branch of the Russian Academy of Sciences, Malygina str. 86, Tyumen, 626026, Russia*
[6] *LLC Severavtodor, Komsomolskaya str. 10B, Nadym, Yamal-Nenets Autonomous District, 629730, Russia*

This study presents new data on the cryolithological structure of a ridge-shaped peat plateau typical for the north of Western Siberian, located in the lower reaches of the Nadym River. Two wells were drilled at the top of the ridge and in the inter-ridge depression, with subsequent core analysis. Grain-size distribution, shape and surface structure of sand quartz grains, botanical composition and radiocarbon age of organogenic deposits were determined. The study revealed the presence of a three-layer peat-sand-loam ridge structure. The lower loam layer with a ~60 % volumetric ice content was affected by frost heaving. Layers of pure ice are identified below this loam layer. The ridge was formed as a result of water migration with the complementary influence of ice injection; it is of the peat-mineral type. In the ridge formation history, we identified the stages of loam and sand deposit accumulation at the end of the Late Pleistocene; bogging occurred at the beginning of the Holocene (10.6–9.8 ka BP), while active frost heaving was during the Subboreal stage (5.5–5.0 ka BP). Currently, there is a decrease in the upper organic horizon thickness and some erosion. It is proposed to consider peat-mineral and mineral frost heave landforms (mounds and ridges) as a separate type of cryogenic landforms.

Key words: *frost mound, frozen ground, permafrost zone, Upper Quaternary deposits, Nadym region.*

INTRODUCTION

Heaving processes of various types of deposits are common within large peat massifs in the north of Western Siberia, as well as in other arctic regions of the Northern Hemisphere [*Evseev, 1976; Landscapes..., 1983*]. Migrational frost mounds (MFM), the formation of which is related to the migration of water from shallow-lying water-bearing horizons to the freezing front, are distinguished among various forms of cryogenic landscapes [*Popov, 1967*]. Use of this term stems from the need for genetic characterization when describing convergent landscape forms, as well as from the fact that the peat, mineral, and peat-mineral mounds stand out in deposit composition among MFM [*Evseev, 1976; Landscapes..., 1983*].

In the north of Western Siberia, MFM are seen predominantly in the southern tundra, forest-tundra, and in the northern taiga region of the irregular bedding of the contemporary and ancient permafrost thicknesses [*Shpolyanskaya, Evseev, 1972*]. The northern boundary of their distribution matches the northern boundary of the discontinuous development of permafrost (MFM are rarely seen north of the river mouth of the Nyda and Taz rivers), the southern boundary is the southern boundary of the distribution of sporadic permafrost [*Evseev, 1976*].

Frost mound research has a many-year history. The theoretical explanation of the heaving process, the description of the cryogenic structure, genesis and MFM morphology are given in various works of Russian scientists [*Popov, 1967; Shpolyanskaya, Evseev, 1972; Evseev, 1976; Berdnikov et al., 2019*]. Individual studies are dedicated to the results of annual monitoring of cryogenic heaving [*Moskalenko, Ponomareva, 2004; Ponomareva et al., 2012*]. The dynamic of the vegetation cover on large-mound peat bogs has been thoroughly analysed, as well as their typical identifying features, which persist in the identification of landscape peculiarities of the territory and the drafting of integral ecological maps [*Tyrtikov, 1979; Ponomareva, 2010*].

MFM of the peat-mineral type, which significantly differ from classic peat mounds in their structure and development dynamic, are particularly in-

teresting. They form in areas of distribution of deposits of various genesis and composition (loams, clays and sometimes dusty loams) and can be morphologically expressed both as hills and ridges. An ice core (a local accumulation of segregated ice) is often absent here, and heaving horizons are covered by a thickness of sand deposits and a thin peat layer from the surface. A separate type of mineral MFM is also identified, the top peat layer of which has been removed by erosion and deflation [*Vasi'lchuk, 2008*]. In Western literature the term "lithopalsa" or "lithalsa" is usually used to signify mineral MFM [*Calmels et al., 2008; Wolfe et al., 2014*]. Peat-mineral and mineral MFM frequently signify genetically different landscape forms complicated by heaving (kames and moraine hills, eskers, etc.) in complex geomorphological conditions [*Wolfe et al., 2014*], which creates additional ambiguity for conducting field research in thematic cartography. There are almost no special studies of age, the history of development and peculiarities of the distribution of peat-mineral MFM, although these questions are considered key in regard to the conditions of the northern taiga of Western Siberia [*Vasil'chuk, 2008*].

The goal of the present work is the reconstruction of the formation history of a peat-mineral MFM (as a frost ridge) in the lower course of the Nadym River.

AREA AND OBJECT OF RESEARCH

The studied territory is located within the bogged and lakeside second above-floodplain terrace of the Kheygiyakha River (left tributary of the Nadym River, 15 km south of the river mouth) (Fig. 1). The absolute heights of the surface fluctuate within 20 to 36 m.

The thickness of the peat in the peat bogs is 1.0–1.5 m on average (up to 5 m in depressions). Alluvial deposits present as fine-grained and medium-grained sands with rare inclusions of quartz gravel and quartz pebbles, as well as vegetation remains of various degrees of decomposition [*Braduchan et al., 2015*]. The sands are 4 to 10 m thick and are underlain by icy loams [*Geological survey..., 1954; Braduchan et al., 2015*]. There is clear oblique or lens-like stratification of the river mouth facies in the sands, which changes into horizontal stratification upon transition into the floodplain facies. The age of the sands was determined using the radiocarbon dating method and optically infrared stimulated luminescence (IR–OSL) in two sections: in the sand quarry near the river mouth of the Kheygiyakha River (dated using oblique stratification sands of the river mouth facies) and directly within the work area in one of the lakeshore outcrops (dated using vegetation remains). In the first case, an age of 24 ka BP was obtained; in the second, an age of 27 ka BP [*Sizov et al., 2020*], which corresponds to the beginning of the Sartan cryochrone (marine isotope stage 2 – MIS 2). The spore and pollen analyses indicate the existence of typical tundra and forest-tundra conditions during the formation period of the terrace [*Braduchan et al., 2015*].

The contemporary average annual air temperature is –5.6 °C. Data from years of observations reveal that the MFM temperature at a depth of 10 m has increased since the end of the 1970s: from –1.8 to –0.4 °C on large-mound peat bogs and from –1.0 to –0.2 °C on flat-mound peat bogs [*Moskalenko et al., 2012*]. The minimum temperature (–1.5...–2.0 °C) was recorded from 2009 to 2017 in the well drilled at the top of the peat-mineral mound.

The vegetation cover of the region belongs to the woodland subzone of the boreal zone [*Vegetation..., 1985*]. Larch and spruce-larch woodlands and open forests with *Larix sibirica* Ledeb. and *Picea obovata* Ledeb., which alternate with moss, lichen, and subshrub tundras, are typical for the flat interfluve zones of the region. Bogging of the territory is very high and reaches 70 % in the Nadym-Pursk interfluve.

The object of research is a small (approximately 300 m in length) peat-mineral frost ridge located near the inner margin of the second above-floodplain terrace of the Kheygiyakha River (Fig. 1) – the distance to the slope of the third above-floodplain terrace of lake-alluvial origin is less than 400 m. The ridge is complicated by thermoerosional scours and is washed away by lakes from the north, west and east. The studied object is located in the center of the area of heaving, where six ridges and 10 separate mounds of different heights can be distinguished. The length of some of the ridges attains 700 m, and the absolute height is 36.0 m. The ridges are divided by inter-ridge depressions with an amplitude of relative heights of over 10 m. The general direction of the ridges is northwest and west, often the ridges are divided by scour into local hills which form extended chains. Sparse forest vegetation consisting predominantly of cedar and larch is seen on the surface of individual ridges.

RESEARCH METHODS

Two wells were drilled using a drilling rig installed onto the chassis of a "Trekol" all-terrain vehicle: well 2 on the top of the ridge (absolute height: 34 m; coordinates: N 65°17′08.58″, E 72°50′39.75″) and well 3 in the inter-ridge depression (absolute height: 27 m; coordinates: N 65°17′01.02″, E 72°50′44.11″). Drilling took place from July 28, 2018 with a 10 cm-diameter core sample taken from peaty and loamy horizons. There was no core sample from sandy horizons. Samples were collected from deposits every 0.5–1.0 m for granulometry, morphoscopy, and morphometry of sand quartz grains. Well structure diagrams are presented in Fig. 2.

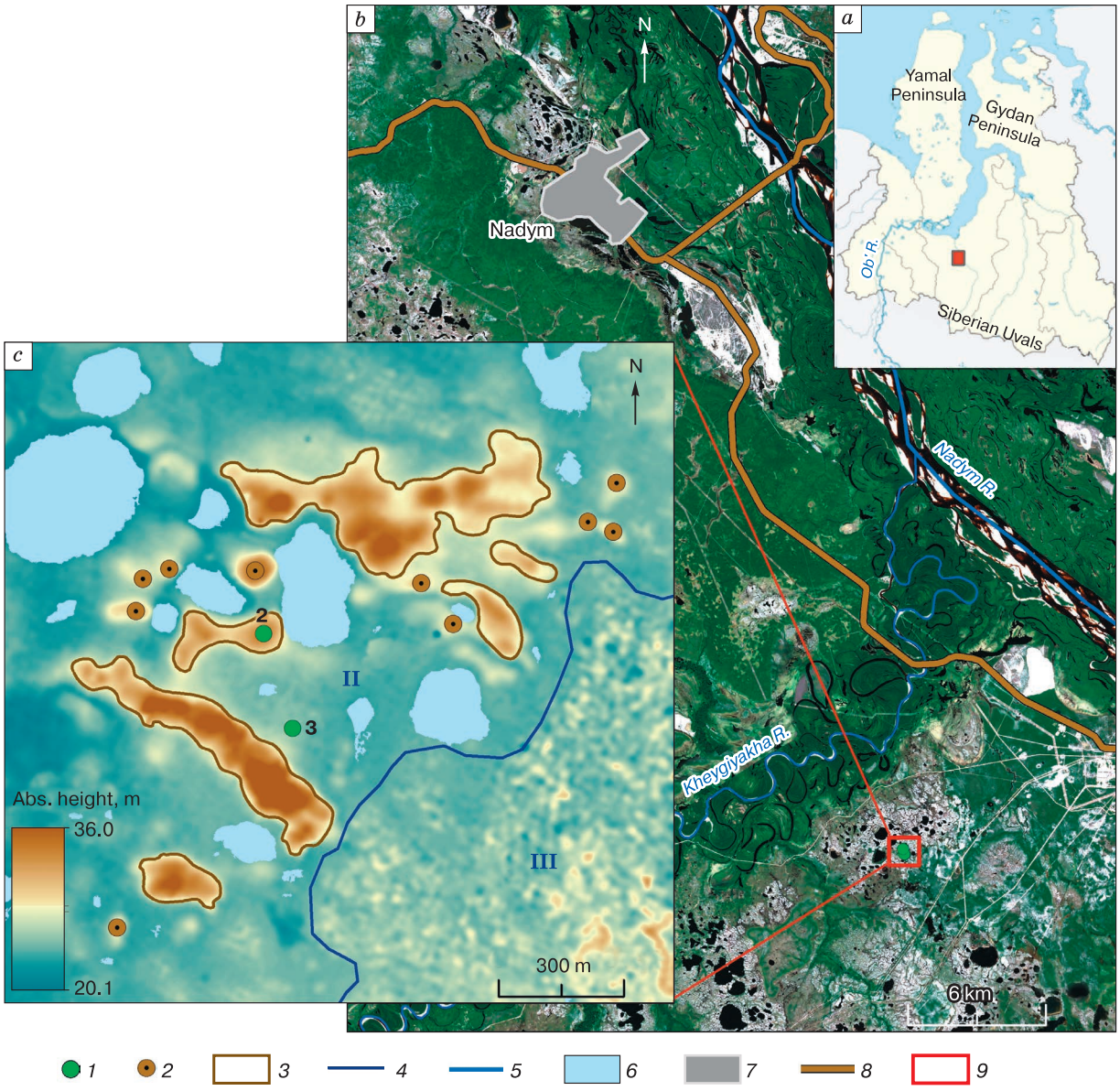

Fig. 1. Overview map of the work area:

a – key map of the north of Western Siberia (work area indicated using red rectangle); *b* – Sentinel-2A satellite image (resolution: 10 m, date the photo was taken: June 18, 2016); *c* – ArcticDEM digital model of landscape (resolution: 2 m). *1* – wells; *2* – migrational frost mounds; *3* – migrational frost ridges; *4* – boundary between the II and III above-floodplain terraces of lake-alluvial origin [*Braduchan et al., 2015*]; *5* – rivers; *6* – lakes; *7* – Nadym Town boundaries; *8* – roadways; *9* – work territory boundary.

The granulometric composition of sand samples weighing 500 g was determined using the dry method according to the traditional sieving method (sieve analysis) on the Analysette 3 PRO vibratory sieve shaker (Fritsch, Germany) in the range from 0 to 2000 μm, fractions were then weighed on laboratory scales with a resolution of 0.1 g. Fractions <125 μm were divided using the Analysette A22 laser particle sizer (Fritsch, Germany), after which the mass percents of each fraction were calculated in Excel 2013 (Microsoft, USA). The granulometric composition of loamy samples was determined directly using the Analysette A22 laser particle sizer (Fritsch, Germany) (the required size of the sample was calculated automatically in the device). The Friedman-Sanders classification was used to describe results [*Friedman, Sanders, 1978*].

Analysis of quartz grains from medium-grained and coarse sand was carried out under a binocular microscope using a method created in the RAS Geo-

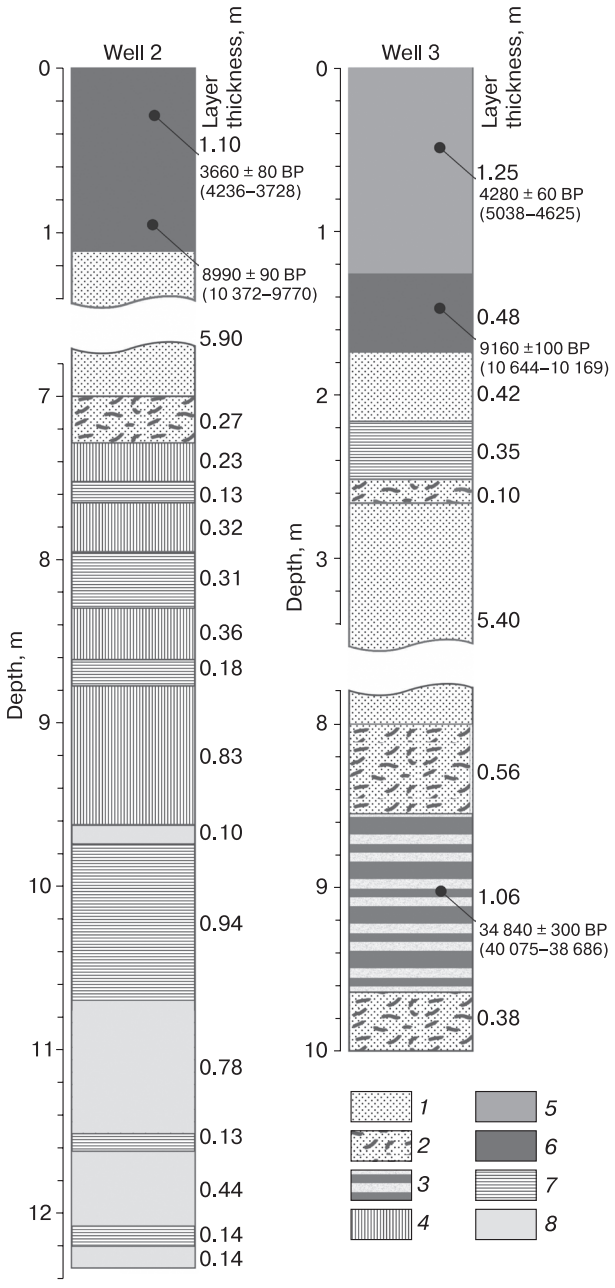

Fig. 2. Structure of deposits in wells 2 and 3 based on results of drilling.

1 – sand, *2* – sand with vegetation detritus, *3* – interlayering of vegetation detritus and sand, *4* – icy loam, *5* – transitional peat, *6* – lowland peat, *7* – loam, *8* – ice.

graphy Institute [*Velichko, Timireva, 1995*]. Analysis of the microstructure of grain surface was carried out on the JSM-6510LV scanning electronic microscope (SEM) (JEOL, Japan) using secondary electrons (SEI – secondary electron image) in the Analytical Center for multi-elemental and isotope research SB RAS (Novosibirsk). Grain roundness was determined using L.B. Rukhin's template [*1969*] and A.V. Khabakov's five-grade scale [*1946*], where 0 is angular and IV is perfectly rounded. The roundness coefficient and degree of matting were determined for each sample [*Velichko, Timireva, 1995*]. Grain matting was determined visually from glossy to dull. Study of grain surface microrelief structure was carried out using published diagnostic features of grains of various genesis and deposition conditions [*Krinsley, Doornkamp, 2011*].

Botanical analysis of the peat and the degree of its decomposition were carried out by the microscopic method (with up to 5 % accuracy) in the Mire Ecosystems Laboratory of the Biology Institute of the RAS Karelian Research Center (Petrozavodsk) by N.V. Stoykina using the atlas of plant remains in peat [*Katz et al., 1977*] and by way of comparison with herbarium samples of plants. Peat typification based on botanical composition was completed using [*Tyuremnov, 1976*].

The liquid scintillation count method was applied for determining the absolute age of the peat and vegetation remains. The analysis was completed by the Radiocarbon Laboratory of the Institute of Environmental Geochemistry of the NAS of Ukraine (Kiev). The obtained radiocarbon dates were recalculated into calendar years through calibration using the publicly accessible program OxCal 4.3 [*Bronk, Lee, 2013*] based on the IntCal13 calibration curve.

RESEARCH RESULTS

1. Granulometric composition and morphoscopy of sand quartz grains. The results of granulometric composition analysis demonstrate a clear differentiation of sand and clay layers distinguished during describing (Fig. 3).

Fine and medium-grained sand fractions dominate in the composition of sand horizons (well 2: 1.1–7.27 m, well 3: 2.6–8.0 m). A fine and medium dust fraction with particle size 0.016–0.002 mm dominates in the clay deposits (well 2: 7.27–10.7 m). Horizons with predominantly large dust are seen in the top part and at a depth of 8.0 m in well 3. Thus, the base of the heaving ridge is composed of a dusty core which is not seen in the inter-ridge depression.

Morphoscopy results (Fig. 4) demonstrated that the roundness coefficient (Q) of quartz grains at a depth of 7 m in the sand horizon in well 2 was 80 %, degree of matting (Cm) was 50 %. The main element of grain surface morphology in well 2 is small pits (Fig. 5, *a–d*), and individual V-shaped grooves (Fig. 5, *b*, *c*) and sickle-shaped hollows are frequently seen. These elements indicate subaqueous grain processing. The presence of small pits in some grains (Fig. 5, *b–d*), most often developed in protruding parts of the grain, indicates the influence of aeolian processes.

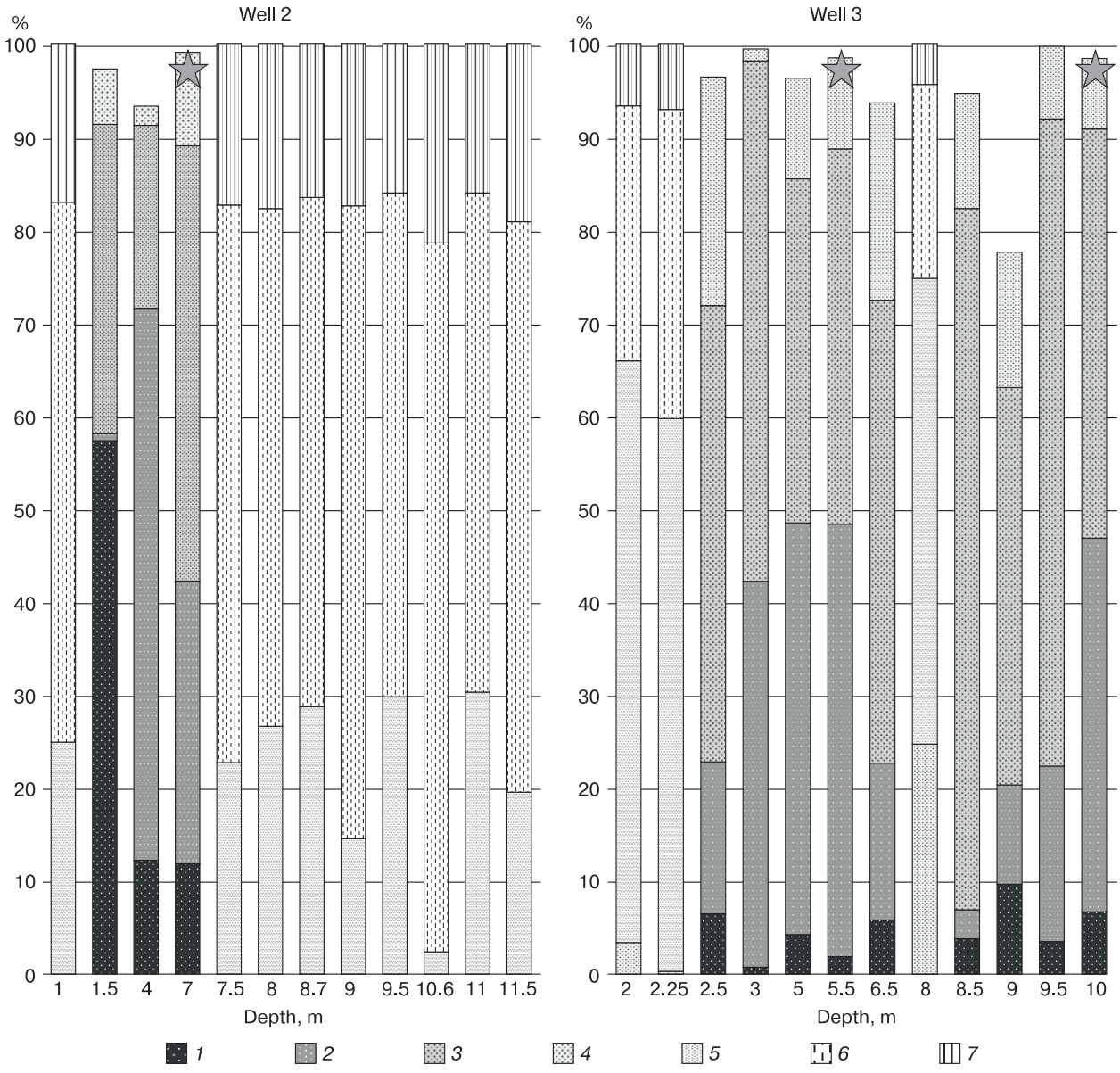

Fig. 3. Granulometric composition of deposits exposed by wells 2 and 3.

Stars mark sand quartz grain morphoscopy and morphometry samples. *1* – coarse sand, 0.5–1.0 mm; *2* – medium-grained sand, 0.25–0.50 mm; *3* – fine-grained sand, 0.125–0.250 mm; *4* – very fine-grained sand, 0.125–0.063 mm; *5* – large dust, 0.063–0.016 mm; *6* – medium and fine dust, 0.016–0.002 mm; *7* – clay, <0.002 mm.

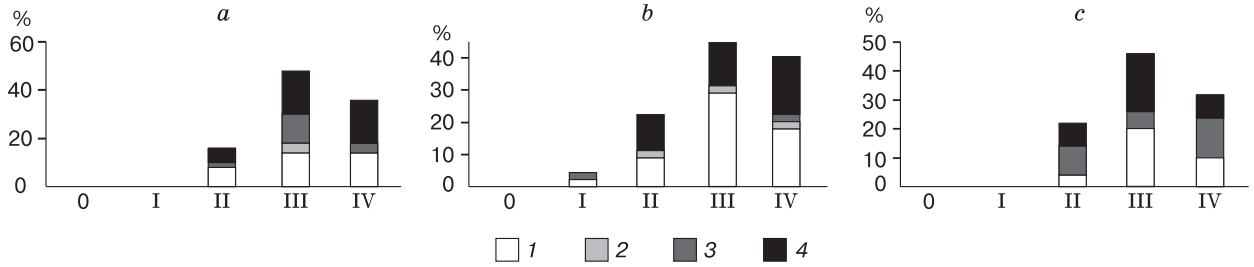

Fig. 4. Distribution based on grain roundness and matting of sand quartz grains from well samples.

a – well 2, depth 7 m; *b* – well 3, depth 5.5 m; *c* – well 3, depth 10 m. *1* – glossy surface, *2* – quarter-matted surface, *3* – half-matted surface, *4* – matted surface. 0, I, II, III, IV – roundness grades according to A.V. Khabakov's scale [*1946*].

The roundness coefficient in well 3 (sand sample from 5.5-m depth) is 77 %, the degree of matting is 41.5 %. Most grains have a well-defined small-pit surface (Fig. 5, *e*, *f*, *i*) which formed as a result of active water transport. Crescent-shaped depressions can also be seen in some grains (Fig. 5, *g*, *h*), which also indicates subaqueous processing, but in a calmer environment. Sometimes, small pits are seen (Fig. 5, *g*, *h*), which indicates transport in subaerial conditions.

The roundness coefficient (*Q*) in the sand sample from well 3 (10-m depth) is 77.5 %, the degree of matting (Cm) is 51 %. Regardless of surface matting, the predominance of well-developed small pits of the surface (Fig. 5, *j*, *k*) is typical for grains, being an indicator of fairly active river transport. Individual cres-

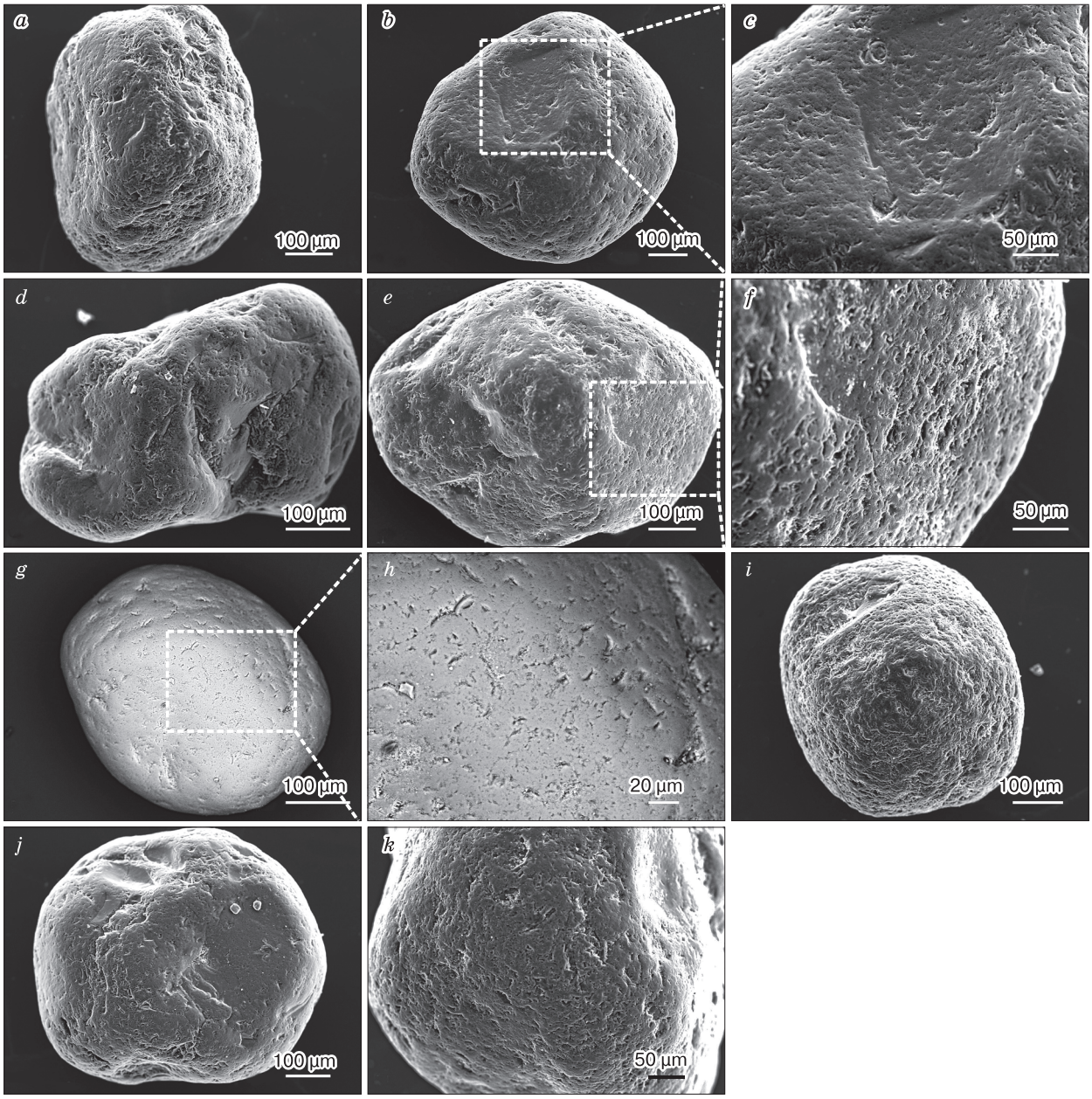

Fig. 5. SEI photographs of sand quartz grains.

a–d – well 2, sampling depth 7 m (*a* – half-matted grain with a small-pit surface; *b*, *c* – glossy grain with a small-pit surface and individual V-shaped grooves, micro pits are seen on protruding areas of the grain; *d* – half-matted grain with small-pit and micro-pit surfaces); *e–i* – well 3, sampling depth 5.5 m (*e*, *f* – glossy grain with a small-pit surface; *g*, *h* – glossy grain with sickle-shaped hollows and micro pits; *i* – glossy grain with a small-pit surface); *j*, *k* – well 3, sampling depth 10 m (*j* – half-matted grain with a small-pit surface; *k* – glossy grain with a small-pit surface).

cent-shaped hollows, usually forming in calmer aqueous environments, can be seen on some grains. Both features indicate water transport with varying flow rate: small-pit surfaces form during transport in an intense river flow, and crescent-shaped depressions form in calmer aqueous conditions.

It can be assumed that the formation of deposits in well 2 (depth 7 m) and in well 3 (depth 5.5 m) occurred owing to alluvial processes and insignificant aeolian processing. Despite similarities in indicators of degree of matting in grains from well 2, the absence of small pits typical for aeolian transport has allowed us to conclude that the formation of the deposits in well 3 (depth 10 m) had occurred under conditions of water flow.

2. Botanical composition of peat. Samples from well 2 were obtained from depths of 0.05 m (recent sample), 0.05–0.10 m and from the base of the peat bog from a depth of 1.0–1.1 m. Samples for well 3 were obtained from depths of 0.45–0.50 m and from the base of the peat bog from depths of 1.60–1.73 m. One sample was obtained from buried interlayers of vegetation detritus from well 3 from a depth of 8.8–8.9 m.

The botanical composition of the surface peat (well 2, depth 0–0.05 m) corresponds to contemporary vegetation: subshrub-moss-lichen groups of hilly peat bogs (Fig. 6). Peat from well 2 from a depth of 0.05–0.10 m is lowland, wood-bog, strongly decomposed (degree of decomposition is 45–50 %), and formed under taiga conditions of a lowland swamp forested by birches and willows. Peat from well 2 from a depth of 1.0–1.1 m is lowland, strongly decomposed, degree of decomposition is 45–50 %, belongs to the forest subtype (birch), formed under plant communities common in low (flood) banks of water objects (lakes, river floodplains). Peat from well 3 from a depth of 0.45–0.50 m is transitional, *Eriophorum-Sphagnum*, medium decomposed (approximately 35 %), formed under a *Gramineae-Eriophorum-Sphagnum* transitional swamp. Peat from well 3 from a depth of 1.65–1.73 m is marsh, quagmire, strongly decomposed, degree of decomposition is over 50 %.

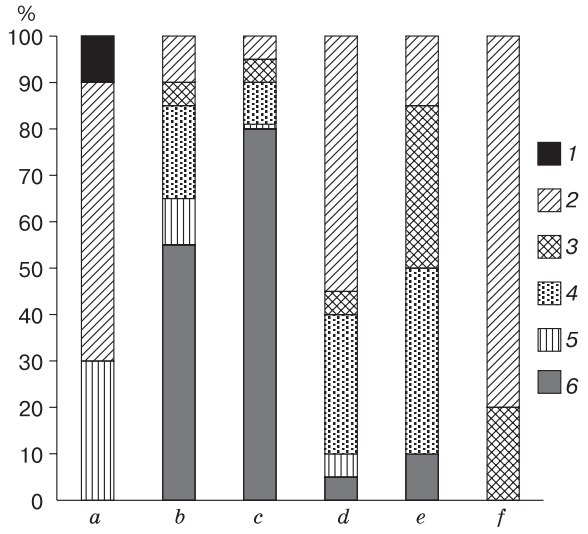

Fig. 6. Relationship between main botanical groups of plants in peat samples.

a – well 2, depth 0–0.05 m; *b* – well 2, depth 0.05–0.10 m; *c* – well 2, depth 1.0–1.1 m; *d* – well 3, depth 0.45–0.50 m; *e* – well 3, depth 1.65–1.73 m; *f* – well 3, depth 8.8–8.9 m. *1* – lichens, *2* – mosses, *3* – grasses, *4* – sedges and Cyperaceae, *5* – subshrubs, *6* – woody plants.

Peat of the given type could have formed under *Gramineae-Cyperaceae* swamps. Vegetation detritus from well 3 from a depth of 8.8–8.9 m is strongly decomposed (degree of decomposition is 35–40 %), formed under conditions of a mineral-peat *Gramineae-Hypnales* swamp.

3. Absolute dating. Radiocarbon dating was completed from five samples of buried peat collected from the same depths as samples for botanical composition analysis, excluding the recent peat sample (well 2: 0.05–0.10 m and 1.00–1.10 m; well 3: 0.45–0.50 m, 1.65–1.73 m, and 8.80–8.90 m). The results reveal a Middle Holocene formation time frame of the top part of the peat bog in well 2 and the middle part of the peat bog in well 3, an Early Holocene formation time frame of the base of the peat bog in wells 2

Table 1. **Radiocarbon dating results of peat samples obtained from wells 2 and 3**

No.	Sample collection depth, m	Dating laboratory number	^{14}C age, years	Calibrated age (2σ, 95.4 %)	Calibrated age (1σ, 68.2 %)
				calibrated y.a.	
			Well 2		
1	0.05–0.10	Ki-19584	3,660 ± 80	3,982 ± 254	3,996 ± 115
2	1.0–1.1	Ki-19596	8,990 ± 90	10,071 ± 301	10,085 ± 139
			Well 3		
3	0.45–0.50	Ki-19598	4,280 ± 60	4,832 ± 207	4,845 ± 98
4	1.65–1.73	Ki-19613	9,160 ± 100	10,407 ± 238	10,358 ± 117
5	8.8–8.9	Ki-19626	34,840 ± 300	39,381 ± 695	39,372 ± 358

Note: σ – standard deviation.

and 3, a Kargin formation time frame of the vegetation detritus in well 3 at a depth of 8.8–8.9 m (Table 1).

DISCUSSION OF THE RESULTS

The characteristic feature of migrational mounds and heaving ridges to form groups has been described in both Russian and Western literature. Thus, a typical area where mounds and ridges are concentrated has been studied by V.P. Evseev [*1976*] in the area of the Pangoda River (tributary of the Pravaya Khetta River). Mounds of various heights stretch in a narrow line along a small stream for 1.5–2.0 km. The mounds are of various types (peat and peat-mineral) and heights (from 3–5 to 10–12 m), with asymmetric slopes and a base diameter of 30–100 m. It is noted that some mounds merge into each other through saddles, creating an illusion of a ridge, which is particularly typical for marginal mounds. According to V.P. Evseev [*1976*], such groups of mounds are linked to inner margins of alluvial terraces and peripheral areas of lake-swamp basins on the border of changing rock composition and freezing conditions.

Another peculiarity of large peat-mineral MFM is a multi-layer structure. In the top part there is usually strongly decomposed peat up to 1.5–2.0 m thick. Below lie sands or loamy sands 3.0–3.5 m thick. The bottom loamy part of the section can reach up to 10–13 m (from 50 to 90 % of the thickness of the drilled deposits) [*Evseev, 1976*]. Loams (predominantly of marine or lacustrine genesis) undergo heaving, the majority of migrational ice accumulation occurs here in the form of ice interlayers, and in some cases by way of the formation of an ice core.

According to Yu.K. Vasil'chuk [*2008*], questions related to intermediate forms between frost mounds of the palsa type and buglunnyakhs (pingo) remain unanswered. According to his data, the ice lens within the mound core could be the criterion for separating palsas and lithopalsas from pingos. However, cases have been described in areas of classical distribution of palsas (in the lower course of Ob' near the village Azovy) when ice lenses over 1 m thick lying in frost mound sections have been classified as the migrational type [*Vasil'chuk, 2008*].

Modern paleogeographic insights indicate that permafrost and MFM had formed in climate conditions that were apparently harsher than contemporary ones. Results of studies which used the palynological, isotopic and radiocarbon methods have revealed that intense bogging in the northern taiga subzone of Western Siberia had begun not earlier than 10 ka, almost at the very beginning of the Holocene, and had ended (for the largest MFM in the northern taiga subzone) with the cooling in the beginning of the Subboreal period (approximately 5.5–5.0 ka) [*Evseev, 1976; Vasil'chuk, 2008; Ponomareva et al., 2012*].

The studied migrational heaving ridge is located in an area typical for palsa distribution. In the section of well 2 at depths of 7.27–10.70 m lies ground ice: there are large grains and ice lenses with loamy material between them. The cryogenic texture in ice ground horizons is thick schlieren (schlieren up to 3 cm). The cryogenic texture in loamy horizons is thin schlieren (schlieren up to 0.5 cm). Ice volume in swelled loams is ~60 %. Below the depth of 10.7 m, up to the well bottomhole (12.35 m), the ice which composes the ice core of the heaving ridge is found. The ice is pure, is broken by chaotic fractures, and is interrupted by thin (not more than 0.15 m) loam interlayers. The significant thickness of ice lenses (0.78 and 0.44 m) may indicate an injectional mechanism of their formation. However, even the presence of pure ice lenses cannot unequivocally exclude a segregational migrational nature [*Vasil'chuk, 2008*] because an intense migrational ice accumulation in ice ground horizons of swelled loam has been identified. It can be said that the studied ridge has a predominantly migrational genesis with a complementary influence of ice injections.

The studied heaving ridge is analogous in structure to a well-studied, large MFM [*Berdnikov et al., 2019*] located 2.35 km northeast of well 2 (Table 2). One difference which can be noted is the presence of pure ice lenses in well 2, while well 1-2009 has only a schlieren cryostructure typical for migrational ice discharge [*Berdnikov et al., 2019*].

The reconstruction of the development of the studied heaving ridge allows us to preliminarily identify the following stages:

– formation of loamy, presumably lacustrine deposits of the Yermakov period (MIS 4), which are observed in the bottom part of well 2;

– the scour of the lacustrine deposits by the meandering stream bed of the Kheygiyakha River and the formation of floodplain deposits presented in the bottom part of well 3 (the beginning of the second half of the Kargin interstadial – MIS 3; 40–38 ka BP);

Table 2. **Comparison of descriptions of migrational peat-mineral frost mound and frost ridge on the second above-floodplain terrace of the Kheygiyakha River**

Heaving shape	Relative height, m	Thickness, m			Ice volume*, %
		peat	sand	loam	
Frost mound***	6.7	0.5	6.7	2.8	35
Frost ridge****	7.5	1.1	5.9	3.7	up to 60**

* Owing to ice volume from ice injections (loams).
** In the ice ground layer.
*** Using [*Berdnikov et al., 2019*] results.
**** Present work.

– the formation of the sand deposits of the second above-floodplain terrace of the Kheygiyakha River (the top part of wells 2 and 3) in streambed and, partly, subaerial conditions in the beginning of the Sartan cryochrone (MIS 2; 27–24 ka BP);

– a hiatus in the Sartan cryochrone (MIS 2; 24.0–11.7 ka BP) induced by cooling and by weakening of surface runoff, the appearance of frost fissures and cryoturbations;

– bogging of the terrace in the beginning of the Holocene (MIS 1), confirmed by the peat dates in wells 2 and 3 (10.6–9.8 ka BP). The formation of swamps on river terraces took place in northern taiga conditions;

– the beginning of heaving and the formation of mounds and ridges was apparently due to cooling in the Subboreal period (5.5–5.0 ka BP). Heaving could have occurred in colder climate conditions than contemporary ones.

The results of a series of works [*Ponomareva et al., 2012; Zykina et al., 2017*] allow us to make deductions about repeatedly changing climate conditions in the studied area during the late Holocene (from 2.0 ka BP – to contemporary time). Cryogenic processes (ice accumulation and heaving) activated during periods of cooling, peat formation processes intensified during periods of warming. Today, the top organic layer on large mounds and ridges is gradually becoming thinner, the depth of seasonal thawing is increasing, drainage conditions are improving, erosion processes are activating, i.e. there is a transition from the peat-mineral to the mineral type [*Berdnikov et al., 2019*].

CONCLUSION

The results of the research allow us to come to the conclusion that the studied heaving ridge has a predominantly migrational genesis (with a complementary influence of ice injections) and belongs to the peat-mineral type. The ridge is characterized by a three-layer peaty-sandy-loamy structure. The bottom loamy horizon, the ice volume of which is ~60 %, is affected by heaving. The sand horizon had formed at the end of the Kargin (MIS 3) and beginning of the Sartan (MIS 2) periods (40–24 ka BP). Bogging of the area occurred at the beginning of the Holocene (MIS 1; 10.6–9.8 ka BP). The beginning of active heaving and the formation of mounds and ridges in the studied area was apparently related to cooling in the Subboreal period of the Holocene (5.5–5.0 ka BP). Heaving processes had taken place during colder climate conditions than contemporary ones. Today, the top organic layer of the heaving ridge is gradually becoming thinner. It should be noted that during detailed studies of large-mound peat bogs in Western Siberia it is reasonable to consider peat-mineral and mineral forms of heaving (mounds and ridges) as a separate type of cryogenic landform.

Acknowledgements. *The study was carried out with financial support from RFBR and the* Yamalo-Nenets Autonomous Okrug within the scientific project *No. 19-45-890008, as well as within the scientific project No. 19-29-05267 and within the government contract of IGM SB RAS.*

References

Berdnikov, N.M., Gravis, A.G., Drozdov, D.S., et al., 2019. Ground ice content of frost mounds in the Nadym river basin. Earth's Cryosphere (Kriosfera Zemli), XXIII (2), 25–32.

Braduchan, Yu.V., Vasilenko, E.P., Voroninь A.S., et al., 2015. State Geological Map of the Russian Federation. Scale 1:1,000,000 (third generation). Series West Siberian. Sheet Q-43 – Novy Urengoy Explanatory Note. VSEGEI, St. Petersburg, 320 pp. (in Russian).

Bronk, R., Lee, S., 2013. Recent and Planned Developments of the Program OxCal. Radiocarbon 55 (2/3), 720–730.

Calmels, F.C., Delisle, G., Allard, M., 2008. Internal structure and the thermal and hydrological regime of a typical lithalsa: significance for permafrost growth and decay. Can. J. Earth Sciences 45 (1), 31–43.

Evseev, V.P., 1976. Migrational frost mounds of the northeast of the European part of the USSR and Western Siberia. In: Problems of cryolithology. Moscow university publishing house, Moscow, No. V, pp. 95–159 (in Russian).

Friedman, G., Sanders, J., 1978. Principles of Sedimentology. Wiley, New York, 792 pp.

Geological survey M 1:1,000,000 of the Heygi-Yakha basin (Long-Yugan) (report of group No. 4), 1954. VSEGEI, Leningrad, 200 pp. (in Russian).

Katz, N.Ya., Katz, S.V., Skobeeva, E.I., 1977. AAtlas of Plant Remains in Peat. Nedra, Moscow, 370 pp. (in Russian).

Khabakov, A.V., 1946. On indices of roundness of gravels. Sovetskaya Geologiya (Soviet Geology), No. 10, 46–52.

Krinsley, D.H., Doornkamp, J.C., 2011. Atlas of Quartz Sand Surface Textures. Cambridge University Press, Cambridge, 102 pp.

Landscapes of the permafrost zone of the West Siberian oil and gas province, 1983. Nauka, Novosibirsk, 159 pp. (in Russian).

Moskalenko, N.G., Ponomareva, O.E., 2004. Changes of frost mounds, disturbed by linear building in northern taiga of West Siberia. Kriosfera Zemli (Earth's Cryosphere), VIII (2), 10–16.

Moskalenko, N.G., Ponomareva, O.E., Gravis, A.G., Berdnikov, N.M., 2012. Change in geocryological conditions. In: Integrated monitoring of northern taiga geosystems of Western Siberia. Academic Publishing House Geo, Novosibirsk, pp. 105–119 (in Russian).

Ponomareva, O.E., 2010. Nature conservation zoning in Nadum river basin (West Siberia). Kriosfera Zemli (Earth's Cryosphere), XIV (2), 46–55.

Ponomareva, O.E., Gravis, A.G., Berdnikov, N.M., 2012. Contemporary dynamics of frost mounds and flat peatlands in north taiga of West Siberia (on the example of Nadym site). Kriosfera Zemli (Earth's Cryosphere) XVI (4), 21–30.

Popov, A.I., 1967. Permafrost Phenomena in the Earth's Crust (Cryolithology). Moscow university publishing house, Moscow, 304 pp. (in Russian).

Rukhin, L.B., 1969. Basics of lithology: The doctrine of sedimentary rocks. Nedra, Leningrad, 703 pp. (in Russian).

Shpolyanskaya, N.A., Evseev, V.P., 1972. Convex peatlands of the northern taiga of Western Siberia. In: Natural conditions of Western Siberia. Moscow university publishing house, Moscow, pp. 134–146 (in Russian).

Sizov, O.S., Volvakh, A.O., Vishnevsky, A.V., Soromotin, A.V., 2020. Lithological and geomorphological signs of the genesis of the upper stratum of Quaternary deposits in the lower reaches of the river. Nadym. Problemy Regional'noy Ekologii, No. 3, 84–97.

Tyrtikov, A.P., 1979. The dynamics of vegetation cover and the development of permafrost landforms. Nauka, Moscow, 116 pp. (in Russian).

Tyuremnov, S.N., 1976. Peat Deposits. Nedra, Moscow, 488 pp. (in Russian).

Vasil'chuk, Yu.K., 2008. Convex frost mounds of permafrost peat massifs. Moscow university publishing house, Moscow, 571 pp. (in Russian).

Vegetation of the West Siberian Plain, 1985. Nauka, Novosibirsk, 248 pp. (in Russian).

Velichko, A., Timireva, S., 1995. Morphoscopy and morphometry of quartz grains from loess and buried soil layers. GeoJournal 36 (2/3), 143–149.

Wolfe, S., Stevens, C., Gaanderse, A., Oldenborger, G., 2014. Lithalsa distribution, morphology and landscape associations in the Great Slave Lowland, Northwest Territories, Canada. Geomorphology 204, 302–313.

Zykina, V.S., Zykin, V.S., Vol'vah, A.O., et al., 2017. Upper Quaternary deposits of the Nadym Ob area: stratigraphy, cryogenic formations, and deposition environments. Earth's Cryosphere (Kriosfera Zemli), XX (6), 12–20.

Received April 20, 2020
Revised version received November 5, 2020
Accepted December 24, 2020

EARTH'S CRYOSPHERE
SCIENTIFIC JOURNAL

Kriosfera Zemli, 2021, vol. XXV, No. 2, pp. 13–21

SURFACE AND GROUND WATERS IN TERRESTRIAL PERMAFROST REGION

THERMAL SPRING AT THE POLE OF COLD (EASTERN YAKUTIA)

V.N. Makarov, V.B. Spektor

Melnikov Permafrost Institute, Siberian Branch of the Russian Academy of Sciences, Merzlotnaya str. 36, Yakutsk, 677010, Russia; vnmakarov@mpi.ysn.ru

The work reports on new data on geochemistry of water of the Sytygan-Sylba Thermal Spring located in the permafrost zone in the northeast of Yakutia. Data on the content of rare and trace elements, elements of a rare-earth group, oxygen and hydrogen isotopes in the studied waters have been obtained for the first time. Groundwaters of the spring are classified as low-mineralized siliceous thermal waters of the deep origin, which are seasonally fed due to the inflow of more mineralized suprapermafrost waters. The year-round activity of the thermal spring in the zone of continuous permafrost 300–500 m thick is associated with the significant heat flow in the anomalous mantle uplift zone. Geochemical signs of the thermal water of the spring involve an increased concentration of sulfates, anomalous contents of Ge, Mo, W, As and other elements, which may be indicators of halo waters and proximity of ore accumulations.

Key words: *hydrogeochemistry, isotopes, Sytygan-Sylba Spring, permafrost, trace elements, rare earth elements, Northeast of Yakutia, thermal waters.*

INTRODUCTION

Thermal waters in the area of the distribution of thick permafrost in the Northeast of Russia have engaged attention of scientists for a long time [*Obruchev, 1927, 1954; Shvetsov, 1951*]. However, these waters remain poorly studied due to remoteness and inaccessibility. The Sytygan-Sylba Spring is the only warm spring in Eastern Yakutia. The spring is famous for its location near the Pole of Cold, 80 kilometers south of the Oymyakon village.

The toponym *Sytygan-Sylba* is translated from Yakut as "*rotten, slowly flowing water*". The original name *Khuksichan* (Ev. *Нуксичан*) which is translated from the Even language as "hot", is almost forgotten. The water here is warm, both in winter and in summer.

The Sytygan-Sylba Spring was discovered in 1926 by geologist S.V. Obruchev, who described it for the first time and made the chemical analysis of mineral water [*Obruchev, 1927*].

In terms of location, physical nature, and composition, water of the Sytygan-Sylba Spring is close to the Talaya Deposit of thermal waters, which is located 400 kilometers to the east on the territory of the Magadan Oblast. The Talaya balneological resort operates on the basis of this thermal spring [*Hydrogeology..., 1972; Shepelev, 1987*].

The main purpose of this work was to study geological, hydrogeological, and geocryological conditions in the discharge area of the thermal waters and their chemical composition. Data on the content of rare and trace elements, oxygen and hydrogen isotopes, and elements of a rare-earth group were obtained in the studied waters for the first time.

METHODS

Water samples were taken from the Sytygan-Sylba Spring on February 17, 2018. Chemical analyses were performed in the analytical departments of the Melnikov Permafrost Institute, Siberian Branch, Russian Academy of Sciences (MPI SB RAS) and Analytical Certification Test Center of the Institute of Microelectronics Technology and High-Purity Materials, Russian Academy of Sciences (ACTC IMT RAS). A complete chemical analysis of water samples was performed by capillary electrophoresis at the MPI SB RAS. Concentrations of microcomponents, trace and rare-earth elements were determined using the inductively coupled plasma mass spectrometry (X-7, Thermo Elemental, USA) and atomic emission methods at the ACTC IMT RAS. The stable reproducible geochemical data have been provided for most chemical elements. These data have been obtained by the analysis of subclarke sensitivity, i.e., at the detection limits, which are close to clarke of an element in the analyzed medium.

GEOLOGICAL AND HYDROGEOLOGICAL CONDITIONS

In winter, the spring is a small stream flowing out from under a snow-ice dome, which is formed due to evaporation over the water discharge zone. The

water is cooled at a distance of 15–20 m from the snow dome, and an icing of about 50 × 200 m in size and 1.0–1.2 m thick is formed. According to V.F. Shishkina, who carried out the geological survey in the spring area in 1960, the volume of the icing was 4000 m^3, and its area was 10 000 m^2. Trunks of the trees, surrounding the valley, bear traces of mechanical and chemical impact of the icing.

The Sytygan-Sylba Spring (62°45′39.5″ N, 144°13′55.5″ E) is situated in the Oymyakon district of the Sakha Republic (Yakutia) of the Russian Federation, 8 km west of Lake Alysardakh, about 1050 m above the sea level (Fig. 1).

The spring is located at the foot of a gently sloping hill about 2 m high. The water flows out of a small sinkhole (about 0.3 m in diameter and 0.2 m deep) formed in loose sediments. Directly at the discharge zone, the temperature varies from 24.5 °C to 26.6 °C in different periods of the year, even during the Oymyakon winter, which is coldest in the Northern Hemisphere. A stable flow rate of about 0.25 L/s is typical for the spring. In summer, a creek formed by the spring has a wide, more than 50 m, valley, which is associated with the formation of the icing in the winter period. Below the slope, there is a small pond about 2 × 3 m in size, which does not freeze all year round. Further, 30–40 m downhill, a pond about 10 m in diameter was formed. Mineral mud is accumulated in this pond; a color of the mud changes from black to gray with depth [*Cherepanova, 1988*].

The Sytygan-Sylba Spring is located in the southern part of the Oymyakon highlands, which is part of the long (about 1200 km) and wide (about 300 km) belt of relatively leveled low relief. This part of the highlands can be called the Yana-Indigirka intermountain region. The morphostructure of the intermountain region is characterized by predomination of plateaus and tablelands, that occupy the central part of the Verkhoyansk-Kolyma mountain system between its high-mountain structures – the Chersky and Verkhoyansk ranges. The top surface within the intermountain region is located at the elevation about 1000 m on average. However, on the framing ridges, the top surface rises to the heights of 2000–2500 m, sometimes reaching the heights of about 3000 m. It is likely that the most significant amount of water penetrates into the subsurface within this part of the ridges, and the geological, geomorphological, and, partially, climatic conditions of these areas determine the volume of water resources, isoto-

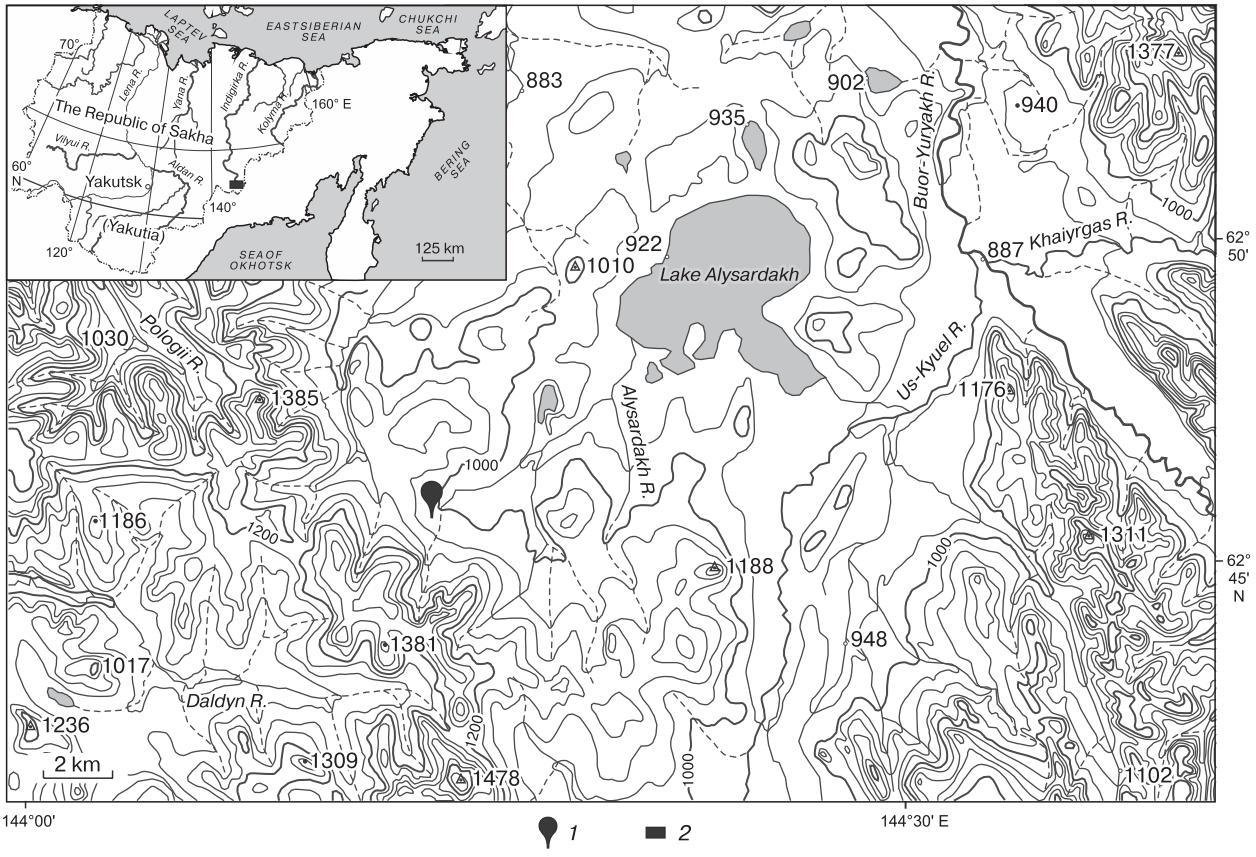

Fig. 1. The overview map of the Sytygan-Sylba Spring.

1 – location of the Sytygan-Sylba Spring; *2* – the studied area in the inset-map.

pic and, to some extent, chemical composition of thermal waters.

The current relief was formed during the Late Cenozoic (Pliocene–Quaternary) after the prolonged (Paleogene–Miocene) stable (quasi-plate) stage, during which the relief was levelled and low-thick continental coal-bearing deposits were accumulated [*Zonenshayn, Savostin, 1979; Spektor, 1987*].

The river network of the Oymyakon area belongs to the basins of the rivers of the Indigirka River upstream that originate in the Suntar-Khayata Ridge. Icings, the origin of which is associated with river waters and confined subpermafrost waters, are widespread in river valleys. The icings play a great role in the ice regime of the rivers and in the runoff redistribution. The geological structure of the area, where the spring is located [*Matveenko, 1972*], points to its long and multistage history, which is partially manifested in outcrops of the structural-material complexes (Fig. 2). The most ancient of them is the Verkhoyansk Complex, which is composed of the Permian and Triassic marine terrigenous rocks dislocated into northwest-striking linear folds in the Late Mesozoic. The poorly dislocated Cretaceous volcanic rocks of the intermediate and felsic composition, which belong to the marginal continental Okhotsk-Chukotka volcanic belt, occupy the higher stratigraphic position. Large granite massifs, the outcrops of which are located at a distance of 5–10 km from the spring, were formed in the same time. The Quaternary deposits, represented by pebbles, boulders, sands, and silts of the glacial, alluvial, and slope origin complete the section. The spring is confined to the slope of the hill, which is composed of the Cretaceous volcanics and the Verkhoyansk Complex.

The Verkhoyansk Complex and the Late Mesozoic volcanic and magmatic rocks were frozen epigenetically, while the Quaternary deposits were frozen syngenetically. The permafrost within the Yana-Indigirka intermountain area and the framing ridges were formed at the end of the Pliocene–the beginning of the Quaternary.

Location of the spring is unique. The structural position of the study area has determined the significant modern tectonic activity and seismicity. Horizontally oriented compressive stresses have been reconstructed in the earthquake sources at the depths of the first tens of kilometers.

According to the model, proposed by V.T. Balobaev [*1991*], the Verkhoyansk-Kolyma system is characterized by the weighted average value of geothermal heat flux of 65 mW/m^2, which is twice higher than the flux within the Siberian Platform. In view of a small thickness of the continental lithosphere and the granitic layer of the crust in this area, V.T. Balobaev [*1991*] concludes that the background flux increases due to the significant heat flux from mantle. The highest values of the heat flux, ranging from 80

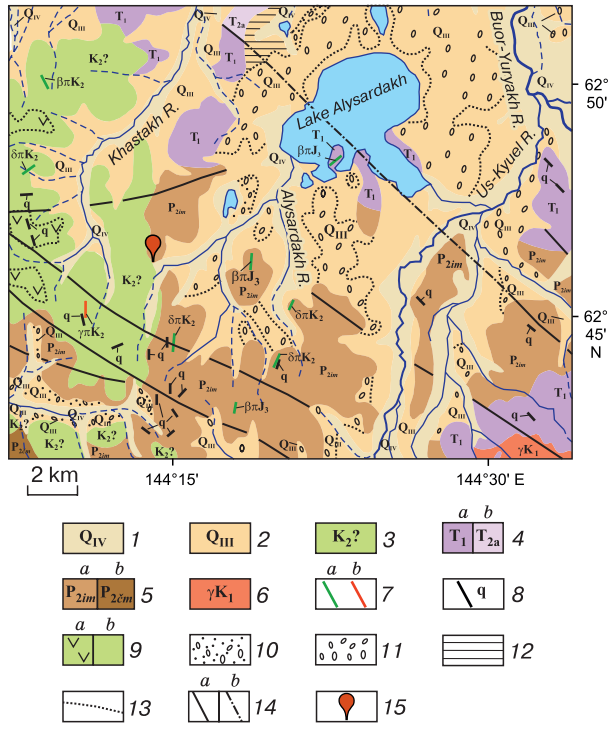

Fig. 2. The overview geological map of the spring location (Scale 1:200 000. Sheet P55-VII).

1, 2 – the complex of the Quaternary deposits: *1* – Holocene, alluvial deposits, *2* – Late Neopleistocene, alluvial deposits; *3* – Late Cretaceous marginal continental volcanogenic complex; *4, 5* – Late Paleozoic–Mesozoic Verkhoyansk terrigenous complex of the passive continental margin: *4* – Triassic deposits: *a* – Lower Triassic deposits, *b* – Middle Triassic deposits, Anisian; *5* – Upper Permian deposits: *a* – Imtachan Formation, *b* – Chamba Formation; *6* – Early Cretaceous granite batholites, proto-orogenic complex; *7* – dikes: *a* – porphyry dikes of mafic and intermediate composition, *b* – granitoid dikes; *8* – hydrothermal quartz veins (q); *9* – the composition of the Late Cretaceous volcanogenic complex: *a* – rocks of intermediate composition, *b* – rocks of felsic composition; *10–12* – genetic types of the Late Neopleistocene deposits: *10* – water-glacial, *11* – glacial, *12* – lacustrine; *13* – facies boundaries; *14* – faults: *a* – established, *b* – assumed; *15* – location of the Sytygan-Sylba Spring.

to 100 mW/m^2, are common in the territory of the Yana-Oymyakon intermountain area. According to V.T. Balobaev it "*...may be an anomalous mantle of asthenospheric type, the appearance of which leads to partial melting of the Earth crust, transformation of its mineralogical composition, formation of depressions and filling them with sediments*" [*Balobaev, 1991, p. 135*].

The spring belongs to an increased type of thermal regime of thermal waters with a heat flux density of 80–100 mW/m^2. Such heat flux provides the temperature, which exceeds 1000 °C at a depth of 40 km [*Balobaev, 1991, p. 137*]. A geothermal gradient (an increase in temperature with depth, usually per 1 km

or 100 m of depth) is 40–50 °C/km. We consider that the location of the spring over the central part of the anomalous mantle ledge and the high heat flow accompanying this ledge explain the very existence of the thermal spring, the relatively high temperature of water (+26.6 °C), and year-round activity of the spring in the field of continuous permafrost 300–500 m thick with the mean annual ground temperature of –3 to –5 °C or lower [*Ershov, 1991*]. This geothermal anomaly should have formed an extensive hydrogeogenic talik zone. The existence of this zone can be indirectly evidenced by the presence of relatively mineralized water in the Lake Alysardakh, which is located near the area of thermal water discharge. The mineralized water of the lake is unusual for surface waters of the region.

In terms of hydrogeology, the area of groundwater discharge belongs to the Alysardakh geocryological intermountain artesian basin of the Yana-Kolyma cryo-pressure basin. This area is attributed to the zone of continuous permafrost, a thickness of which exceeds a thickness of the sedimentary cover. The significant tectonic fragmentation of rocks and the presence of large tectonic faults determined the wide distribution of subpermafrost fracture-vein waters and icings, associated with local discharges of groundwater in the area.

Geological and structural features of the area determine the specific character of the hydrogeological conditions of the area of thermal water discharge. In accordance with the conditions of occurrence and circulation, these waters are fracture-vein thermal waters, which are attributed to the zone of active latitude- striking faults at the place of their junction with the north-northwest-striking faults [*Parfenov, 2001*].

The Sytygan-Sylba Spring is a unique thermal mineral spring in the studied area. However, it is possible that, in the Indigirka River upstream, discharges of thermal waters are more widely distributed, and Sytygan-Sylba is not the only spring of thermal waters within the Yana-Oymyakon intermountain area [*Shvetsov, 1951*]. We consider that there are "warm lakes" to the north of this area, in the same morphostructural zone, and further north, beyond the Arctic Circle, there are discharges of subthermal water in the Kular Ridge area.

RESULTS AND DISCUSSION

Results of chemical analyses of water of the spring, which were obtained by different researchers from 1926 to 2018, are given in Table 1. The data demonstrate that the chemical composition of waters of the Sytygan-Sylba Spring has remained stable during almost a century of observations. These waters are mixed in their anion composition with the strong predominance of sodium: sodium bicarbonate-sulfate-chloride, weakly alkaline (pH 8.2–8.48), with a high silica content of 21–81 mg/L (about 10 % of the total dissolved solids) and low mineralization (0.40–0.51 g/L):

$$(17.02.2018)\ M\ 0.437\frac{Cl\ 54\ SO_4\ 24(HCO_3+CO_3)22}{Na\ 90\ Ca\ 6\ K\ 2\ Mg\ 2}$$

$$pH\ 8.48\ Eh\ 0.386\ SiO_2\ 30\ F\ 19.6.$$

The geochemical conditions are oxidizing (Eh = 0.25–0.38 V). Water is slightly carbonaceous, CO_2 content is 48.4, and H_2S is 0.45 mg/L. A specific feature of the springs is a relatively constant water temperature (24.5–26.6 °C) in cold and warm seasons. Low mineralization of thermal waters of the Sytygan-Sylba Spring is explained by their formation in terrigenous rocks, which are well washed off water-soluble salts by intensive groundwater circulation.

The basic components, providing mineralization of waters of the spring, are sodium, silica, fluorine, chlorides, sulfates, and bicarbonates. Cl predominates (48–61 %-eq.) among anions. Besides chloride ions, sulfates (up to 110 mg/L) and bicarbonates (up to 109 mg/L) are present in rather high amounts. Among cations, Na^+ predominates (92–95 %-eq.) with the concentration up to 195 mg/L. The content of other cations is low: K^+ content is no more than 8.0 mg/L, Ca^{2+} content is up to 5.8 mg/L and Mg^{2+} is up to 3.0 mg/L.

The studied thermal waters are rich in fluorine with the concentration of 19.6 mg/L. The fluorine content is similar to that in the thermal waters of the Talaya Spring (15–20 mg/L) in the Magadan region [*Hydrogeology..., 1972*]. Low activity of calcium also creates the favorable conditions for the increased activity of fluorine and its accumulation in water.

There are certain variations in the chemical composition of water of the spring in different months: July, November, February, April (Fig. 3). Data obtained in different years have been compared, because no single annual cycle of observations has been carried out. In April, at the end of winter (when the active layer freezes to the maximum), the chemical composition of water of the spring should completely correspond to the composition of deep thermal waters. During this period, as thermal waters of the Sytygan-Sylba Spring move toward the surface through permafrost, they are not supplied by surface waters and not diluted by frozen suprapermafrost waters. In winter time, the temperature of water in the spring remains positive at the discharge zone; however, mineralization of water steadily decreases due to reduction of Na^+ and SO_4^{2-} concentration (Fig. 3).

In the warm season, when the spring water should be desalinated, mineralization should be decreased, and a role of bicarbonates in the chemical composition of the waters should be increased due to input of less mineralized waters from the free ex-

Table 1. **The chemical composition of thermal waters of the Sytygan-Sylba Spring**

Parameters	Date of sampling				
	10–16.11.1926 [*Obruchev, 1927*]	02.04.1948 [*Shvetsov, 1951*]	28.07.1984 [*Cherepanova,1988*]	14.04.2013 [*Trofimova, 2013*]	17.02.2018 (authors' data: V.N. Makarov, V.B. Spektor, R.N. Ivanova)
Rate, L/s	0.20	0.25	–	0.25–0.30	–
Water temperature, °C	+26.0	+25.6	+26.6	+25.1	+24.5
Air temperature, °C	–40.0	–11.5	–	–	–
pH	–	–	8.2	9.5	8.48
Eh, mV	–	–	250	–	386
Mineralization, mg/L	483.1	396.6	513	439	436.8
Content*					
Ca^{2+}	7.7/0.38	1.0/0.03	4.0/0.20	8.0/0.8	7.76/0.39
Mg^{2+}	0.2/0.02	6.0/0.47	3.0/0.25	2.24/0.2	1.43/0.12
Na^{+}	186.4/7.90	140.0/6.10	195.5/8.50	179.4/7.8	158.2/6.09
K^{+}	186.4/7.90	140.0/6.10	8.0/0.20	179.4/7.8	4.20/0.13
CO_3^{2-}	–	–	–	–	4.65/0.15
HCO_3^{-}	108.6/1.78	57.2/0.95	85.0/1.39	103.7/1.7	86.22/1.41
Cl^{-}	142.5/4.02	141.0/4.00	150.0/4.23	149.1/1.7	134.99/3.81
SO_4^{2-}	94.0/1.96	80.0/1.65	110.0/2.29	48.0/1.0	82.32/1.71
SiO_2^{2-}	20.6	–	81.0	–	65.3
NO_3^{-}	–	–	–	–	0.10
NO_2^{-}	–	–	2.0	–	0.12
NH_4^{+}	–	–	–	–	0.05
HPO_4	–	–	–	–	0.12
CO_2	–	48.4	–	66.0	–
H_2S	–	0.45	–	9.22	–
Fe^{3+}	–	0.24	–	0.12 (Fe)	0.056 (Fe)

* In a numerator – mg/L, in a denominator – mg-eq.

change zone, the opposite events are observed. In summer, in the water of the Sytygan-Sylba Spring, mineralization significantly increases (by 50–100 mg/L) due to sulfates and sodium chlorides (Fig. 3). The content of Na^{+} and SO_4^{2-} ions increases by about 30 % in July compared to April, when suprapermafrost waters is affected by the maximum winter freezing. Obviously, during the warm season, suprapermafrost waters with higher mineralization inflow to the spring. The very fresh surface bicarbonate waters do not influence the chemical composition of waters of the spring.

In 2018, we obtained new data on the chemical composition of thermal waters of the spring. High concentrations in the thermal spring are typical for strontium – 0.16 mg/L, lithium – 1.39 mg/L, and fluorine – 19.6 mg/L.

Of siderophile elements, only iron and molybdenum have significant concentration in the waters. Fe_{tot} content in thermal waters of the Sytygan-Sylba Spring varies from 56 to 240 μg/L, Mo content is 0.443 μg/L. The concentration of other siderophiles is below the detection limit: Co, Ni < 0.*n*; Pd, Rh, Au < 0.0*n*; Re, Os, Ir, Pt, Ru < 0.00*n* (*n* = 1–9), in particular: Co and Ni is <0.2 μg/L; Pd is <0.014 μg/L, Rh is <0.012 μg/L, Au is <0.014 μg/L; Re is <0.001 μg/L, Os <0.001 μg/L, Ir is <0.001 μg/L, Pt is <0.002 μg/L, Ru is <0.008 μg/L. The concentra-

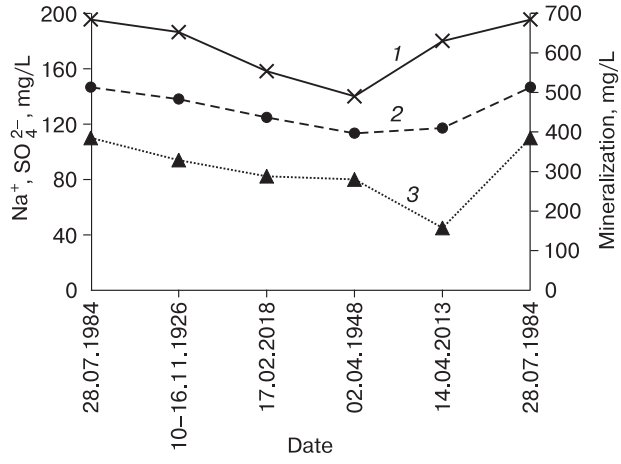

Fig. 3. Variations in mineralization (*2*) and Na^{+} (*1*) and SO_4^{2-} (*3*) content in water of the Sytygan-Sylba Spring on months in different years.

Table 2. **Concentration of REEs in thermal waters of the Sytygan-Sylba Spring**

Element	REE content		Element	REE content	
	μg/L	Normalized to NASC		μg/L	Normalized to NASC
La	0.0165	$5.3 \cdot 10^{-7}$	Tb	0.00086	$1.0 \cdot 10^{-6}$
Ce	0.0501	$7.5 \cdot 10^{-7}$	Dy	0.006	$1.2 \cdot 10^{-6}$
Pr	0.004	$5.4 \cdot 10^{-7}$	Ho	<0.0008	–
Nd	0.0215	$7.8 \cdot 10^{-7}$	Er	0.0019	$5.3 \cdot 10^{-7}$
Sm	0.0049	$8.8 \cdot 10^{-7}$	Tm	<0.0008	–
Eu	0.0023	$1.9 \cdot 10^{-6}$	Yb	<0.0008	–
Gd	0.0086	$1.7 \cdot 10^{-6}$	Lu	<0.0008	–

Note. Mass-spectral and atomic-emission analyses have been performed at the Analytical Certification Test Center of the Institute of Microelectronics Technology and High-Purity Materials, Russian Academy of Sciences (ACTC IMT RAS, Chernogolovka).

tion of silicon is 30.48 μg/L, the concentration of phosphorus is less than 30 μg/L.

Of lithophile elements, the high content (>*n*, μg/L) was established for Li (1390–2050), Br (275), Sr (160–212), Al (24.9), Mn (3.1), B (1.68), and Ba (1.1). The content of other lithophile elements ranged from 0.*n* to 0.00*n* μg/L: W (0.715), V (0.17), Cs (0.088), Rb (0.085), Be (0.048), Zr (0.038), Th and U (0.008), Hf (0.007). B/Cl ratio = $1.24 \cdot 10^{-5}$, which is almost 4 orders of magnitude lower than in seawater, and close to this parameter (<0.007) in thermal springs in the areas of active volcanism.

Gallium, zinc, arsenic, germanium, lead, and antimony should be highlighted in a group of chalcophile elements. Their concentrations range from *n* – 0.*n* μg/L: Ga (1.8), Zn (1.2), As (0.85), Ge (0.762), Pb (0.14), Sb (0.105). Cu content in the studied thermal waters is less than 0.7 μg/L, Ti content is less than 1 μg/L. The following elements have concentrations below the detection limit: Se <5 μg/L; Hg <0.7; Sc < 0.3; Sn <0.022; Te <0.018; Ag <0.01; Cd <0.009; Nb <0.008; In <0.005; Ta <0.003; Te <0.001; Bi <0.001 μg/L*.

The geochemical characteristics of thermal spring waters, which contain sulfates and anomalous amounts of ore elements (germanium, molybdenum, tungsten, arsenic and others) may be indicators of the halo waters suggesting close proximity to ore bodies [*Makarov, 1998*].

We have obtained the first data on the content of rare-earth elements (REE) in the studied thermal waters (Table 2). The concentration of REE is generally low: ⩾0.0*n* μg/L. The spectrum of the REE distribution, normalized to North American Shale Composite (NASC), is characterized by a high content of light REEs (more than 80 %), which are moderately enriched in medium REEs and depleted in heavy REEs. Low concentration of REEs in the waters may be caused by alkaline values of pH in thermal waters, controlling the REE content and determining decrease in the REE content [*Sholkovitz, 1995*].

A poor cerium anomaly and an apparent europium anomaly are indicated. The tetrad effect is insignificant. This pattern of the REE distribution with the well-manifested Eu anomaly is typical for hydrothermal solutions [*Haas et al., 1995; Dubinin, 2006*]. The high positive Eu anomaly may be an indirect indicator of the thermal impact during the formation of a liquid phase. Although, we cannot exclude the possibility that the enrichment by europium occurred during diagenesis of marine sediments under anaerobic conditions [*Ivanova, 2020*].

The similarity of the composition of REE in the spring water with sandstones and siltstones of the Verkhoyansk Complex points to inheritance of their composition, particularly, in terms of the significant amount of light REEs and the europium anomaly. The lack of heavy REEs may be associated with a geochemical barrier (influence of suprapermafrost waters, chemisorption on clayey minerals) during discharge.

Such characteristics of the REE spectrum as well as the anionic composition and low content of macrocomponents, indicate the location of the spring in the zone of discharge of fracture waters.

The relationship between the thermal spring and the suprapermafrost and surface waters can be established on the basis of the comparison of the REE spectra of the spring waters and the samples from wedge ice, massive ground ice, and river water, which were obtained in Eastern Yakutia [*Ivanova, 2020*] and normalized to the NASC standard (Fig. 4) [*Gromet et al., 1984*].

* Mass-spectral and atomic-emission analyses have been performed at the Analytical Certification Test Center of the Institute of Microelectronics Technology and High-Purity Materials, Russian Academy of Sciences (ACTC IMT RAS, Chernogolovka).

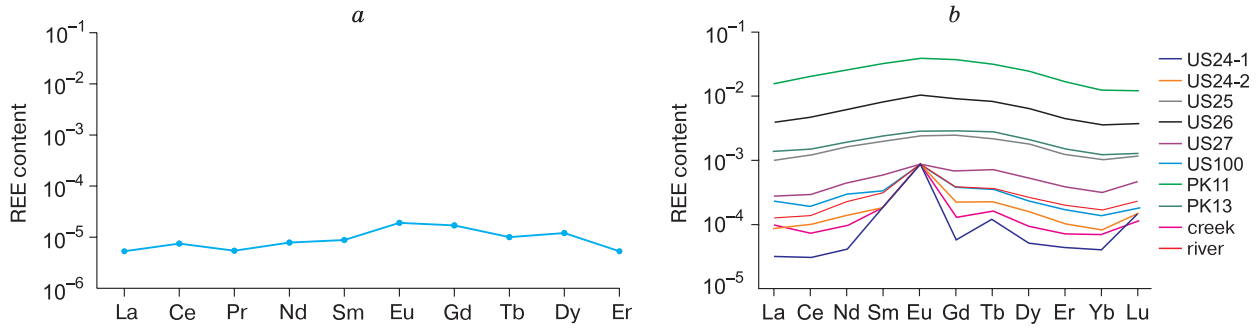

Fig. 4. REE content, normalized to NASC:

a – in water of the Sytygan-Sylba Spring; *b* – in ground ice (US: 24–27,100; PK: 11,13) and surface waters (creek, Adycha River).

However, there are almost no data on the distribution of REEs in the components of the hypergenesis zone in the region. Therefore, when interpreting the obtained data, we have used the results of the studies of V.V. Ivanova in the basin of the Adycha River [*Ivanova, 2020*]. Terrigenous sediments and granitoids are widespread in this area, as well as in the area of the spring. These regions are characterized by the similar chemical composition of atmospheric precipitation [*Makarov, 2014*]. These data suggest that the chemical composition of natural waters of the hypergenesis zone was formed under similar conditions in both regions.

The REE spectrum of wedge ice and massive ground ice reflects the chemical composition of soil solutions penetrating into ice from the suprapermafrost perched aquifer. The positive Europium anomaly of ice is associated with the groundwater composition and the increasing of the concentrations of chemical elements due to cryogenic or ore concentrating. REE content in water of the Sytygan-Sylba Spring is significantly lower than their content in river water and wedge ice (Fig. 4). This indicates that the spring is located in the groundwater discharge zone, which is poorly associated with the background surface waters and ground ice.

Mineralization and Na^+ and SO_4^{2-} content in the spring water significantly increase in the summertime. This points to the very weak (almost zero) dilution of water of the Sytygan-Sylba Spring by surface and suprapermafrost waters (Fig. 3).

Data on oxygen and hydrogen isotopes in water of the spring have been obtained for the first time. Isotope analysis has been carried out at the MPI SB RAS on the Picarro L2140-i Isotope and Gas Concentration Analyzer (analysts N.I. Lykhota and G.T. Maksimov). This allowed us to measure simultaneously $\delta^{18}O$, $\delta^{17}O$ and δD in solids, liquids, and vapor. Table 3 demonstrates characteristics of the oxygen and hydrogen isotopic composition of atmospheric precipitation and water of the thermal spring. The calculated value of meteoric waters $\delta D = a \cdot \delta^{18}O + 10$ ‰. Substituting the value $^{18}O = -21$ ‰ for rainwater (Table 3), we obtain $\delta D = -178$ ‰, the real, current value of –169 ‰. Some enrichment of the modern meteoric waters in heavy hydrogen may result from the increased role of precipitation due to the sources of evaporation located nearby (Pacific Ocean).

In water of the spring, $\delta D = -179.31$ ‰, which is very close to the calculated parameters of atmospheric precipitation. They reflect the composition of atmospheric precipitation for a long period of time preceding the modern one, when the Atlantic transfer prevailed. This is evidenced by the lowering of deuterium in water of the spring, which has been lost during the long-distance transfer of atmospheric moisture. The small amount of precipitation, enriched in heavy hydrogen, falls during the summer. This precipitation is consumed generally by accelerated evaporation.

In terms of balneology, warm (subthermal) waters of the spring can be used as therapeutic, anion mixed, sodium waters in a similar way to thermal waters of the Talaya Deposit. The presence of such balneological components as fluorine, metasilicic acid, rare elements, many of which are biologically active components, allows us to recommend the waters of

Table 3. **The isotopic composition of oxygen and hydrogen of atmospheric precipitation and water of the thermal spring**

Natural waters	$\delta^{18}O$	δD
Atmospheric precipitation, March–June	–21...–23	–160...–169
Spring	–20.89	–179.31
Snow, March (Oimyakon Area)	–37.44	–
	–38.08	–
Standard Mean Ocean Water (SMOW), ‰	–0.1985	–0.01985

Note. Isotope analysis has been carried out at the MPI SB RAS (analyser Picarro L2140-i Isotope and Gas Concentration Analyze).

the Sytygan-Sylba Spring for external therapeutic and prophylactic use in the form of baths.

CONCLUSIONS

Almost a lapse of a hundred years of observations reveals that waters, heated up to 26 °C in the Triassic terrigenous fractured sediments, are not subjected to significant temperature fluctuations and variations in the chemical composition. Specific features of nitrogen thermal waters of the Sytygan-Sylba Spring are low mineralization (0.4–0.5 g/L), complex anionic composition, predomination of sodium in the cation composition, weakly alkaline reaction, predomination of nitrogen in the gas composition, significant concentrations of silicic acid, fluorine, tungsten, molybdenum, germanium, arsenic and others. A distinctive feature of thermal waters of the Sytygan-Sylba Spring is the presence of sulfates in the ionic composition.

Very low (ng/L) REE contents were established in the water of the Sytygan-Sylba Spring. In terms of REE contents and correlation with spectra of river water and ground ice, these waters are thermal waters of the groundwater discharge zone, poorly related to the background regional surface waters and ice.

The isotopic composition of the thermal waters may indicate a certain role of snow recharge in the formation of a hydrogenous component of the Sytygyn-Sylba Spring waters.

There is the significant increase in mineralization (by 50–100 mg/L) due to the concentration of sulfates and sodium chlorides in the water of the Stygan-Sylba Spring in summertime. It can be assumed that during the warm period, when thermal waters enter the active layer, groundwater mixes with mineralized permafrost waters. Subsequently, since mid-November, as the active layer freezes and the inflow of groundwater decreases, mineralization of the spring water has decreased (by 15–20 % by the end of the winter period as compared to the summer period of time).

Stability of the hydrogeothermal parameters of the spring points to the relatively deep propagation of fracture systems, which serve as the regulating reservoirs and make their long-term regimes consistent. A crucial role of deep factors in the stable hydrogeochemical character of the thermal spring is clearly in evidence.

The characteristics of the REE spectrum as well as the anionic composition and the low content of macrocomponents, suggest that the spring is located in the zone of fracture water discharge. Based on the chemical composition and geological conditions of the discharge area of the Sytygan-Sylba Thermal Spring, the groundwaters belong to the low-mineralized siliceous thermal waters of the deep origin, which are recharged seasonally due to the inflow of more mineralized suprapermafrost waters.

The geochemical features of waters of the thermal spring (the increased concentration of sulfates in the ionic composition, the anomalous content of germanium, molybdenum, tungsten, arsenic and other elements) can be valuable in geochemical exploration of ore accumulations in this region.

In terms of balneology, these waters can be used as therapeutic waters for external treatment and prophylactic in the form of baths, by analogy with the thermal water of the Talaya Deposit.

Acknowledgements. *The authors are grateful to V.V. Ivanova Doctor of Geological-Mineralogical Sciences (post-doctorate degree in Russia) (Gramberg All-Russian Scientific Research Institute for Geology and Mineral Resources of the Ocean – VNIIOkengeologia) and researcher R.N. Ivanova (Melnikov Permafrost Institute, Siberian Branch, the Russian Academy of Sciences) for help in the collection of the factual material and data interpretation.*

References

Balobaev, V.T., 1991. Geothermy of the frozen zone of the lithosphere in the northern Asia. Publishing House of the SB RAS, Novosibirsk, 193 pp. (in Russian).

Cherepanova, A.P., 1988. New data on the Sytygan-Sylba Mineral Spring (Yakutia). Research of frozen strata and cryogenic events. IMZ SO AN SSSR, Yakutsk, pp. 90–97 (in Russian).

Dubinin, A.V., 2006. Geochemistry of rare earth elements in the ocean. Nauka, Moscow, 359 pp. (in Russian).

Ershov, E.D. (Ed.), 1991. Geocryological Map of the USSR. Izd-vo Mosk. Un-ta, Moscow (in Russian).

Gromet, L.P., Dymek, R.F., Haskin, L.A., Korotev, R.L., 1984. The North American Shale Composit: Its composition, major, and trace element characteristics. Geochim. et Cosmochim. Acta 48, 2469–2482.

Haas, J.R., Shock, E.L., Sassani, D.C., 1995. Rare earth elements in hydrothermal systems: estimates of standard partial modal thermodynamic properties of aqueous complexes of the rare earth elements at high pressures and temperatures. Geochim. Cosmochim. Acta 59, 4329–4350.

Hydrogeology of the USSR. Vol. XXVI. North-East of the USSR, 1972. Nedra, Moscow, 296 pp. (in Russian).

Ivanova, V.V., 2020. Geochemical features of spectra of rare earth elements in deposits of the Eastern Siberia as a new indicator of the Late Pleistocene climate change in the zone of periglacial lithogenesis–Dissertation for the degree of Doctor of geol.-mineral. sciences, St. Petersburg, 408 pp. (in Russian).

Makarov, V.N., 1998. Geochemical Fields in Permafrost. IMZ SO RAN, Yakutsk, 116 pp. (in Russian).

Makarov, V.N, 2014. Geochemistry of the snow cover of the taiga and mountain permafrost landscapes. Led i Sneg (Ice and Snow), No. 1 (125), 73–80.

Matveenko, V.T. (Ed.), 1972. State Geological Map of Russian Federation at a scale of 1:200 000. List P-55-VII. Izd-vo "Aerogeologiya", Leningrad (in Russian).

Obruchev, S.V., 1927. The Sytygan-Sylba Spring on the Indigirka River (YaASSR). Kurortnoye Delo, No. 4, p. 8.

Obruchev, S.V., 1954. Unknown lands. Travels to the North 1917–1930. Molodaya gvardiya, Moscow, 347 pp. (in Russian).

Parfenov, L.M., 2001. Tectonics, Geodynamics and Metallogeny of the Territory of the Republic of Sakha (Yakutia)/ M.I. Kuz'min (Ed.). MAIK Nauka/Interperiodika, 571 pp. (in Russian).

Shepelev, V.V., 1987. Spring waters of Yakutia. Knizhnoye izdvo, Yakutsk, 27 pp. (in Russian).

Sholkovitz, E.R., 1995. The aquatic chemistry of rare earth elements in rivers and estuaries. Aquat. Geochem. 1, 1–34.

Shvetsov, P.F., 1951. Groundwaters of the Verkhoyansk-Kolyma Fold Area and Features of their Manifestation Associated with Low-temperature Permafrost. Izd-vo AN SSSR, Moscow, 280 pp. (in Russian).

Spektor, V.B., 1987. Structure and kinematic of the Verkhoyansk–Kolyma folded system. In: The Formation of Relief of the Siberia. Nauka, Novosibirsk, pp. 152–156 (in Russian).

Trofimova, T.P., 2013. The chemical composition of waters of the Sytygan-Sylba Mineral Spring. Collection of scientific articles based on the results of the international scientific-practical conference. Kul'tInformPress, St. Petersburg, pp. 147–149 (in Russian).

Zonenshayn, L.P., Savostin, L.A., 1979. Introduction to Geodynamics. Nedra, Moscow, 311 pp. (in Russian).

Received August 30, 2020
Revised version received October 22, 2020
Accepted December 18, 2020

EARTH'S CRYOSPHERE
SCIENTIFIC JOURNAL

Kriosfera Zemli, 2021, vol. XXV, No. 2, pp. 22–34

PERMAFROST ENGINEERING

AFFECTIVITY OF SURFACE COOLING OF FROZEN GROUND IN CONNECTION WITH MECHANISM OF TEMPERATURE SHIFT FORMATION

J.B. Gorelik[1], A.K. Khabitov[2]

[1] *Earth Cryosphere Institute, Tyumen Scientific Centre, Siberian Branch of the Russian Academy of Sciences, Malygina str. 86, Tyumen, 625026, Russia; gorelik@ikz.ru*
[2] *Giprotyumenneftegaz, Respubliki str. 62, Tyumen, 625000, Russia; prof.power@yandex.ru*

The analysis of affectivity of frozen soils surface cooling methods based on the theoretical understanding of temperature shift formation with seasonal processes in the upper ground layers is provided. The surface cooling method for the building with aerated underfloor space is suggested on the base of this analysis. This method includes heat-insulation layer ground surface and free convection cooling system with its horizontal evaporator under insulation layer. Condenser of the cooling system is out of the building contour and it makes evaporator temperature near to winter air temperature. The results of mathematical modelling demonstrate that suggested method provides a significant and rapid decrease of the ground temperature as compared to other methods (up to 1.0–2.5 °C for not more than 1.5 year instead of 3–5 years). An additional temperature decrease by 1.5 °C may be obtained by connecting of the forced cooling device to the cooling system for one summer season. The calculation results allow us to propose the best sequence for connecting the cooling elements of the system at the initial stage of its operation.

Key words: *frozen soils, seasonal thawing layer, ground temperature regime, heat-insulation layer, GET cooling system, forced cooling, relaxation time to project temperature regime.*

INTRODUCTION

The regulation of the temperature regime of structure's foundations, its stabilization and restoration are widely used in the construction and operation of structures, as well as during the repair work in the areas where permafrost soils are distributed. The technical implementation of those measures is associated, as a rule, with the use of various kinds of cooling devices. The constructions of most of them (for example, thermal stabilizers of the vertical and inclined seasonal action), to ensure operability, must be deepened with their parts into the soil base. Providing high work efficiency, that significantly increases the laboriousness of the activities, since it requires drilling operations, which often have to be performed manually on a previously prepared pile field [*Dolgikh, 2014*].

Alternative methods of surface cooling of the soil have also been using in practice for a long time. The most important of them is the method based on the use of an aired underfloor space, which is still the main one in ensuring the design temperature regime of the building foundations and areal structures erected according to the first principle, and maintaining it during operation. However, the possibilities of its application are often insufficient to achieve the required temperatures. For example, for the open underfloor spaces, there is a high probability of snow accumulation on the ground surface in winter, which entails a corresponding decrease in the cooling efficiency. For the underfloor spaces with a reduced ventilation module (with airholes in the cooling structures), the cooling efficiency decreases due to a decrease in the speed of the air flow, as well as its heating from plumbing communications and the heat release from the floor. In addition to a decrease in the amount of cooling, that also leads to an increase in the time required to reach the required temperature regime of the foundation [*Vyalov et al., 1979*].

To intensify the process of soil cooling from the surface, the so-called surface heat-semiconducting coatings have been proposed, the design of which provides asymmetric heat transfer through the soil surface throughout the year: increased heat removal from the base in winter and a significant decrease in heat supply to the base in summer [*Makarov, 1985; Bubelo, 2003*]. However, they did not give the expected effect, probably because the same negative factors continue to act on the upper surface of those devices as on the underfloor space.

At the same time, it is easy to see that none of the currently known methods of surface cooling excludes the processes of seasonal freezing-thawing and, therefore, the prospects for the development of those methods can be characterized by assessing the ex-

treme values of the temperature shift [*Dostovalov, Kudryavtsev, 1967; Kudryavtsev, 1974*], arising from the application of that group of measures. As is known, the most important parameter that determines the magnitude and dynamics of changes in soil temperature regime under the influence of surface factors, as well as the magnitude of the temperature shift at a given mean-annual temperature of the soil surface, is the value of the mean-annual temperature at the bottom of the active layer. Difficulty of performing an analysis of the effectiveness of surface cooling methods is that until recently there were no simple and at the same time sufficiently general models of the mechanism for the formation of a temperature shift, allowing in simple analytical expressions to obtain estimates of the required calculated values depending on the main group of influencing factors. Such a model has been recently proposed in [*Gorelik, Zemerov, 2020*]. First of all, it is useful here to consider the simple estimates and conclusions derived from the results of that work regarding the effectiveness of surface cooling methods.

Basic relations for the dynamics of temperature in the simplest model of the frozen base

A frozen soil layer of finite thickness has been proposed as the simplest physical model of a frozen base [*Gorelik, Zemerov, 2020*]. That makes it possible, when analyzing seasonal processes, to use quasi-stationary relations for the temperature distribution not only from the side of the thawed zone (as was done earlier [*Balobaev, 1964; Porkhaev, 1970; Feldman, 1977; Shur, 1988*]), but also from the side of the frozen ground. That approach allows one to obtain a fairly simple expression for the mean-annual temperature at the bottom of the seasonal thawing layer t_m [*Gorelik, Zemerov, 2020*] in the following form (this value forms the soil temperature throughout the entire permafrost thickness below the active layer):

$$t_m = t_w \tau_w + t_s \tau_s \frac{\lambda_u}{\lambda_f}. \qquad (1)$$

Hereinafter, the following designations are introduced: t_s, t_w, t_y are mean-summer, mean-winter and mean-annual temperature (°C) of the soil surface under cover of any nature; τ_s, τ_w are the relative duration (u.f.) of the year periods with the positive and negative mean-daily air temperatures; λ_u, λ_f are coefficients of thermal conductivity (W/(m·°C)) of soil in the thawed and frozen states.

The above-mentioned surface temperatures, generally speaking, should be established by calculating the heat exchange between the soil surface and atmospheric air for the given characteristics of the soil cover. However, in some cases, they can be assessed by their extreme values. In the relation (1), the first term is negative, the second one is positive. The relation (1) demonstrates that the temperature shift $\Delta t = t_m - t_y$ depends both on the thermophysical characteristics of the soil and on the climatic parameters of a given area, and also establishes the nature of that dependence. Apparently, the earlier works do not focus on the role of climatic factors (although the influence of the difference in the values of the coefficients λ_u and λ_f is noted [*Dostovalov, Kudryavtsev, 1967; Kudryavtsev, 1974*]), since they remain practically constant for the large territories referenced to a specific meteorological station, while the properties of soils within its limits are subjected to more drastic changes. However, from the point of view of engineering geocryology, the dependence of the t_m value on the entire group of influencing factors is important, as well as the fact that each of the parameters included in the relation (1) can be changed within a specific construction site by technical means.

In the particular case, when $t_s = -t_w$, $\tau_s = \tau_w = 1/2$ (or $t_y = 0$), the expression (1) turns into the following:

$$t_m = -\frac{t_e}{2}\left(1 - \frac{\lambda_u}{\lambda_f}\right),$$

which gives the noted dependence on the ratio of the soil thermal conductivity coefficients.

In accordance with the previously proposed methodology [*Gorelik, Pazderin, 2017*], the direction of change in the temperature of the permafrost (below the bottom of the active layer up to the depth of zero annual amplitudes) is set in relation to the initial state, which is determined empirically at the stage of engineering surveys by two parameters: the depth of the active layer (ξ_m) and the temperature at the depth of zero annual amplitudes (t_0).

To derive the relationship that determines the time of the formation of a new temperature regime, it is assumed that with the beginning of the 'switching on' of the technical method of surface cooling, the conditions of heat exchange between the outside air and the soil surface change rather quickly (abruptly). Taking that into account, the time τ_f of the formation of a new temperature regime (characterized by the temperature t_f at the depth of zero annual amplitudes z_0 under the influence of the changed surface factor is determined by the relations [*Gorelik, Zemerov, 2020*]:

$$\tau_f = \frac{z_0^2}{12\mu_f\left(1-\sqrt{1-n}\right)^2}, \quad n = \left|\delta t_{mf} / \Delta t_{0m}\right|,$$
$$\Delta t_{0m} = t_0 - t_m, \quad \delta t_{mf} = t_f - t_m. \qquad (2)$$

Here: μ_f is thermal diffusivity of frozen soil; t_m is defined by the relation (1). It is important that at a depth of zero annual amplitudes, the temperature t_m is reached in the asymptotic limit of an infinite time interval, while at the bottom of the active layer it is

being established already in the first year after the changing conditions on the surface of the soil [*Feldman, 1977; Gorelik, Zemerov, 2020*]. The δt_{mf} value is the deviation of the current temperature value of t_f (corresponding to the time instant of τ_f) from the asymptotic value t_m. If, using the first of the relations (2), we express the temperature t_f in terms of the time τ_f, then we can also estimate the dynamics of the temperature change at the depth of z_0 during the service life of the structure.

The n parameter demonstrates the degree to which the temperature approaches a new equilibrium state. For $n = 0$, that state exactly corresponds to the temperature of t_m, but the time to reach it is equal to infinity. At $n = 1$, the temperature at the depth of z_0 only begins to change and the time to reach that moment coincides with the time when the radius of the thermal influence reaches the depth of z_0. Taking the standard value of $z_0 = 10$ m, we obtain the dependence of the τ_f time on the n parameter, which is shown by the graph in Fig. 1. In particular, for $n = 0.3$ we get $\tau_f = 10.4$ years, and for $n = 0.5$ we get $\tau_f = 3.2$ years. The characteristic value can be taken as $n = 0.4–0.5$, which demonstrates that the proximity of the intermediate temperature state (determined by the parameter of δt_{mf}) to a new stable one corresponds to approximately half the maximum length of the full range of temperature changes (from t_0 to t_m). That is, $\delta t_{mf} \approx (0.4–0.5)\ \Delta t_{0m}$ and the corresponding change occurs within 3–5 years. That corresponds to the rate of commonly observed processes [*Vyalov et al., 1979; Khrustalev, Nikiforov, 1990*]. The important thing here is the dependence of the τ_f time on the design (required) temperature of t_f and its limiting values of t_0 and t_m. It is easy to see that a decrease in the value of t_m, with the other two fixed, brings the value of n closer to one, while the value of τ_f decreases rapidly.

Evaluation of the effectiveness of the proposed method of cooling the foundation

It is easy to make certain that for fixed values of τ_s, τ_w, the minimum temperature of t_m, according to the relation (1), can be achieved when two conditions are met: a) minimization of the mean-summer temperature t_s (within the limits of up to 0 °C); b) reaching a minimum value of the mean-winter temperature t_w (within the limits of up to equal in magnitude to the air temperature). In that case, it is important to ensure the conditions under which the value of t_w does not depend on side factors (for example, snow-carrying of the surface, negative heat release in the underground, etc.). The first of those conditions can be ensured by the use of a layer of high-quality thermal insulation, which minimizes the heat flux to the surface in the warm season. In the construction of the heat-insulating layer, standard heat-insulating panels of light enclosing structures can be used, which have an external metal casing that protects against mechanical stress and performs the functions of waterproofing. The second condition can be achieved by using the GET cooling system [*Dolgikh et al., 2011*], the evaporative element of which is placed under the thermal insulation layer over the entire soil surface inside the structure contour (Fig. 2). The principle of operation, design and application possibilities of the GET system is summarized in the article [*Gorelik, 2015*]. The optimum pipe laying density must be determined by calculation. The evaporator temperature of the GET system is determined only by the outside air temperature (according to the test data of existing

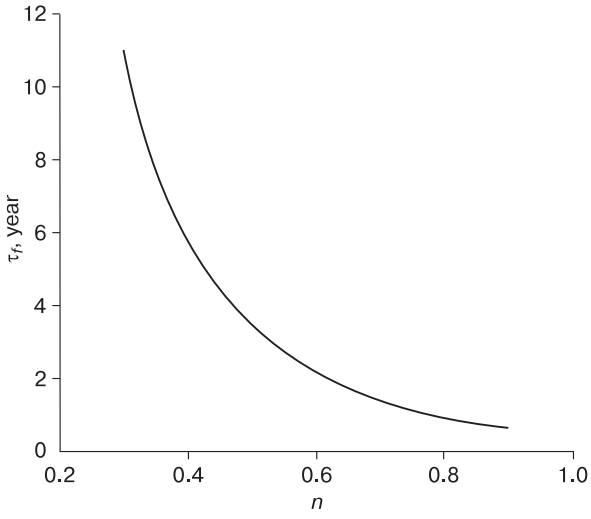

Fig. 1. The dependence of the time of approach τ_f to the new temperature state on the approximation parameter n.

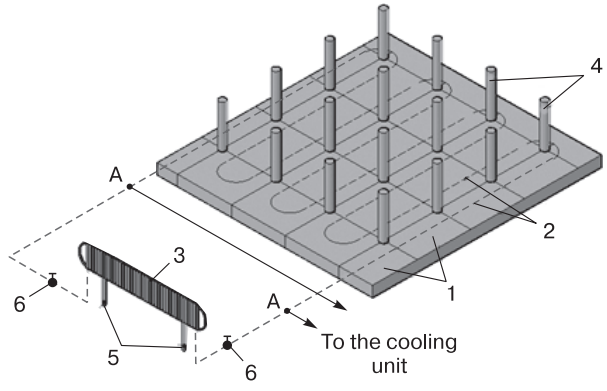

Fig. 2. The layout of the elements of the GET system near the underfloor space (above-foundation structures are not shown):

1 – thermal insulation plates; 2 – evaporator pipe (cooling element); 3 – condenser of the GET system; 4 – foundation piles; 5 – support legs of the condenser; 6 – valves for cutting off the condenser from the evaporator. The letter A indicates the connection points of the refrigeration unit to the evaporator.

structures, that temperature is approximately by 5–6 degrees higher than the air temperature and is practically constant along the length of the evaporator [*Dolgikh, Okunev, 1989; Feklistov et al., 2008*]). The independence of the evaporator temperature on the conditions inside the underfloor space is ensured by the fact that the condenser of the device is taken out of the contour of the structure. Shown in Fig. 2, the design of the cooling method should be especially convenient when restoring the temperature regime of the foundation that was disturbed during the operation of the structure. The use of vertical thermal stabilizers in that case encounters additional difficulties in their installation, associated with the limitation of the height of the underfloor space. To install such devices, special designs with a flexible evaporator are used [*Abrosimov et al., 2018*], which, however, does not eliminate the main disadvantages of the method. It should be noted that, in conventional applications, the cooling element of the GET system is also deepened in the basement soils [*Dolgikh et al., 2011*].

Here are some estimates for the case of restoration of the temperature regime of the basement disturbed during the operation. Let the current temperature at the structure's basement at a depth of zero annual amplitudes have reached a value of t_0, which has exceeded the design value of t_f. As an example, let us take the duration of the winter period of 8 months, $\tau_w = 8/12 = 2/3$. Assuming that the thermal insulation is ideal, we will neglect the second term in the formula (1). Taking $t_w = -15$ °C, according to the formula (1) we obtain $t_m \approx t_w\tau_w = -15(2/3) = -10$ °C. Let $t_0 = -0.7$ °C, $t_f = -2.0$ °C, then $\Delta t_{0m} = 9.3$ °C, $\delta t_{mf} = 8.0$ °C, $n = 0.86$. According to the graph (Fig. 1) we find that the required temperature regime is reached after about one year of cooling. In another example, let us take $t_0 = -2$ °C, $t_f = -3.0$ °C, $\tau_w = 2/3$, then $\Delta t_{0m} = 8.0$ °C, $\delta t_{mf} = 7.0$ °C, $n = 0.88$. Accordingly, we find that in that case the required temperature regime is also reached after about one year of cooling. The specified time is counted from the beginning of the first summer season, by the time of the onset of which a layer of thermal insulation and cooling elements of the GET system must be laid on the soil surface (as described below when characterizing the design option Ib in the section 'Calculation results and their discussion'). It is important that the speed of reaching the design temperature is determined by the low mean-annual soil temperature at the bottom of the active layer, as well as by a significant increase in the duration of the cooling impulse [*Gorelik, Zemerov, 2020*].

An even greater efficiency of the described method can be achieved if, in the summer period of the first year of its application, a forced cooling unit is connected to the evaporator pipes. In that case, the duration of the summer period turns to zero, and the duration of the winter period coincides with the duration of the year ($\tau_s = 0$, $\tau_w = 1$), while the value of t_w decreases accordingly. The temperature t_m will also decrease, and the time of τ_f will decrease even more (at the same values of t_f and t_0). After the first summer season, the forced cooling unit can be dismantled without any damage, and there is no need for its further use at that facility.

However, it should be remembered that the above methods for estimating the temperature of t_m, as well as the time interval of τ_f, although convenient, are approximate and only the main trends in the dependences can be understood with their help. It is difficult to predict quantitative differences from the exact values, since the estimates do not take into account many important details of specific design solutions for the cooling method. Strict calculation procedures must be followed to obtain reliable results. In addition to increasing the accuracy due to the procedure itself, those methods allow taking into account the dynamics of the air temperature, the real properties of the applied thermal insulation, the density of the evaporator pipes, the heterogeneity of soil properties, changes in the temperature field in space and other factors. In the next section, the results of calculating the dynamics of the recovery of the temperature-regime restoring in the basement of the building with the underfloor space are presented using the strict numerical methods for the two examples considered above.

Calculation procedure for soil cooling using the GET system

Calculations of the dynamics of temperature restoring in the basement soils with a surface cooling method using the GET system have been performed for a building with an underfloor space with dimensions in the plan of 12 × 24 m. The design and location of the cooling system elements within the pile field are demonstrated in Fig. 2. The evaporator pipes of the GET system are laid in a coil along the major axis of the building and covered with a leveling layer of sand. Standard heat-insulating panels are laid end-to-end along the leveling layer (with the necessary trimming at the points of pile bypass) within the entire surface of the underfloor space. The condenser of the GET system is located on a special site outside the building contour on support racks. If it is necessary to connect the unit for forced circulation of the refrigerant, the condenser is cut off from the evaporator using special valves.

The horizontal distance between the axes of adjacent evaporator's tubes (L) is taken in two versions, 1 m and 0.7 m, the diameter of the tubes (D) is 37 mm. Thermal insulation thickness of a standard panel (h) is 100 mm, material thermal conductivity coefficient (λ_i) is 0.03 W/(m·°C).

Table 1. **Annual variation of average monthly air temperature according to the Urengoy Meteorological Station**

Month	Average air temperature, °C	Month	Average air temperature, °C
January	–26.4	July	15.4
February	–26.4	August	11.3
March	–19.2	September	5.2
April	–10.3	October	–6.3
May	–2.6	November	–18.2
June	8.4	December	–24.0

The main trends in the behavior of temperature fields can be established for a soil homogeneous in terms of thermophysical characteristics. The heterogeneity of those properties can only be associated with local quantitative deviations from the general trend in the behavior of temperature, which do not fundamentally affect the general nature of its change. Below, for all calculation options, the following soil characteristics are adopted (for the thawed and frozen soil, the *u* and *f* indexes are adopted correspondingly): thermal conductivity coefficients $\lambda_u = 1.75$ and $\lambda_f = 1.80$ W/(m·°C); volumetric heat capacity $C_u = 2.68 \cdot 10^6$ and $C_f = 2.20 \cdot 10^6$ J/(m^3·°C); dry density $\gamma_s = 1500$ kg/m^3; moisture content $w = 0.2$. The transition of a unit volume of frozen soil to a thawed state is characterized by the value of latent volumetric heat $\kappa_v = \kappa\gamma_s w$, where $\kappa = 3.34 \cdot 10^5$ J/kg ($\kappa_v = 10^8$ J/m^3). Soil moisture due to unfrozen water $w_u = 0$. Freezing point of soil $t_b = 0$ °C. The course of air temperature throughout the year is taken as a fragmentary-constant function of mean-monthly temperatures. Air temperature data were taken from the Urengoy Meteorological Station (Table 1).

The initial temperature of the soil at the basement in the disturbed state of the design thermal regime was taken, as above, in two versions: $t_0 = -0.7$ °C and $t_0 = -2.0$ °C. In accordance with the methodology of [*Gorelik, Pazderin, 2017*], the calculated values of the summer (α_s) and winter (α_w) coefficients of heat transfer between air and the underlying surface for the variant with $t_0 = -0.7$ °C are $\alpha_s = 23.2$, $\alpha_w = 1.12$ W/(m^2·°C); and for the variant with $t_0 = -2.0$ °C are $\alpha_s = 23.2$, $\alpha_w = 1.39$ W /(m^2·°C). As above, the corresponding design temperatures for those two options are taken as $t_f = -2.0$ and -3.0 °C.

The boundary condition on the wall of the evaporator tube during the active period of operation of the device was selected on the basis of experimental data on the testing device [*Dolgikh, Okunev, 1989; Feklistov et al., 2008*] in the form of setting its temperature $t_t(\tau)$ by a condition of the first kind:

$$t_t(\tau) = t_a(\tau) + 6,$$

where $t_a(\tau)$ is the air temperature (°C), given as a function of time (τ) according to Table 1. The interruption of the device operation during the passive period is determined by the disturbance of the condition of heat sink (q_t) from the ground to the evaporator wall: $q_t < 0$.

The boundary condition on the upper surface of the soil is set by the condition of the third kind:

$$\alpha\left(t_a(\tau) - t_s\right) = -\lambda\left(\frac{\partial t}{\partial z}\right)_s.$$

Here: z is vertical coordinate; t_s is the temperature of the soil surface (determined during the calculating process); λ is the coefficient of thermal conductivity of the soil, which, depending on its state, takes the values of λ_u or λ_f; α is the coefficient of heat exchange of the surface of the soil covering with air, takes the values of α_s, or α_w in the corresponding seasonal periods of time. Within the underfloor space, the soil massif is considered as two-layered vertically, where the top layer corresponds to thermal insulation with the above-mentioned characteristics.

The coordinate system is located in a horizontal plane that coincides with the soil surface, its center coincides with the geometric center of the building in the plan. The *Oz* axis is directed vertically downwards, the *Ox* and *Oy* axes lie in the horizontal plane and are directed, respectively, along the long and short axes of the building. The dimensions of the computational domain along each of the axes are determined by the radius of the thermal influence [*Gorelik, Pazderin, 2017*], and when calculating, for no more than a 5-year period, that radius does not exceed 35 m. Thus, the boundaries of the computational domain should be removed by 35 meters from the boundaries of the underfloor-space contour in plan and at the same distance into the depth of the massif vertically. At those boundaries, the heat flux is set to zero.

The calculation procedure used here is based on numerical methods, has been repeatedly tested on various problems and described earlier [*Gorelik et al., 2019; Gorelik, Khabitov, 2019a,b*].

Calculation results and their discussion

When carrying out the calculations, two technological cooling schemes have been considered: a) using only the seasonally operating GET system; b) with additional connection to the evaporator pipes of the forced cooling unit during one summer season. It should be borne in mind that the connection of various elements of the cooling system can be carried out at different points in time in the annual cycle, which can affect the cooling efficiency. The purpose of the calculations was, among other things, to determine the optimal time for connecting the cooling systems. Here is a brief description of the options for the technological schemes considered below and their designations.

Option Ia: the GET system together with thermal insulation is installed at the end of the summer season; the seasonally thawed layer is formed under the influence of natural factors (its thickness is close to the average long-term value); the GET system turns on with the onset of the winter season and automatically turns off at the end of winter; the second and all subsequent cycles of thawing of the seasonally thawed layer occur under the influence of thermal insulation. That process is cyclically repeated from the second year to all subsequent ones.

Option Ib: the GET system together with thermal insulation is installed at the end of the winter season; the seasonally thawed layer is formed under the influence of natural factors and thermal insulation (its thickness is close to the minimum value); the GET system turns on with the onset of the winter season and automatically turns off at the end of winter; the first and all subsequent cycles of thawing of the seasonally thawed layer occur under the influence of thermal insulation. That process is cyclically repeated from the first year to all subsequent ones.

Option IIa: installation and start of operation of the GET system before the end of the first winter period is similar to the option Ia; at the beginning of summer, a forced cooling unit is connected to the evaporator pipe, which operates during the summer; at the end of summer, forced cooling is turned off and dismantled (no longer used); further in the winter season, the GET system works together with thermal insulation; the second and all subsequent cycles occur under the influence of thermal insulation and winter switching-on of the GET system.

Option IIb: the GET system is mounted similarly to the option Ib; at the beginning of the summer season, a forced cooling unit is connected, which operates during the summer; at the end of summer, forced cooling is turned off and dismantled (no longer used); then only the GET system works together with thermal insulation.

Option IIc: the GET system is mounted similarly to the option Ib; the forced cooling unit is connected at the beginning of the second summer season, which operates during the summer; at the end of the second summer, forced cooling is turned off and dismantled (no longer used); then only the GET system works together with thermal insulation.

The first two options correspond to the scheme without using a forced cooling method, the next three include that method. Each of the presented options is characterized by an additional set of parameters: an initial soil temperature (t_0); the distance between the parallel sections of the evaporator pipes (L); the coordinate (x) of the cross-section of the basement, in which the results of the calculation are considered; the time interval (τ) from the start of the cooling system, which corresponds to the presented calculation results. The calculation results for the options Ia and IIa are displayed at the end of the first, second, etc. annual cycles. The calculation results for the items Ib, IIb and IIc are displayed at the end of the second, third, etc. summer seasons (with a summer season duration of 5 months – after about 1.4; 2.4, etc. years from the moment of installation of the cooling system). The output of the results corresponds to the maximum ground temperature (at the end of the summer season). The calculation results are presented in Figures 3–8. The lines in the figure field represent the position of the isotherms in the considered section of the basement, the numbers along the line indicate the corresponding temperature of the isotherms. The color scale at the bottom shows the correspondence of a certain color in the picture field to the calculated temperature value.

Figures 3 and 4 demonstrate the results of calculating the soil temperature when using cooling systems in the options Ia and Ib for two values of its initial temperature (−0.7 and −2.0 °C). As can be seen from a comparison of soil temperatures, from the surface to the depth of zero annual amplitudes (10 m), the cooling efficiency in the second of those options is significantly higher than in the first one. Based on the values of the design temperature t_f (−2.0 and −3.0 °C) for the corresponding initial soil temperatures given in the examples of the 'Evaluation of efficiency ...' section, it can be argued that for the option Ib, the design values are achieved for the central section (Figures 3, *b* and 4, *b*), and they are achieved with a slight disadvantage for the edge section (Figures 3, *d* and 4, *d*) after completion of one cycle of operation of the cooling system (1.4 years) with a standard distance between the evaporator tubes (L = 1 m).

The corresponding temperature distribution in the option Ia demonstrates that both in the central and in the edge sections the temperature remains significantly higher than the design value (Figures 3, *a*; 4, *a*; 3, *c*; 4, *c*) even for a denser pipe laying (L = 0.7 m) and with a longer (two-year) cycle of the cooling system. That difference has a simple explanation, which is that the first activation of the GET system in the option Ia is spent on a very energy-intensive process of freezing the layer of seasonal thawing, which in that option has a maximum value. As a result, the duration of the cooling impulse, which determines the process of cooling the basement [*Dostovalov, Kudryavtsev, 1967; Feldman, 1977; Gorelik, Zemerov, 2020*], is significantly reduced. The option Ib is free from that drawback, since the layer of seasonal thawing is formed under the influence of thermal insulation and has a minimum value.

The results of short-term use of a forced cooling system in combination with thermal insulation and the GET system are shown in Fig. 5–8. The presented results demonstrate that the use of technological op-

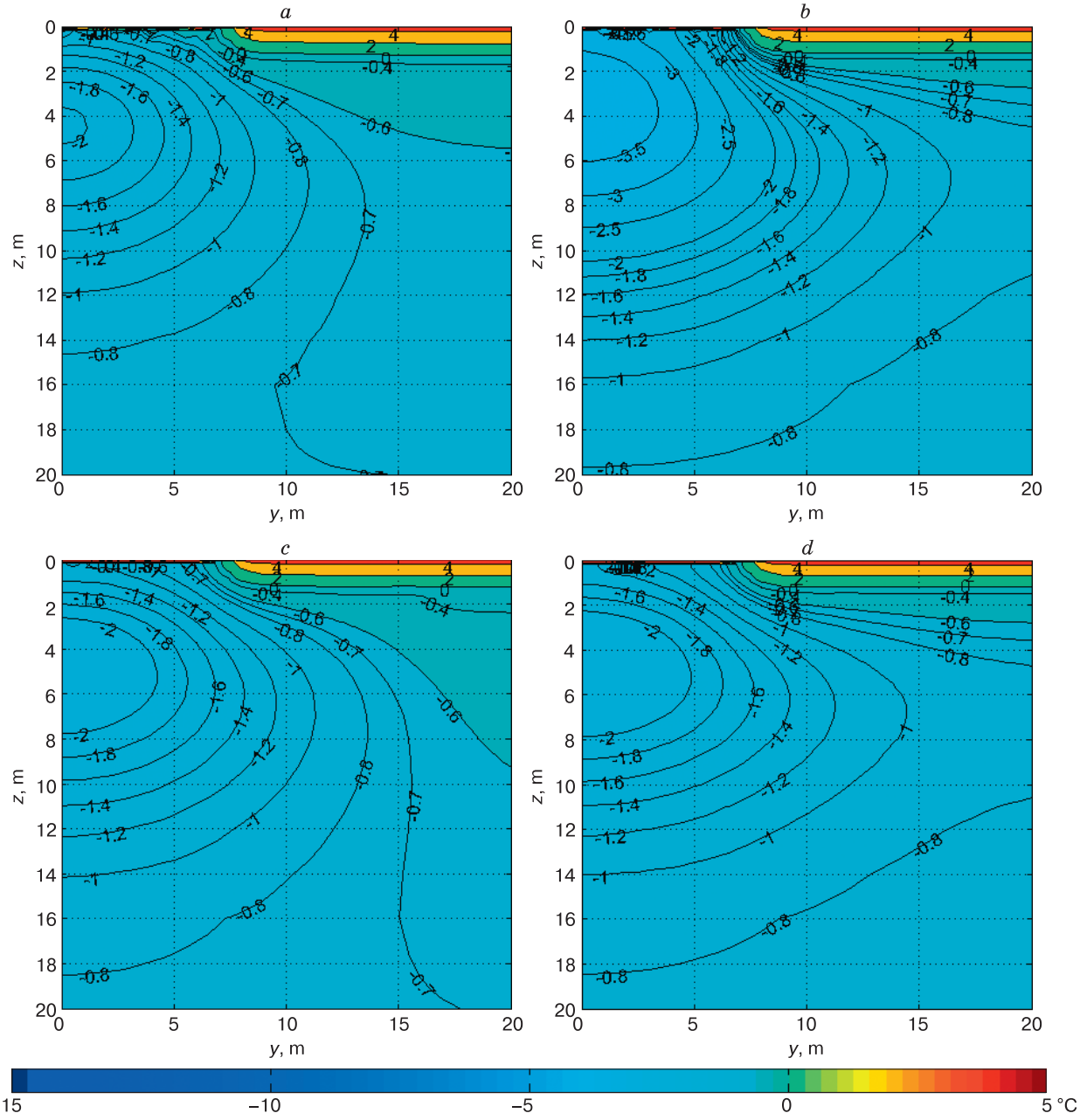

Fig. 3. The results of soil temperature calculations during the cooling only with the use of the GET system at t_0 = –0.7 °C:

a – option Ia (L = 0.7 m, x = 0 m, 1 year); *b* – option Ib (L = 1.0 m, x = 0 m, 1.4 year); *c* – option Ia (L = 0.7 m, x = 12 m, 2 years); *d* – option Ib (L = 1.0 m, x = 12 m, 1.4 year).

tions IIb and IIc in all cases ensures the achievement of the design temperature for both the central and the edge sections in the basement after completion one cycle of the cooling system (1.4 years) with a standard distance between the evaporator tubes (L = 1 m). Moreover, in the option IIb, that temperature is reached with a noticeable margin of 0.5–1.0 °C (Fig. 5, *c*, *d*; 6, *c*, *d*; 7, *c*, *d*; 8, *c*, *d*). Fragments of the same figures (Fig. 5, *a*, *b*; 6, *a*, *b*; 7, *a*, *b*; 8, *a*, *b*) demonstrate that the scheme IIa does not ensure the attainment of design temperature within the minimum period of its operation. The reason for the lack of effectiveness of the option IIa is similar to that stated when comparing the options Ia and Ib. The highest efficiency of the cooling system in the option IIb is due to the fact that the duration of the continuously

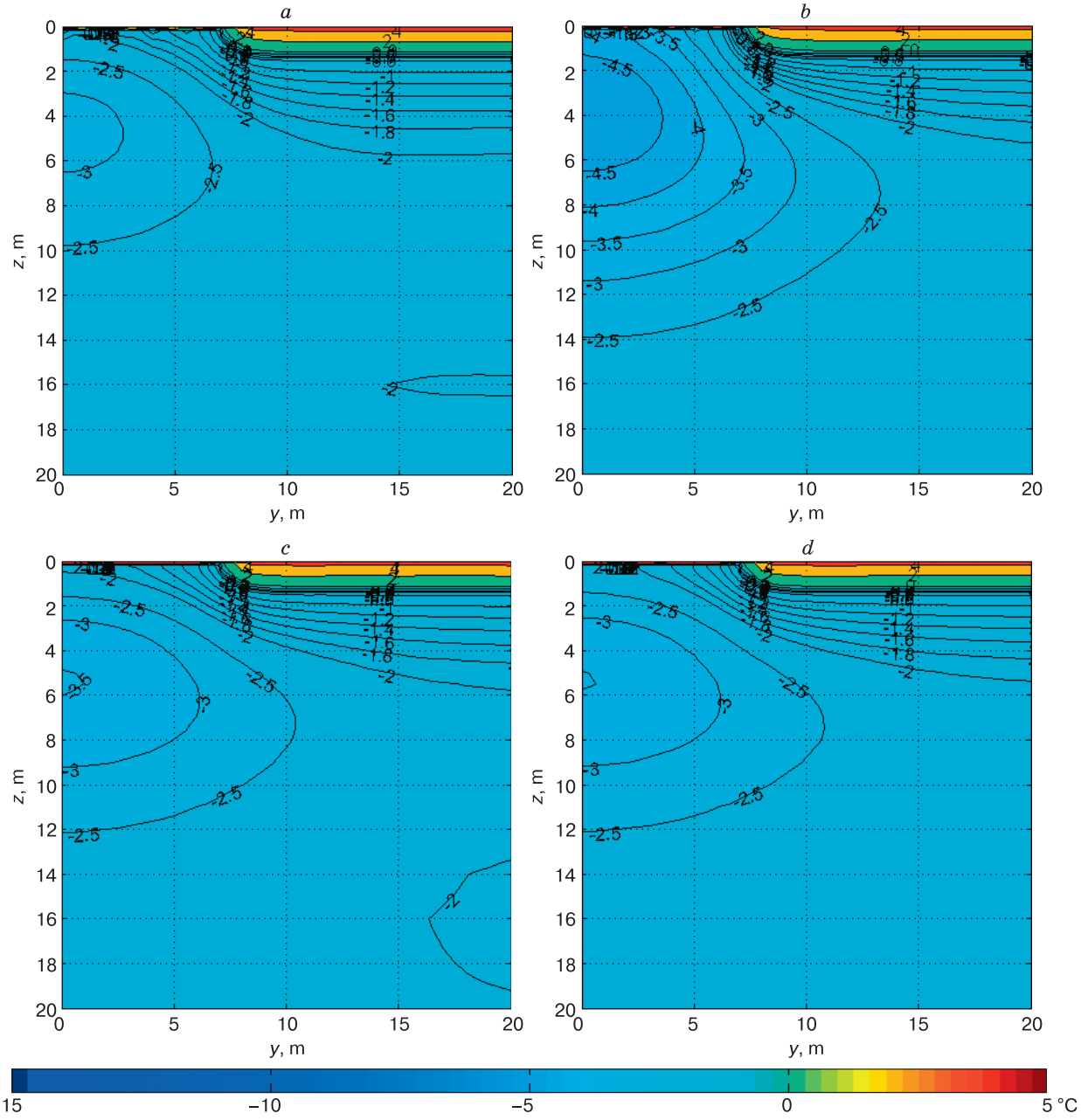

Fig. 4. The results of soil temperature calculations during the cooling only with the use of the GET system at t_0 = −2.0 °C:

a – option Ia (L = 0.7 m, x = 0 m, 1 year); *b* – option Ib (L = 1.0 m, x = 0 m, 1.4 year); *c* – option Ia (L = 0.7 m, x = 12 m, 2 years); *d* – option Ib (L = 1.0 m, x = 12 m, 1.4 year).

operating cooling impulse in that case turns out to be as high as possible. The time of τ_f is determined by the sum:

$$\tau_f = \tau_{w1} + \tau_s + \tau_{w2}, \quad (3)$$

where τ_{w1} is the duration of the impulse in the winter period preceding the moment of assembly of the GET system (natural cooling factors are at work); τ_s is the duration of the summer period (during which forced cooling is active); τ_{w2} is the duration of the subsequent winter period (during which the GET system is in effect). The duration of the cooling pulse in variant IIc is shorter than the value determined by the formula (3) by the τ_{w1} value. In fact, the winter conditions on the soil surface in the option IIb continuously exist for about 1.5 years.

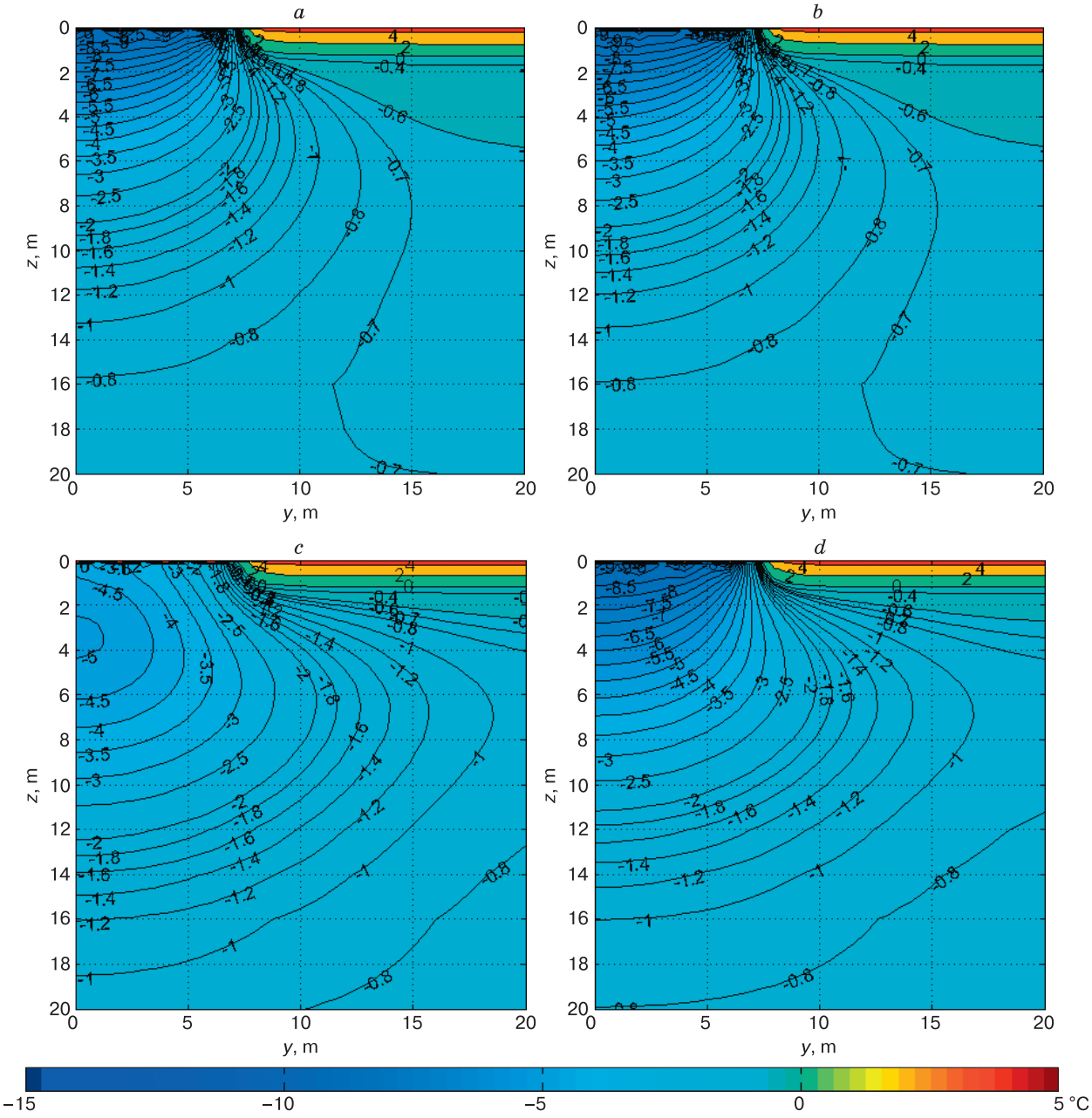

Fig. 5. Results of calculations of soil temperature during cooling using forced cooling and the GET system for the central section (x = 0 m) at t_0 = −0.7 °C:

a – option IIa (L = 1.0 m, 1 year); *b* – option IIa (L = 0.7 m, 1 year); *c* – option IIb (L = 1.0 m, 1.4 year); *d* – option IIc (L = 1.0 m, 1.4 year).

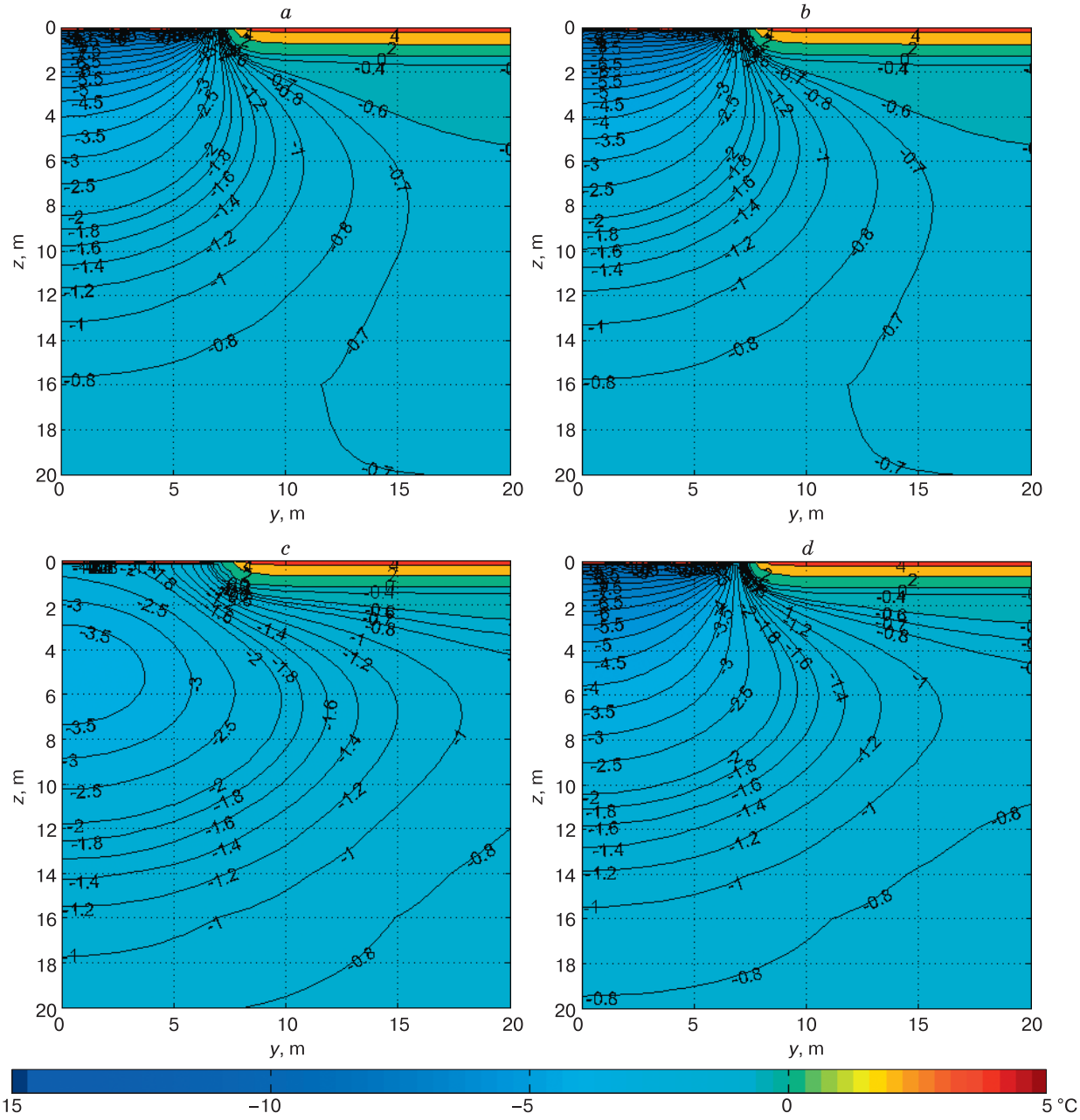

Fig. 6. Results of calculations of soil temperature during cooling using forced cooling and the GET system for the edge section (x = 12 m) at t_0 = –0.7 °C:

a – option IIa (L = 1.0 m, 1 year); *b* – option IIa (L = 0.7 m, 1 year); *c* – option IIb (L = 1.0 m, 1.4 year); *d* – option IIc (L = 1.0 m, 1.4 year).

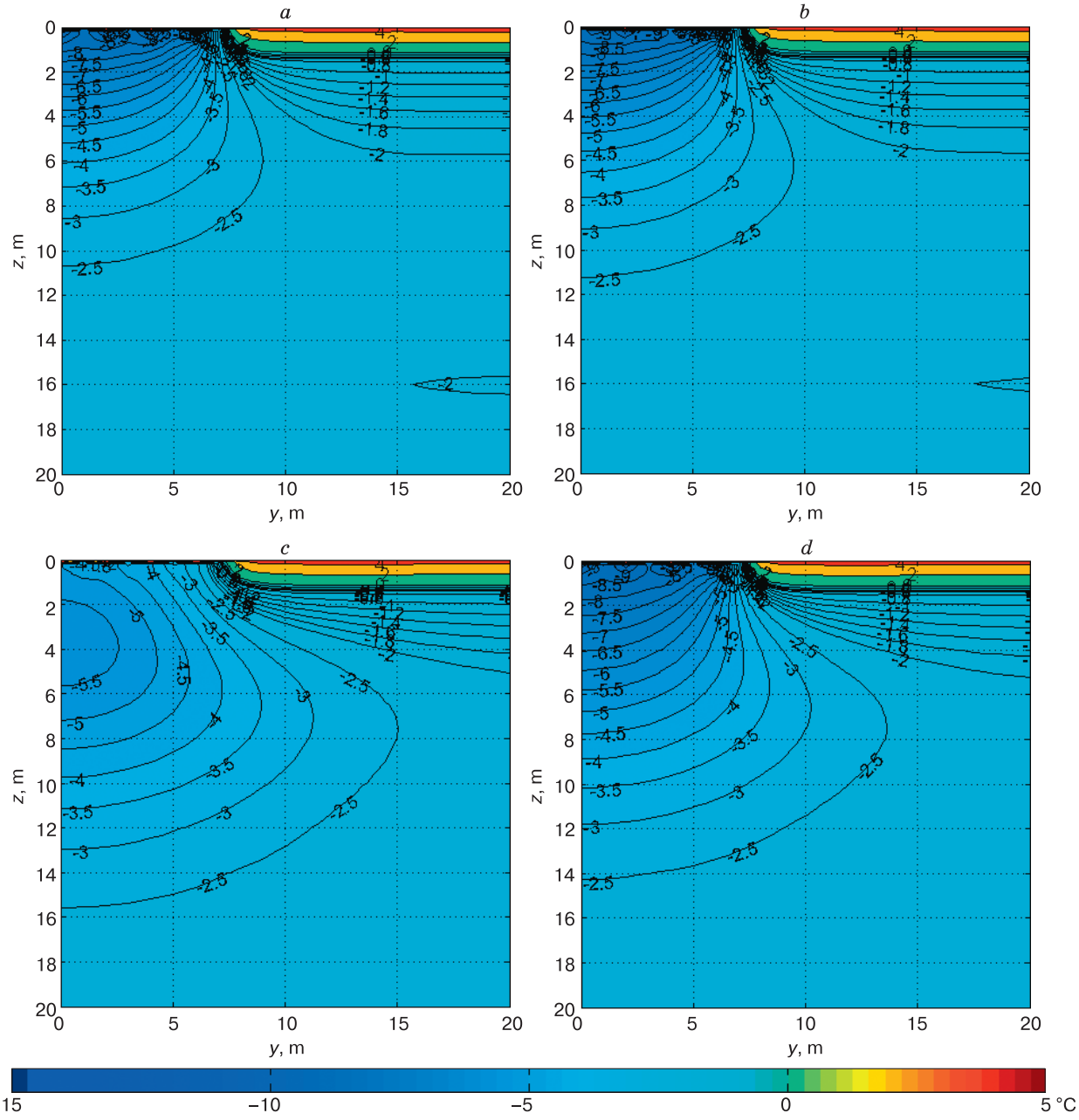

Fig. 7. Results of calculations of soil temperature during cooling using forced cooling and the GET system for the central section (x = 0 m) at t_0 = –2.0 °C:

a – option IIa (L = 1.0 m, 1 year); *b* – option IIa (L = 0.7 m, 1 year); *c* – option IIb (L = 1.0 m, 1.4 year); *d* – option IIc (L = 1.0 m, 1.4 year).

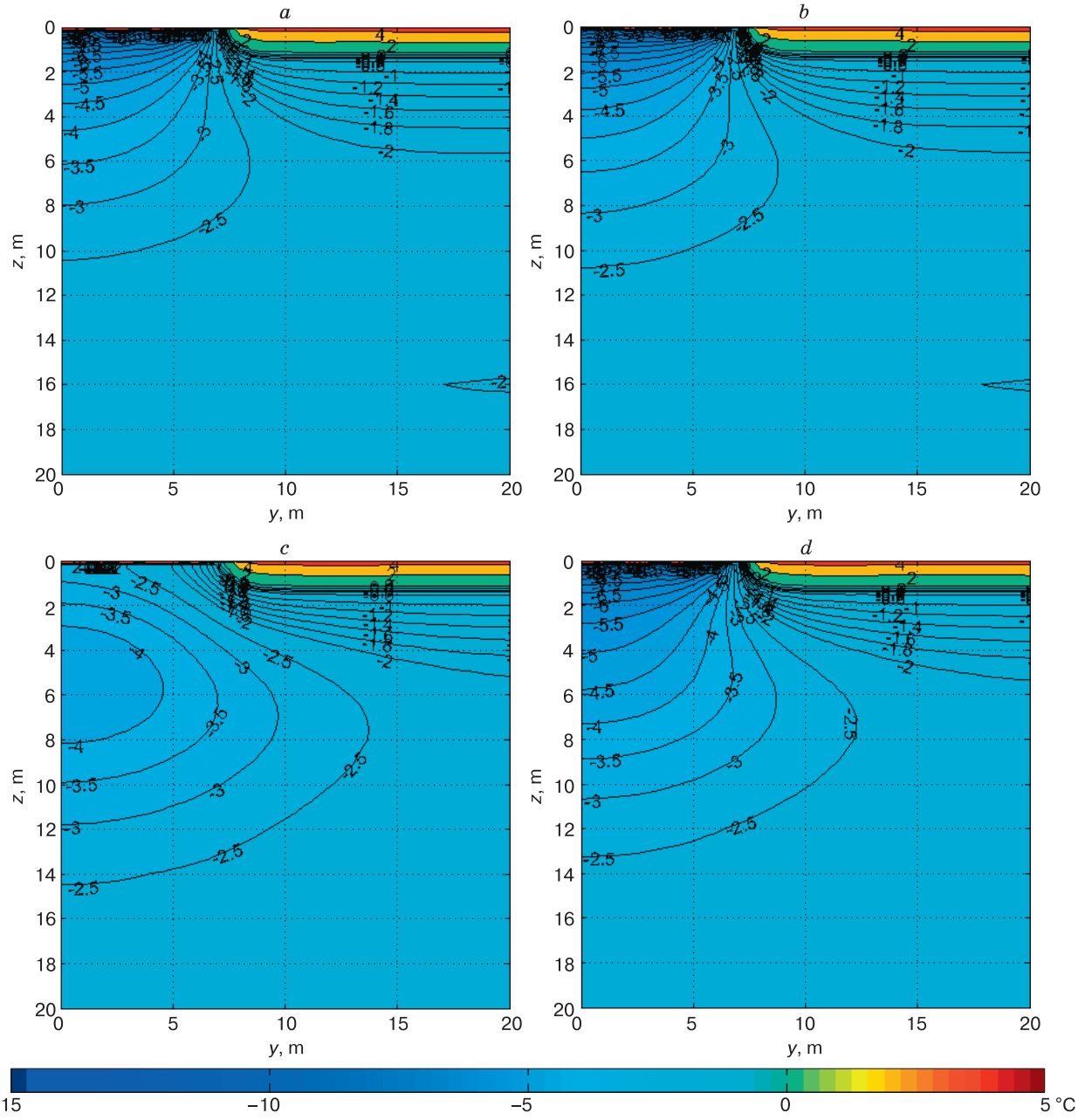

Fig. 8. Results of calculations of soil temperature during cooling using forced cooling and the GET system for the edge section (x = 12 m) at t_0 = –2.0 °C:

a – option IIa (L = 1.0 m, 1 year); *b* – option IIa (L = 0.7 m, 1 year); *c* – option IIb (L = 1.0 m, 1.4 year); *d* – option IIc (L = 1.0 m, 1.4 year).

CONCLUSION

The results of mathematical modeling of the process of formation of a temperature field in a frozen ground with a surface cooling method using the considered technical means, presented in the article, allow us to draw the following conclusions:

1. The proposed method of surface cooling of the structure foundations (with the use of thermal insulation, the GET system and a forced cooling method (if necessary, for a short time) allows the soil temperature to be lowered by 1.0–2.5 °C to a depth of zero annual amplitudes, which in many cases is sufficient to ensure their solid-frozen state. At the same time, the time for reaching the design temperature value is significantly reduced in comparison with other methods (1.5 years instead of 3–5 years). The method is characterized by a decrease in labor intensity for the installation and mantling of cooling systems due to the absence of the need to perform the drilling and other laborious earthworks.

2. The efficiency of the proposed method is highest if the active elements of the cooling system (GET, forced cooling unit) are switched on at the moment when the layer of seasonal thawing is in a completely frozen state. In that case, the duration of the cooling impulse, which forms the temperature of the soil to a depth of zero amplitudes, turns out to be more than one year.

3. The earlier proposed [*Gorelik, Zemerov, 2020*] simple quantitative estimates of the time to reach the design temperature in the soil based on the existing ideas about the mechanism of the formation of the temperature shift generally correspond to the calculation results obtained by strict numerical methods.

The work has been carried out within the framework of the theme of the state assignment Reg. R&D No. AAAA-A17-117051850061-9.

References

Abrosimov, A.I., Teplyakov, A.V., Zaletaev, S.V., et. al., 2018. The increezing of pile stability by employment of cooling systems in the aired underfloor space. In: Proceeding of Council of Earth's Cryology (Moscow, May 15–16, 2018), MGU, Moscow, vol. 2, pp. 9–15 (in Russian).

Balobaev, V.T., 1964. Influence of the surface layer to thermal regime and to depth of seasonal thaw penetration of the frozen ground. In: Thermal processes in the frozen ground. Nauka, Moscow, pp. 7–38 (in Russian).

Bubelo, R.V., 2003. Stabilization of Negative Temperature in the Base's Frozen Soils by Surface Cold Accumulators. Author's abstract of PhD thesis. Moscow, 23 pp. (in Russian).

Dolgikh, G.M. (Ed.), 2014. Systems for Thermal Stabilization of Grounds in Permafrost Zone. Collection of Papers by Specialists from Fundamentstroiarkos R&D Company for 2010–2014. Geo, Novosibirsk, 218 pp. (in Russian).

Dolgikh, G.M., Okunev, S.N. (Eds.), 1989. The Elaboration of Ecologically Acceptable Technologies and Devises for Development of Gas and Gas-Condensate Deposits of Yamal Peninsula. Scientific Report. Tyumen, Gyprotyumenneftegas, 152 pp. (in Russian).

Dolgikh, G.M., Okunev, S.N., Velchev, S.P., 2011. Stages, problems and technical decisions for building activity in Permafrost. In: Proceeding of International Conference of XX Year of NPO "Fundumentstroiarkos" (Tyumen, November 7–10, 2011). NPO "Fundumentstroiarkos", Tyumen, pp. 12–23 (in Russian).

Dostovalov, B.N., Kudryavtsev, V.A., 1967. General Geocryology. MGU, Moscow, 403 pp. (in Russian).

Feklistov, V.N., Dolgikh, G.M., Okunev, S.N., Pazderin, D.S., 2008. The Investigation of Cooling System of Type as GET for Thermostabilization of Ground Bases. In: Proceeding of International Conference "Cryogenic Resources of Polar and Alpine Regions. State and Outlook of Engineering Geocryology", Tyumen, TGNGU, 2008, p. 165–168 (in Russian).

Feldman, G.M., 1977. Prognoses of Temperature Regime for Grounds and Evolution of Cryogenic Processes. Nauka, Novosibirsk, 102 pp. (in Russian).

Gorelik, J.B., 2015. Operation of two-phase thermosyphons with horizontal evaporation tubes: causes of instability. Earth's Cryosphere (Kriosfera Zemli), XIX (4), 74–83.

Gorelik, J.B., Khabitov, A.K., 2019a. The influence of the boreholes' heat insulation on the determination of the minimal distance between its outfalls at permafrost. Bulletin of Tyumen State University. Physical and Mathematical Modeling. Oil, Gas, Energy, 5 (2), 10–26.

Gorelik, J.B., Khabitov, A.K., 2019b. About efficiency of adaptation of the thermostabilizers for building activity in Permafrost. Bulletin of Tyumen State University. Physical and Mathematical Modeling. Oil, Gas, Energy, 5 (3), 25–46.

Gorelik, J.B., Pazderin, D.S., 2017. Correctness of formulation and solution of thermotechnical problems of forecasting temperature field dynamics in the ground base of structures on permafrost. Earth's Cryosphere (Kriosfera Zemli), XXI (3), 44–54.

Gorelik, J.B., Romanyuk, S.N., Khabitov, A.K., 2019. Constraining thaw boundary around multipe wells with regard to their joint thermal effect. Earth's Cryosphere (Kriosfera Zemli), XXIII (2), 67–73.

Gorelik, J.B., Zemerov, I.V., 2020. Influence of the surface water reservoir to the thermal regime of frozen ground. Bulletin of Tyumen State University. Physical and Mathematical Modeling. Oil, Gas, Energy, 6 (1), 10–40.

Khrustalev, L.N., Nikiforov, V.V., 1990. A Stabilization of Permafrost in the Building's Bases. Nauka, Novosibirsk, 209 pp. (in Russian).

Kudryavtsev, V.A. (Ed.), 1974. Bases of prognoses for permafrost in engineering and geological investigations. MGU, Moscow, 432 pp. (in Russian).

Makarov, V.I., 1985. Thermosyphons in High-Latitude Construction Engineering. Nauka, Novosibirsk, 169 pp. (in Russian).

Porkhaev, V.G., 1970. Thermal Interaction of Buildings and Constructions with Permafrost. Nauka, Moscow, 208 pp. (in Russian).

Shur, Yu.L., 1988. Upper Horizon of Frozen Ground and Thermokarst. Nauka, Novosibirsk, 213 pp. (in Russian).

Vyalov, S.S., Alexandrov, Yu.A., Mirenburg, Yu.S., Fedoseev, Yu.G., 1979. Artificial cooling of the ground with employment of the thermal piles. In: Engineering Geocryology. Nauka, Moscow, pp. 72–90 (in Russian).

Received May 5, 2020
Revised version received November 9, 2020
Accepted December 5, 2020

EARTH'S CRYOSPHERE
SCIENTIFIC JOURNAL

Kriosfera Zemli, 2021, vol. XXV, No. 2, pp. 35–43

SNOW COVER AND GLACIERS

IMPLICATIONS OF CHANGES IN INSOLATION CHARACTERISTICS FOR LONG-TERM SEA ICE EXTENT DYNAMICS IN THE NORTHERN HEMISPHERE

V.M. Fedorov, P.B. Grebennikov

Lomonosov Moscow State University, Faculty of Geography,
Leninskie Gory 1, Moscow, 119991, Russia; fedorov.msu@mail.ru

A correlation analysis of long-term dynamics of sea-ice extent in the Northern Hemisphere involving calculations of insolation characteristics with high spatial resolution was performed. The revealed close negative relationships between multi-year variations in sea ice extent, winter insolation and irradiance contrast were calculated in model cells with resolution of 1° × 1° for the period 1901–2018. The linkage density maps have been constructed to analyze relationships between multi-year change in sea ice extent and insolation characteristics based on annual, semi-annual and monthly (March, September) means of sea ice extent. It is revealed that the correlation between multi-year variations in sea ice spatial distribution in the Northern Hemisphere and insolation contrast is interpreted as cause and effect relationship, while insolation contrast can be used as a predictor in statistical models for the sea-ice extent dynamics. A close relationship between spatial distribution of sea ice and insolation contrast throughout the entire Northern Sea Route has been determined. This gives a perspective for long-term forecasting of the sea-ice extent for the Northern Sea Route based on calculations of the intensity of insolation contrast for the Northern Hemisphere.

Key words: *sea ice area, seasonal, interannual and multi-year variability, insolation, insolation contrast, correlation analysis, Northern Sea Route, solar climate theory.*

INTRODUCTION

The distribution of sea ice depends on many factors determined by geophysical processes. Those are, first of all, the air temperature and humidity, ocean surface temperature, cloudiness, river runoff, albedo, etc. However, the energy basis of those factors, as well as of the circulation processes in the atmosphere and ocean, is the solar radiation coming to the Earth – the main source of energy for hydrometeorological processes. Heat exchange mechanisms ('heat engine of the first and second kind') are the consequence of the irregularity of the irradiation time and the uneven distribution of solar radiation in space. Due to the heterogeneity of the components of the natural environment, heat exchange mechanisms are formed between the atmosphere, the ocean and the sea ice. That implies the importance of the radiation factor in the dynamics of the spread of sea ice and the need to determine the relationship between those variables. That is also relevant for improving the methods of predicting the spread of sea ice in the changing climate. Forecasting the spread of sea ice is important for long-term planning the strategy of using the Northern Sea Route and the socio-economic development of the Arctic regions [*Fedorov, 2015; Fedorov, Grebennikov, 2018*].

The spread of the area of sea ice (drift) is influenced by sea currents and tides associated with the gravitational interaction of the Earth with the Moon and the Sun. That influence is not considered in this work.

The aim of this work is to determine the correlation and cause-and-effect relationships of long-term changes in the area of sea ice with the characteristics of insolation in the Northern Hemisphere with a high spatial resolution. That block of studies is one of the constituent parts of the statistical model of the distribution of sea ice in the Northern Hemisphere developing by the authors. The other two blocks of the statistical model will include relationships between the seasonal and interannual variability in sea ice area and insolation characteristics. As a result, an assessment of the influence of the insolation factor on the dynamics of the sea ice area and the possibility of modeling and forecasting the spread of sea ice, taking into account the seasonal, the interannual and the long-term changes in insolation characteristics, calculated with high spatial and temporal resolution in the future, will be carried out. In addition to insolation factors, it is assumed that air humidity and other factors will be taken into account on the basis of a multi-factorial multiple regression equation. The elaboration of a specialized statistical model for the distribution of sea ice is relevant and justified taking into account the problems noted for physical and

mathematical models, in which sea ice is one of the fragments of climate modeling [*Fedorov, 2019a,b*].

INPUT DATA AND RESEARCH METHODOLOGY

The database of the Hadley Meteorological Center (Hadley Center for Climate Prediction and Research, Met Office, UK) HadISST1 (Hadley Center Sea Ice and Sea Surface Temperature data set) has been used as an input data (http: //www.metoffice.gov.uk/...html).

The information presented in the HadISST1 database on the mean-monthly temperature of the ocean surface (TOS) and the area of sea ice in the Northern and Southern Hemispheres has been obtained as a result of the consolidation of the reanalysis's data (ERA40) into a single data set. The reanalysis has been carried out using empirical orthogonal functions (EOF) and instrumental data (primarily the shipboard and satellite data) of observations. Reconstruction of the sea ice area in the massif on a 1° × 1° grid has been carried out on the basis of the approximation and extrapolation algorithms for available data (digitized sea ice area maps, ship and satellite observation data) taking into account the TOS [*Rayner et al., 2003*]. Since the insolation characteristics are calculated by the authors for the future, the determination of close correlations and cause-and-effect relationships seems to be a possible basis for statistical and probabilistic forecasts of changes in the area of sea ice.

The input data containing information on the area of sea ice (HadISST1) are presented in several text files, which have been combined by the authors into a single array in Excel format. The array is consisted of data on the area of sea ice in the Northern Hemisphere in a 1° × 1° spatial cell as a percentage of the cell area. In total, the array, collected in that way, has covered about 7400 cells, each of which provides information on the sea ice area with monthly values for the period from 1901 to 2018. The array is completely filled with monthly values (no gaps). The monthly values were used to calculate the mean-annual (as averages for all months of the year) and semiannual (as averages for the months from April to September for the summer half of the year and from October to March for the winter half of the year) values of the sea ice area.

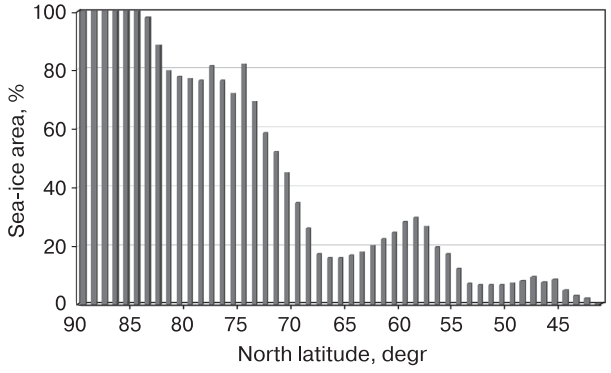

Fig. 1. Distribution by latitudes of the average perennial values of the area of sea ice for the period from 1901 to 2018 in a 1° × 1° cell.

The analysis of the values of the sea ice area within the latitudinal range of 90° N up to 42° N have been accomplished. We have adopted the lower boundary conditions on the basis of the typical 0.5 % mean-multi-year value of the annual sea ice area in the cell at latitude of 42° N. At lower latitudes, the long-term average value does not exceed 0.5 % of the cell area. For latitude of 42° N the mean long-term value of the cell area occupied by sea ice exceeds 0.5 % (0.556 %). For latitude 41° N the ice area on average for the period from 1901 to 2018 is 0.278 % (Fig. 1). The pattern of the distribution remains the same throughout half-years and months, but the latitudinal range with cells, in which the average ice area exceeds 0.5 %, changes. In the winter half of the year, the parameters of the lower values of the sea ice area are identical to the annual ones. In the summer half of the year at latitude of 43° N the average cell area occupied by ice is 1.389 % of the cell area. Sea ice does not spread further southward during that period. In March, the range (at the boundary value of 0.5 %) of the analyzed values is 90–42° N, for September it is 90–54° N (in September, the peak noted in Fig. 1 in the region of 55–65° N disappears). Thus, we have excluded the cells that occurred in seas not covered by ice in the period from 1901 to 2018. The analysis of the results has been carried out and the Table 1 has been compiled.

The previously calculated values have been used as the initial characteristics of insolation in the Northern Hemisphere: 1) the incoming solar radiation per year, summer and winter semesters (J/m^2, W/m^2), 2) the seasonality, i.e. the difference between the incoming solar radiation in the summer and winter semesters (J/m^2, W/m^2), 3) the annual insolation contrast (IC) [*Fedorov, Kostin, 2019*]. The IC (W/m^2) has been determined as the difference between the insolation of the heat source region (0–45° N) and the heat sink area (45–90° N). The IC reflects the change in the meridional gradient of insolation, which regulates the transfer of heat from the equatorial and tropical regions to the polar regions, in a generalized manner (for the regions of the heat source and heat sink) – the operation of the 'heat engine of the first kind' [*Shuleikin, 1953; Fedorov, 2018*].

Correlation analysis of long-term series (118 years long) of average annual, semiannual and monthly (March, September) values of the sea ice area in each 1° × 1° cell with the characteristics of insolation of the Northern Hemisphere has been carried

Table 1. **Distribution of the values of the correlation coefficient of long-term changes in the area of sea ice and the characteristics of insolation in the Northern Hemisphere (%)**

Correlation coefficient	Insolation, J/m²		Seasonality of insolation, J/m²	Insolation contrast, W/m²
	Summer	Winter		
Summer semester				
<–0.9	0.00	0.00	0.00	0.00
<–0.8	0.00	0.38	0.00	0.64
<–0.7	0.04	6.42	0.07	7.63
<–0.6	0.23	21.23	0.22	23.68
<–0.5	0.49	41.58	0.52	43.68
> 0.5	42.41	0.48	43.19	0.53
> 0.6	23.23	0.22	23.70	0.22
> 0.7	6.77	0.03	7.25	0.07
> 0.8	0.53	0.00	0.67	0.00
> 0.9	0.00	0.00	0.00	0.00
Winter semester				
<–0.9	0.00	0.00	0.00	0.00
<–0.8	0.00	0.00	0.00	0.00
<–0.7	0.45	0.94	0.46	1.44
<–0.6	0.73	6.80	0.78	8.28
<–0.5	1.16	21.12	1.13	23.55
> 0.5	22.04	1.12	23.12	1.14
> 0.6	7.86	0.75	8.10	0.78
> 0.7	1.16	0.42	1.32	0.48
> 0.8	0.00	0.00	0.00	0.00
> 0.9	0.00	0.00	0.00	0.00
March				
<–0.9	0.00	0.00	0.00	0.00
<–0.8	0.00	0.00	0.00	0.00
<–0.7	0.38	0.22	0.39	0.41
<–0.6	1.20	2.84	1.30	3.46
<–0.5	3.41	9.47	3.50	10.38
> 0.5	9.90	3.25	10.11	3.39
> 0.6	3.34	1.20	3.40	1.30
> 0.7	0.34	0.34	0.41	0.41
> 0.8	0.00	0.00	0.00	0.00
> 0.9	0.00	0.00	0.00	0.00
September				
<–0.9	0.00	0.00	0.00	0.00
<–0.8	0.00	0.00	0.00	0.02
<–0.7	0.00	0.92	0.00	2.45
<–0.6	0.00	14.33	0.00	16.45
<–0.5	0.07	30.81	0.07	32.11
> 0.5	32.41	0.07	32.49	0.07
> 0.6	16.52	0.00	16.84	0.00
> 0.7	2.11	0.00	2.20	0.00
> 0.8	0.02	0.00	0.02	0.00
> 0.9	0.00	0.00	0.00	0.00

out. Using geoinformation technologies, maps of the correlation coefficient values have been built. The maps reflect the coefficient of correlation between the area of sea ice distribution and the characteristics of insolation. Possible errors in the correlation analysis are associated with the chronological discrepancy between the calendar year, semesters, and months for which there are sea ice area values with the tropical year, semesters, and months for which the insolation characteristics have been calculated. A tropical year is a period of time between the passages of the successive points of the vernal equinox by Earth. The assessment and significance of the linear correlation coefficient when performing the correlation analysis have been carried out in accordance with the existing methods [*Tsymbalenko et al., 2007*].

RESULTS AND DISCUSSION

Close correlations have been found between long-term changes in the sea ice area (annual, semiannual, and monthly) and summer and winter insolation of the Northern Hemisphere (J/m²), seasonality of insolation (J/m²), and annual insolation contrast (W/m²).

The correlation of long-term changes in annual (average for the winter and summer half-year) values of the sea ice area with long-term changes in summer insolation is characterized mainly by positive values (Fig. 2). All values of the correlation coefficient are statistically significant with a probability of 0.99. Out of 7416 values of the correlation coefficient (R) of long-term changes in the annual area of sea ice with summer insolation in the Northern Hemisphere, 541 of them (7.30 %) have negative values and 6875 ones (92.70 %) have positive values (Fig. 2). 70.16 % of them have positive values over 0.5; 42.98 % of them exceed the values of $R = 0.6$, 19.82 % of them exceed the values of $R = 0.7$ and 2.27 % of them have the values of $R > 0.8$ (Table 1).

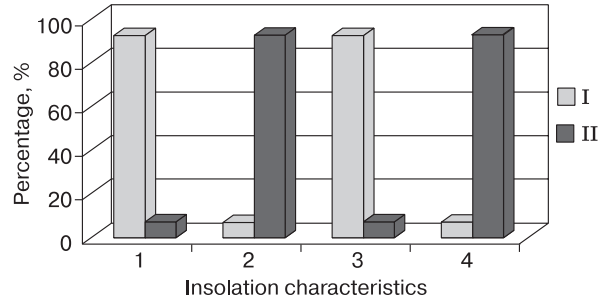

Fig. 2. Ratio of positive (I) and negative (II) values of the correlation coefficient of the annual area of sea ice:

1 – with summer insolation, 2 – with winter insolation, 3 – with seasonality of insolation, 4 – with insolation contrast of the Northern Hemisphere.

The correlation of long-term changes in the annual sea ice area with long-term changes in winter insolation is characterized mainly by negative values. 6895 values of the correlation coefficient (92.97 %) are negative and 521 (7.03 %) are positive. 68.46 % have negative values of $R < -0.5$; 40.17 % have the R values < -0.6; 18.18 % have the R values < -0.7 and 1.35 % have the R values < -0.8.

The correlation of long-term changes in the annual sea ice area with the seasonality of insolation is mainly characterized by positive values (Fig. 2). Out of the 7416 values of R, 6884 ones (92.83 %) have positive values and 531 ones (7.17 %) have negative values. 70.73 % have positive values exceeding 0.5; 44.27 % exceed the values of $R = 0.6$; 20.60 % of the values have $R > 0.7$ and 2.36 % have $R > 0.8$.

The correlation of long-term changes in the annual sea ice area with long-term changes in insolation contrast is characterized mainly by negative values. Among 7416 values of the correlation coefficient, 6901 ones are negative (93.06 %) and 515 ones (6.94 %) are positive. The negative $R < -0.5$ have been obtained for 71.79 % of the values; 44.70 % have the R values <-0.6; 21.14 % have $R < -0.7$ and 2.37 % have $R < -0.8$.

Correlation indicators of the semiannual, the March and the September values of the sea ice area are presented in Table 1. The values of the correlation coefficient in the summer half of the year, in the winter half of the year, in March and in September have been obtained, correspondingly, for 7324, 7354, 7149 and 6079 cells.

In the long-term changes in the annual values of the sea ice area, a close correlation with the insolation characteristics is noted in the vast Arctic region, including the Baffin Sea, Hudson Strait, Fox Basin, the northern part of Hudson Bay, many straits of the Canadian Arctic Archipelago (Lancaster, Barrow, etc.),

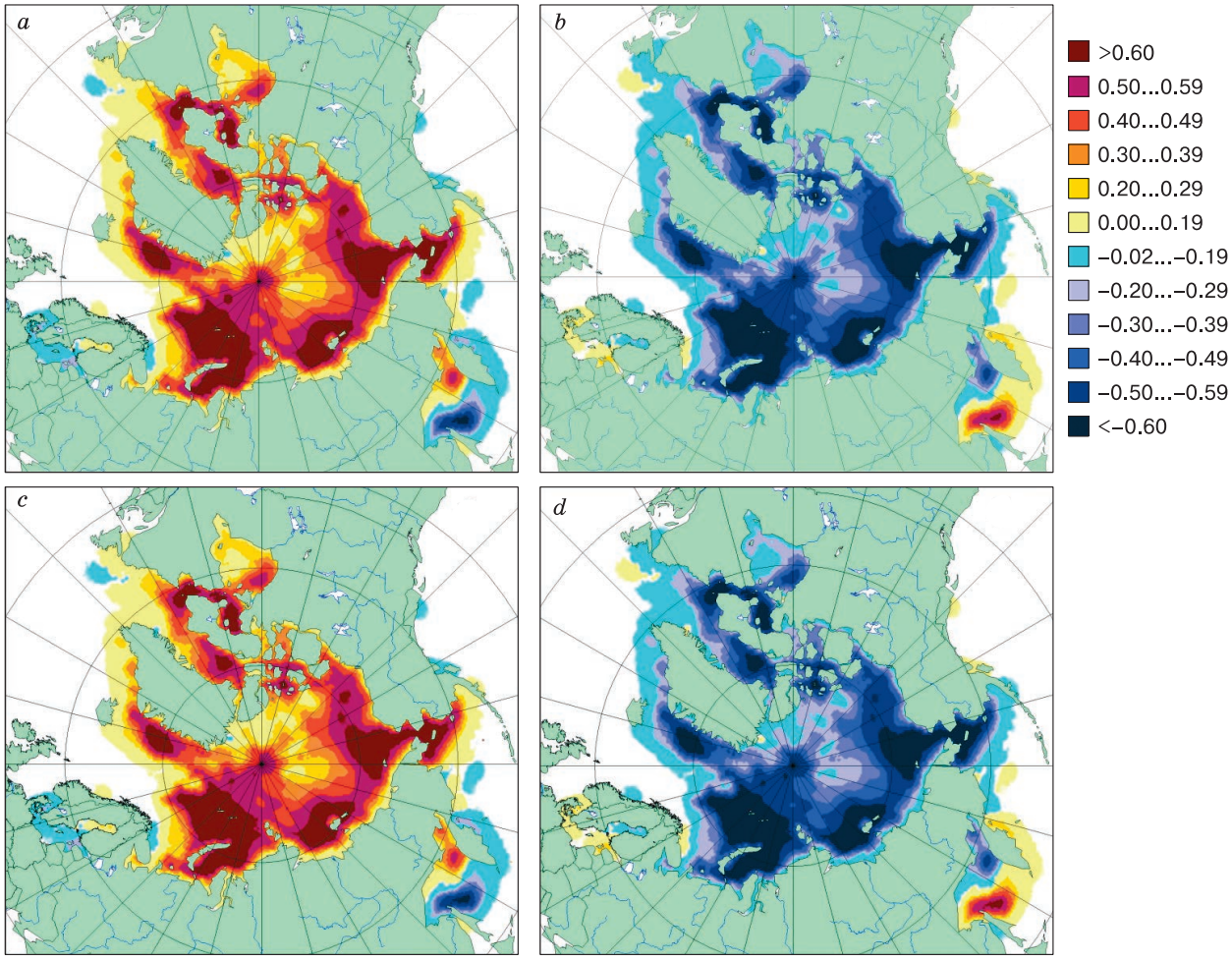

Fig. 3. Distribution of the correlation coefficient of long-term changes in the annual area of sea ice and insolation characteristics:

a – with summer insolation; *b* – with winter insolation; *c* – with seasonality of insolation; *d* – with insolation contrast of the Northern Hemisphere.

Greenland and the Barents Sea, the western part of the Kara Sea, the Laptev Sea and the western part of the East Siberian Sea, the Chukchi Sea and the northern part of the Bering Sea, the western part of the Beaufort Sea (Fig. 3).

The search for cause-and-effect relationships in the pool of found close correlations has been carried out. As noted, the positive relationship between the long-term changes in the area of sea ice (annual, semi-annual, and monthly) with the summer insolation and the seasonality of insolation has been found. A negative relationship with winter insolation and insolation contrast has been marked. However, all those characteristics of insolation are closely related, and, therefore, are not independent variables. Thus, the correlation coefficient of IC with summer insolation within the interval of 1901 to 2018 is –0.950, the same with winter insolation is 0.994, with seasonality it is –0.985. All those characteristics are linearly related to a decrease in the inclination of the Earth's axis of rotation [*Fedorov, 2018*].

Let us consider the possible climatic effects associated with the found connections.

An increase in insolation (winter or summer) should also result in a decrease in the area of sea ice in that season (due to inertia, that effect can manifest itself in both seasons with some delay in time). In the case of a reduction in the incoming radiation, the opposite effect should be expected. During the study period, a decrease in both annual and summer insolation has been registered, yet, a decrease in the annual and summer area of sea ice has been observed. Consequently, the positive relationships (noted for summer insolation) with changes in the sea ice area are correlative, since, based on physical concepts, an increase in summer insolation should correspond to a decrease in the sea ice area. And, conversely, a decrease in summer insolation should correspond to an increase in the area of sea ice distribution. Winter insolation increases during the specified period and, therefore, can be the factor of the long-term changes in the area of sea ice.

A positive relationship between the long-term changes in the area of sea ice and the seasonality of insolation has been found. For the seasonality of insolation in the period under study, there is also a tendency to decrease [*Fedorov, Frolov, 2020*]. That trend is determined by the reduction in summer insolation. It is known that summer insolation is important in the genesis of climate and its changes, which are closely related to the formation and evolution of sea ice. That is determined, firstly, by the fact that the evaporation and the content of water vapor in atmosphere increase with the increasing of summer insolation, which leads to an increase in the greenhouse effect. Secondly, the release of heat is associated with an increase in atmospheric precipitation (transition of water vapor into water and snow). Third, because of decrease in albedo due to a reduction in the area of sea ice and glaciers, the heating of the surface (of continents and oceans) and, hence, the atmosphere increases. With a decrease in summer insolation, the opposite effects obviously occur. As a result, based on the above-mentioned physical concepts, the positive relationship between the long-term changes in the area of sea ice and the seasonality of insolation, characteristic of the period under study, should also be considered a correlative one. A close negative relationship between the long-term changes in the area of sea ice (for annual, semi-annual, and monthly values) and the insolation contrast has been obtained (Fig. 2, 4). In the summer half-year, close correlations between the long-term area of sea ice and the insolation contrast are observed over the vast territory of the Northern Hemisphere. In the winter half of the year, the area of close interrelations is noticeably reduced. There are no responses to long-term changes in IC in the central part of the Arctic Ocean, where the minimal changes in the area of sea ice are observed during the study period. However, a close relation is manifested in the individual marginal and coastal areas (Greenland Sea, northern Barents and Kara Seas, Chukchi Sea, western Beaufort Sea, northern Bering Sea, Hudson Strait, Shelikhov Bay in the Sea of Okhotsk). In March, close relations are noted only in the Greenland Sea, in the north of the Barents and Bering Seas. That time is characterized by the maximum distribution of sea ice in the Northern Hemisphere along with a low (for this month) long-term variability of the ice cover area. In September, a close relation is fixed for all seas of the Russian Arctic, the Beaufort Sea and the Fox Basin. The distribution of ice cover in those areas during that period is subject to the greatest long-term changes [*Frolov, Gavrilo, 1997; Zubakin, 2006*]. The close correlations obtained for September between the long-term changes in the area of sea ice for the seas of the Russian Arctic and the IC provide the basis for long-term forecasting of changes in the distribution of the area of sea ice along the entire length of the Northern Sea Route in summer (Fig. 4, *d*).

Let us consider a possible physical explanation of the found relationship between the long-term changes in sea ice area and the insolation contrast. Due to the uneven distribution of solar radiation on the Earth's surface, a meridional insolation gradient (MIG) occurs. Previously, the authors have obtained a latitudinal profile of changes in the annual MIG for the period from 3000 B.C. to 2999 A.D. [*Fedorov, 2018*]. The maxima of the increase in the MIG are localized near the polar circles (60–70° N, an annual 'turbulence zones'). The annual 'turbulence zones' coincide with the regions of maximum development of extratropical cyclones (cyclogenesis) in the hemispheres [*Pogosyan, 1976*]. The increase in the annual MIG occurs in the area of the Hadley and Ferrel cir-

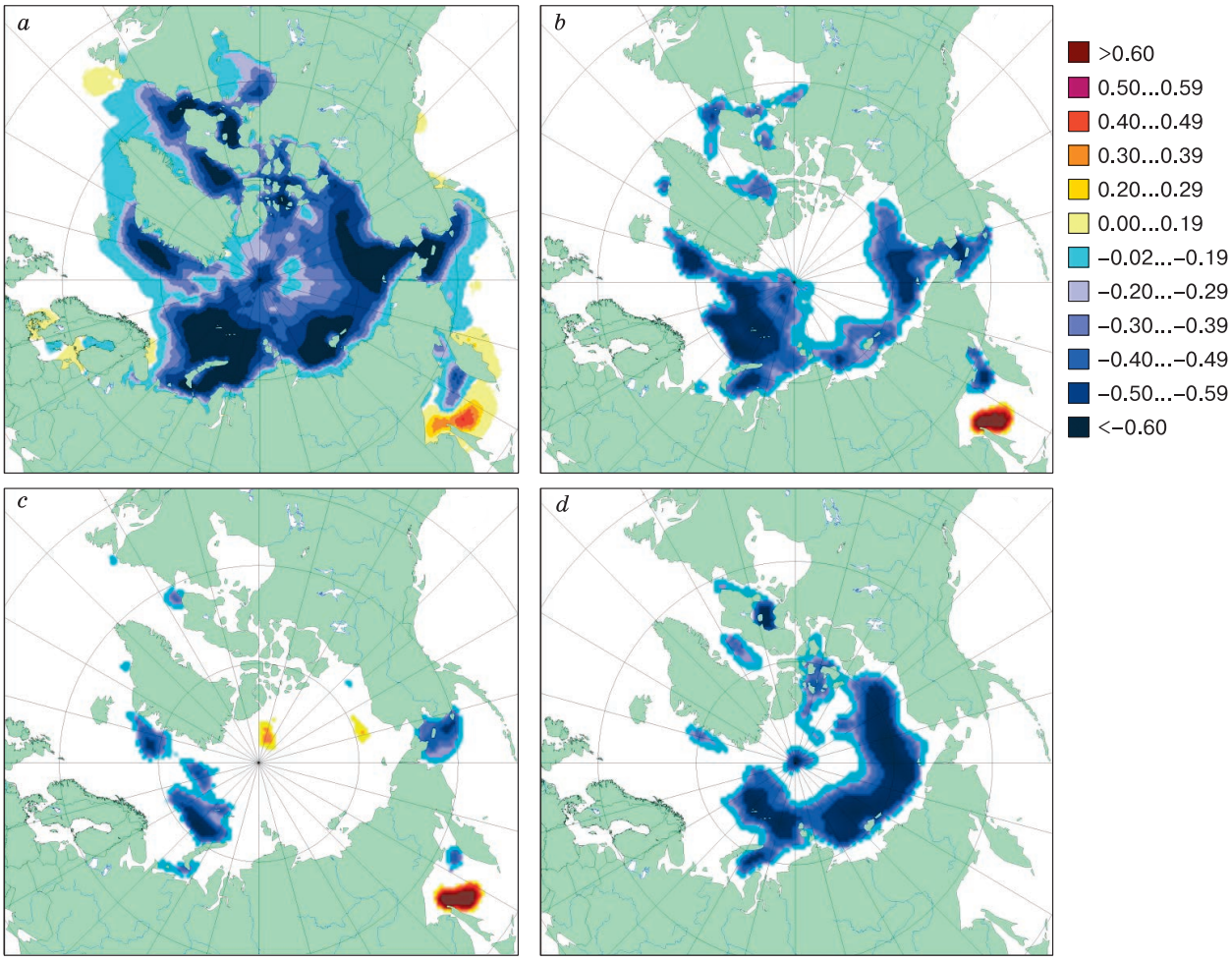

Fig. 4. Distribution of the correlation coefficient of long-term changes in the area of sea ice and insolation contrast in the Northern Hemisphere:

a – in the summer half of the year; *b* – in the winter half of the year; *c* – in March, *d* – in September.

culation cells in the atmosphere. The decrease in the annual MIG falls on the area of polar cells. Thus, the change in the MIG determines the features of both the circulation and vortex activity in the atmosphere. Also, long-term changes in the MIG for the winter and summer semesters have been determined. The MIG values maximally increase in the winter (for the Northern Hemisphere) six months in the latitudinal zone 15–20° S (11.8 %) and decrease maximally in the latitudal zone of 10–15° S (17.8 %). In the summer (for the Northern Hemisphere) six months, the maximum increase (11.8 %) is fixed in the latitudinal zone of 10–15° N, the maximum decrease (17.8 %) is noted in the latitudinal zone of 5–10° N [*Fedorov, 2018, 2019c*].

In the summer half of the year there are seasonal 'turbulence zones' in the hemispheres located within the latitudinal range of 5–20° N. Here, in the neighboring five-degree latitudinal zones, the maximum discrepancies in the trends of changes in the summer MIG are fixed. The seasonal 'turbulence zones' coincide with the areas of tropical cyclone generation (80 % of which are formed within the range of 10–20° N). The vortex transfer of energy is associated with the work of the 'heat engine of the first kind', the mechanism of meridional heat transfer from low latitudes to high ones [*Shuleikin, 1953*]. In the polar regions (polar circulation cells), an increase in the MIG is noted in the hemispheres in the winter semesters, and a decrease is fixed in the summer semesters.

The resulting average distribution of the annual MIG was compared with the meridional distribution of the average annual energy transfer in the ocean-atmosphere system given in [*Lorenz, 1970; Palman, Newton, 1973*]. The correlation coefficient between the mean values of the annual MIG (calculated from the mean long-term values of insolation in the five-degree latitudinal zones for the period from 1900 to

2018) and the values of energy transfer in the ocean-atmosphere system was 0.98 (linear relationship). At the same time, the numerical values of energy transfer in the ocean-atmosphere system in [*Lorenz, 1970; Palman, Newton, 1973*], on average, by 6–7 times exceed the MIG values, which may be due to the participation of water and air masses in the energy transfer in the ocean–atmosphere system. In later works, the values of energy transfer are approximately 3 times higher than the values of the annual MIG [*Peixoto, Oort, 1984*].

Since the energy transfer in the ocean-atmosphere system is determined by the MIG, the features obtained for it can also manifest themselves in the ocean–atmosphere system (an increase or decrease in the intensity of circulation in the cells of the general atmosphere circulation, an increase or decrease in the vortex energy transfer and climatic variability). The features of the Earth's solar climate noted for the modern era are associated with a decrease in the inclination of the Earth's axis of rotation as a result of precession [*Milankovich, 1939; Fedorov, 2018, 2019a,c*].

Earlier, as a result of the correlation analysis, we have determined the relationship between the long-term changes in the anomalies of the surface air temperature (SAT), the temperature of the ocean surface (TOS) of the Earth, the World Ocean and the hemispheres (http://www.cru.uea.ac.uk/cru/data/ temperature) and the long-term changes in the annual insolation contrast. The temperature regime, as noted earlier, is the main factor in the formation and dynamics of the distribution of sea ice. The IC generally (for the regions of the heat source and sink) reflects the change in the MIG. Long-term changes in the MIG and IC are determined by a change in the angle of inclination of the Earth's axis of rotation as a result of precession and nutation [*Fedorov, 2018, 2019c*].

Changes in the SAT and TOS of the Earth and hemispheres (data from the University of East Anglia and the Headley Weather Bureau) are mainly taken into account by trends [*Fedorov, 2018*]. The values of the determination coefficient range from 0.693 to 0.862 (trends are polynomials of the second degree). The coefficient of determination demonstrates the proportion of changes in the SAT and TOS determined by the trend. Consequently, in order to explain the tendencies of long-term changes in global temperature, it is necessary to find a factor that determines the trends of long-term changes in the SAT and TOS. The analysis reveals that long-term changes in the SAT and TOS of the Earth and hemispheres are characterized by close positive correlations with long-term changes in IC and negative correlations with long-term changes in the axis tilt angle. The calculations performed using the regression equation (based on an ensemble of linear and polynomial solutions) has demonstrated that long-term changes in the SAT and TOS are mainly associated with long-term changes in the annual insolation contrast, enhanced by positive feedbacks (Table 2), as shown below.

Table 2. **Long-term changes (%) in near-surface air temperature (SAT) and temperature of ocean surface (TOS), explained by the regression model**

Territory	SAT	TOS
Earth, World Ocean	80.7	79.7
Northern Hemisphere	73.4	69.3
Southern Hemisphere	83.1	84.1

The physical mechanism of the close correlation (found by the authors) of the long-term changes in the area of sea ice in the Northern Hemisphere with the insolation contrast in a generalized form can be reduced to the following. The increase in the IC associated with a decrease in the angle of inclination, which controls the meridional heat transfer or the intensity of the 'heat engine of the first kind', leads to an increase in heat transfer (due to circulation processes in the atmosphere and vortex formations) from the low to high latitudes. As a result, the ocean surface temperatures and near-surface air temperatures rise. That leads to an increase in evaporation and an increase in the content of water vapor in the atmosphere and an intensification of the greenhouse effect. That results in an additional rise in temperature, etc. That process, constantly repeating, increases the climate warming in the Northern Hemisphere and leads to a reduction in the area of sea ice. In addition, as a result of condensation due to the advection of warm air masses to high latitudes, heat is also released, making an additional contribution to the scheme of radiation heat exchange in the atmosphere (Fig. 5).

The three lower blocks in the diagram reflect the mechanism of increasing the warming process in the Arctic and reducing the area of sea ice (Fig. 5). Also, one should take into account the positive feedbacks, a decrease in albedo due to a long-term reduction in the area of sea ice and an increase in the greenhouse effect due to the degassing of permafrost owing to climate warming [*IPCC, 2013*]. Thus, the natural causes of changes in the current global climate are confirmed. The main one is the change in the inclination of the Earth's rotation axis, which regulates the distribution of the solar radiation coming to the Earth by latitudes and seasons and the intensity of the meridional heat transfer (the work of a 'heat engine of the first kind') [*Shuleikin, 1953*].

Taking into account the above-mentioned physical explanation, the found close correlation between long-term changes in annual, semi-annual and monthly values of the sea ice area with the IC of the Northern Hemisphere can be considered the cause-and-effect relationship. The relationship of long-term changes in the area of sea ice with the winter insola-

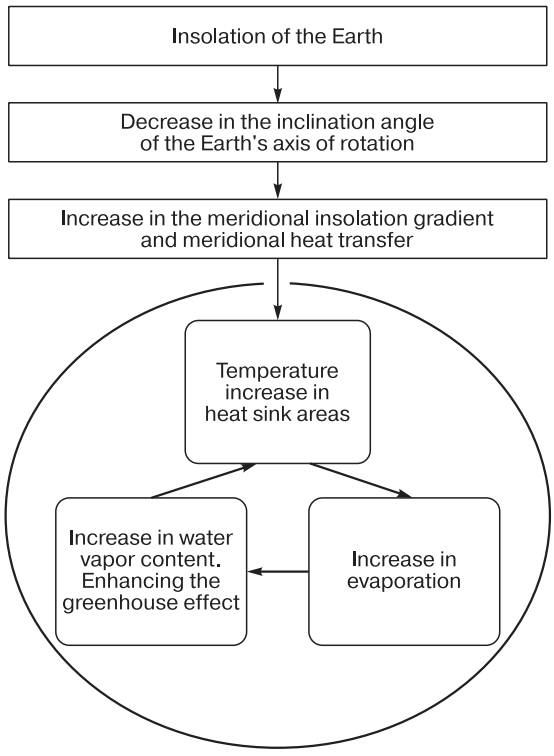

Fig. 5. Schematic diagram of radiation heat exchange in the atmosphere.

tion (its increase corresponds to a decrease in the area of sea ice) can also be considered the causal relationship. The winter insolation in the period of 1901 to 2018 increases by 0.020 %, while the IC increases by 0.048 %, that is, the contribution of the IC to long-term changes in the sea ice area is more significant than the effect associated with an increase in winter insolation. In addition, as follows from the description of the climatic effect of the IC, it manifests itself throughout the year (seasons, months). Wherein the winter insolation is a seasonal factor. At the same time, the variability of the sea ice area mainly falls on the summer half of the year. Therefore, in the statistical model (taking into account the close relationship between the IC and winter insolation and their linear dependence on the axis tilt angle), the IC should be used as a predictor when forecasting long-term changes in the area of sea ice. However, at the same time, it seems necessary to obtain quantitative characteristics of the ratio of the influence of those factors (IC and winter insolation) on the trend of changes in the area of sea ice in the Northern Hemisphere.

CONCLUSIONS

A causal relationship between long-term changes in annual, semi-annual and monthly values of the sea ice area with the characteristics of insolation – winter insolation and insolation contrast of the Northern Hemisphere – on a scale of high spatial resolution has been found. Insolation characteristics are linearly related to the inclination of the Earth's rotation axis and are closely related to each other, therefore, they are not independent parameters, which excludes the possibility of using a two-factor (the winter insolation and the IC) multiple regression model. Due to the large range of the IC changes, that characteristic, taking into account the associated physical mechanism of climate change, is taken as one of the predictors in the developed statistical model of the sea ice area. Thus, the model will take into account long-term changes in the sea ice area associated with changes in the meridional insolation gradient and meridional heat transfer. Long-term changes in the area of sea ice associated with variations in the income of solar radiation (including the winter half of the year) will be taken into account in the block of connections in the annual course of insolation with the annual course of changes in the area of sea ice in the cells. The third block assumes taking into account the relationships between the long-term interannual changes in the sea ice area and the long-term interannual changes in insolation characteristics. Separate blocks and algorithmic scheme (architecture) of the statistical model of sea ice will be presented in the subsequent works.

The close correlations obtained for September between the long-term changes in the area of sea ice for the seas of the Russian Arctic and the IC represent the basis for predicting of changes in the distribution of the area of sea ice along the entire length of the Northern Sea Route in summer.

The work has been performed in accordance with the state budget theme "Evolution, contemporary state and forecast of devolopment of the coastal zone of Russian Arctic".

References

Fedorov, V.M., 2015. Trends of the changes in sea ice extent in the Northern Hemisphere and their causes. Earth's Cryosphere (Kriosfera Zemli), XIX (3), 46–57.

Fedorov, V.M., 2018. The Earth's Insolation and Recent Climate Changes. Fizmatlit, Moscow, 232 pp. (in Russian).

Fedorov, V.M., 2019a. Earth's insolation variation and its incorporation into physical and mathematical climate models. Uspekhi Fizicheskikh Nauk (Advances in Physical Sciences), 62 (1), 32–45, DOI: 10.3367/UFNe.2017.12.038267.

Fedorov, V.M., 2019b. Commentaries on the article "impacts of climate change on long-term dynamics of seasonal freezing in Moscow region: retrospective analysis and uncertainties in forecasting for the second half of the 2nd century " by S.P. Pozdniakov et al. Earth's Cryosphere (Kriosfera Zemli), XXIII (4), 31–36.

Fedorov, V.M., 2019c. The problem of meridional heat transport into the astronomical climate theory. Geofizicheskiye Protsessy i Biosfera (Geophysical Processes and Biosphere), 18 (3), 117–128, DOI:10.21455/gpb2019.3-8.

Fedorov, V.M., Grebennikov, P.B., 2018. Insolation contrast of the Earth and changes in the sea ice extent in the Northern hemisphere. Arktika: Ekologiya i Ekonomika (The Arctic: Ecology and Economy), No. 4 (32), 86–94, DOI: 10.25283/2223-4594-2018-4-86-94.

Fedorov, V.M., Frolov, D.M., 2020. The Little Ice Age in the life of the Earth and its possible causes. Zhizn Zemli (Life of the Earth), 42 (1), 4–12.

Fedorov, V.M., Kostin, A.A., 2019. Calculation of the Earth's insolation for the period from 3000 BC until AD 2999. Protsessy v geosredakh (Processes in Geoenvironments), No. 2, 254–262.

Frolov, I.E., Gavrilo, V.P. (Eds.), 1997. Sea Ice. Gidrometeoizdat, St. Petersburg, 402 pp. (in Russian).

IPCC, 2013: Climate Change 2013: The Physical Science Basis. Contribution of Working Group I to the Fifth Assessment Report of the Intergovernmental Panel on Climate Change. T.F. Stocker, D. Qin, G.-K. Plattner, M. Tignor, S.K. Allen, J. Boschung, A. Nauels, Y. Xia, V. Bex, P.M. Midgley (Eds.). Cambridge Univ. Press, Cambridge, New York, 1535 pp., DOI: 10.1017/CBO9781107415324.

Lorenz, E.N., 1970. Nature and Theory of the General Circulation of the Atmosphere. Gidrometeoizdat, Leningrad, 260 pp. (in Russian).

Milankovich, M., 1939. Mathematical Climatology and Astronomical Theory of Climate Fluctuations. GONTI, Moscow; Leningrad, 208 pp. (in Russian).

Palman, E., Newton, C., 1973. Atmospheric Circulation Systems. Gidrometeoizdat, Leningrad, 616 pp. (in Russian).

Peixoto, J.P., Oort, A.H., 1984. Physics of climate. Rev. Modern Phys. 56, 365–429.

Pogosyan, H., 1976. Cyclones. Gidrometeoizdat, Leningrad, 148 pp. (in Russian).

Rayner, N.A., Parker, D.E., Horton, E.B., et al., 2003. Global nalyses of sea surface temperature, sea ice, and night marine air temperature since the late nineteenth century. J. Geophys. Res. 108, No. D14, 4407 pp., DOI: 10.1029/2002JD002670.

Shuleikin, V.V., 1953. Physics of the Sea. USSR Academy of Sciences, Moscow, 990 pp. (in Russian).

Tsymbalenko, T.T., Baydakov, A.N., Tsimbalenko, O.S., Gladilin, A.V., 2007. Mathematical Statistics Methods in the Processing of Economic Information. Finansy i Statistika, Moscow, 200 pp. (in Russian).

Zubakin, G.K. (Ed.), 2006. Ice Formations in the Western Arctic Seas. AARI, St. Petersburg, 272 pp. (in Russian).

URL: http://www.cru.uea.ac.uk/cru/data/temperature (last visited: 13.05.2020).

URL: http://www.metoffice.gov.uk/hadobs/hadisst/data/download.html (last visited: 13.05.2020).

Received May 15, 2020
Revised version received September 1, 2020
Accepted November 5, 2020

EARTH'S CRYOSPHERE
SCIENTIFIC JOURNAL

Kriosfera Zemli, 2021, vol. XXV, No. 2, pp. 44–55

DISCUSSION

AIR JANUARY PALEOTEMPERATURE RECONSTRUCTION 48–15 CALIBRATED KA BP USING OXYGEN ISOTOPE RATIOS FROM ZELYONY MYS YEDOMA

Yu.K. Vasil'chuk, A.C. Vasil'chuk

Lomonosov Moscow State University, Faculties of Geography and Geology, Leninskie Gory 1, Moscow, 119991, Russia; vasilch_geo@mail.ru

The features of the Late Pleistocene ice wedges in the outcrop of the Zelyony Mys Yedoma located on the right bank of the Lower Kolyma River are considered. The oxygen isotope composition of ice wedges, radiocarbon age, and hydrochemical characteristics have been studied. Stable oxygen isotopes provide the main basis for reconstructing the mean January air temperature history of a site from ice wedges. Detailed quantitative assessments of paleogeocryological and paleoclimatic changes of the region in the Late Pleistocene 48–15 cal ka BP were performed.

Key words: *ice wedge, Late Pleistocene, permafrost, yedoma, oxygen isotopes, radiocarbon age, pollen and spores, hydrochemistry, Zelyony Mys exposure, Lower Kolyma River, north-eastern Yakutia.*

INTRODUCTION

Syngenetic ice wedges were actively accumulated in maritime lowlands during the Late Pleistocene. The yedoma section of Zelyony Mys is located in the boundary between tundra and forest-tundra, i.e. in the area sensitive to climatic and landscape changes. Main purposes of this article are: 1) Study of syngenetic Late Pleistocene ice wedges and host yedoma deposits located on the right bank of the Kolyma River near Zelyony Mys settlement; 2) Study of the oxygen isotope composition in ice wedges; 3) Radiocarbon and hydrochemical analysis of ice wedges and host sediments, generalization of all radiocarbon data available for the section; 4) Air paleotemperature reconstruction for the Late Pleistocene 48–15 thousand calibrated years BP in this region.

ENVIRONMENTAL CONDITIONS OF THE STUDY AREA

Zelyony Mys Yedoma section is located 3 km away from Chersky on the right bank of the Kolyma River, 130 km from its mouth, in the continental region of Northeastern Russian Arctic. The mean air temperature in January is –32.3 °C, that in July is +15.5 °C, in winter is –31 °C, in summer is +15 °C; the mean annual temperature is –10.8 °C. The average annual precipitation is 197 mm; stable snow cover forms from September to mid-May [*Davydov et al., 2008*]. According to Chersky weather station data, in 1940–2020 the lowest January air temperature was observed in 1964 (–41.7 °C), the highest one – in 1969 (–24.4 °C). The lowest mean annual air temperature was observed in 1940 (–14.5 °C), and the highest one in 2003 (–7.4 °C); the maximum July air temperature was observed in 1960 (17.7 °C), and the minimum one – in 1948 (8.6 °C). The maximum annual amount of precipitation was observed in 1968 (439 mm), the minimum one – in 1978 (102 mm) (www.pogoda.klimat.ru). Permafrost thickness reaches 500–600 m; the mean annual ground temperature at the depth of zero annual amplitude varies mostly within the range of –9 to –11 °C [*Fyodorov-Davydov et al., 2004*]. Permafrost distribution is continuous except of taliks under large rivers. During 1970–2009 observation period, the mean annual ground temperature at the depth of zero annual amplitude changed from –12 to –9 °C in the boreholes in Chersky area [*Romanovsky et al., 2010*].

The yedoma deposits exposed in Zelyony Mys outcrop on the right bank of the Kolyma River near the port of Zelyony Mys (Fig. 1), are arguably among the most representative yedoma outcrops. The outcrop vertical wall reached 36 m in its most complete form. At present, the outcrop is covered by landslides.

In 1983, Yu.A. Murzin and Ya.I. Torgovkin [*1984*], simultaneously with the authors, described the outcrop of that Ice Complex and noted that the outcrop had been formed at the spot of a small lake which was drained in 1981. The drained lake basin was about 200 m wide and 400 m long. A deep ravine with several outcrops on its sides has formed after lake drainage. The study of the Zelyony Mys yedoma has a short history, since the outcrop itself did not ex-

Article by Yu.K. Vasil'chuk and A.C. Vasil'chuk is published contrary to the decision of the editorial group, as it contains a significant amount of self-plagiarism and has no scientific novelty. The authors of the article contacted the editor-in-chief of the journal, Academician V.P. Melnikov, who made the decision to publish this article in the "Discussion" section, simultaneously conducting its independent review. In the same issue, an open review by A.A. Galanin for this article has been published.

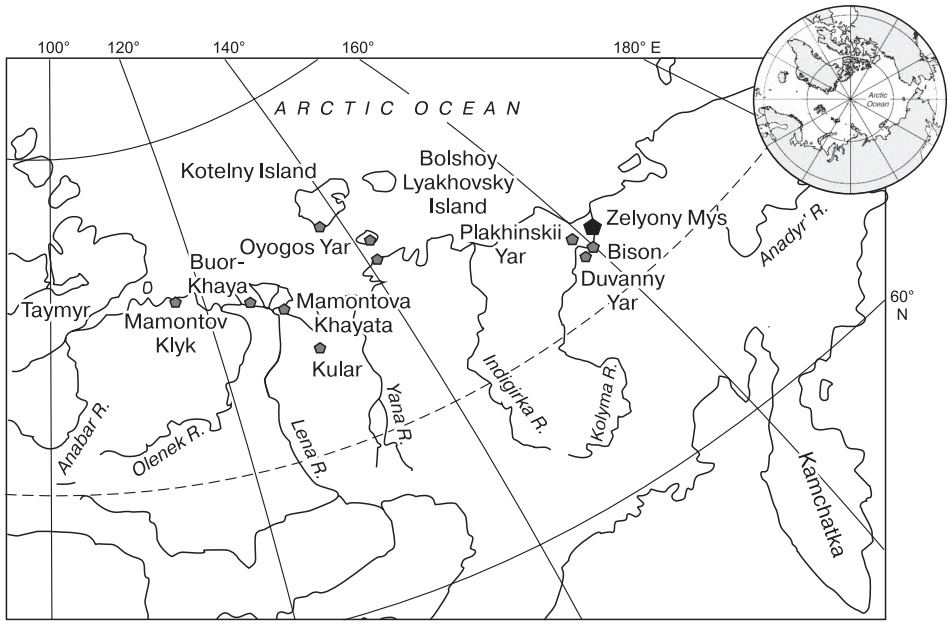

Fig. 1. Location of the Zelyony Mys section and the yedoma sections synchronous to it in the northeast of Yakutia.

ist long [*Vasil'chuk et al., 1985; Vasi'lchuk, 1992; Zanina, 2005; Gubin, Lupachev, 2008; Mikhalev et al., 2012; Gubin, Zanina, 2013*].

Vegetation of the area described, is represented by pre-tundra larch forests. According to Yu.P. Kozhevnikov, the forest-forming specie here is *Larix cajanderi* Mayr. The shrubs understorey is composed of *Betula exilis* Sukacz., *Salix glauca* L., *Rosa acicularis* Lindl., as well as *Vaccinium uliginosum* L., *Arctous erytrocarpa* Small., *A. alpina* (L.) Niedenzu [*Kozhevnikov, 1981*]. According to O.G. Zanina and D.A. Lopatina [*2017*], the vegetation at the drained lake bottom near the Zelyony Mys is characterized by pioneer communities with predominance of *Chamaenerion angustifolium* (L.) Scop., *Tanacetum vulgare* L., *Erigeron acris* L., *Poa pratensis* L., *Hordeum jubatum* (L.) Nevski, *Salix glauca* L.

YEDOMA STRUCTURE AND COMPOSITION

Zelyony Mys yedoma had been studied in 1983 in a ravine 2 km to the north of the Zelyony Mys on the right bank of the Kolyma River (Fig. 1). Ice-rich yedoma has been exposed in the middle part of the ravine (68.7875° N, 161.3806° E) in the outcrop high wall (up to 35–36 m high). The outcrop was subject to annual studies, from 1983 to 1988. At the beginning of 2000s it had been completely covered by landslide deposits.

Stratigraphy and cryolithological features of the yedoma deposits. The 36-meter-high outcrop consists of two parts. The upper gray portion, about 12–13 m thick, is almost free of organic material. The lower brownish gray one, 24 m thick, consists of three peat layers with plant detritus and three layers without visual organic remains. It is these organic-reach layers (Fig. 2, *a*) which studying lead to formulation of the hypothesis of the cyclical development of the yedoma [*Vasil'chuk, 1992, 1999*].

The upper horizon of the outcrop, less than 0.5 m thick, is represented by banded lacustrine loams. The deposits of an Ice Complex 11–12 m thick represented by the dark gray sandy loams with thin or medium ice lenses, rarely with ice belts lie below. The total water content is 75–100 %. Within the interval of 12.5–16.3 m, the upper layer of peaty loam has been exposed. In the middle part, almost pure dark brown peat with reticulate cryostructure is exposed, *in situ* roots have been sampled for ^{14}C dating. At 16.3–18.6 m depth brownish-gray sandy loam with layered cryostructure (thin to medium layers) is exposed. At a depth of 18.6–20.1 m, brown peat with roots and sandy loam with reticulate cryostructure is found. At 20.1–24.2 m, the brownish-gray sandy loam is exposed; cryostructure is reticulate with thin ice layers. At a depth of 24.2–25.4 m lays brown sandy peat with roots, cryostructure is cross-layered and reticulate. Below, up to a depth of 36 m, dark gray sandy loam with horizontal-layered, cross-layered cryostructure with thin ice lenses. In the distribution of ice content and cryostructures through the section, as in the lithological structure, a trinomial mesocyclicity is noted: an increase in ice content, a decrease in the thickness of ice lenses and the distance between them from less peaty horizons up to the base of more peaty ones.

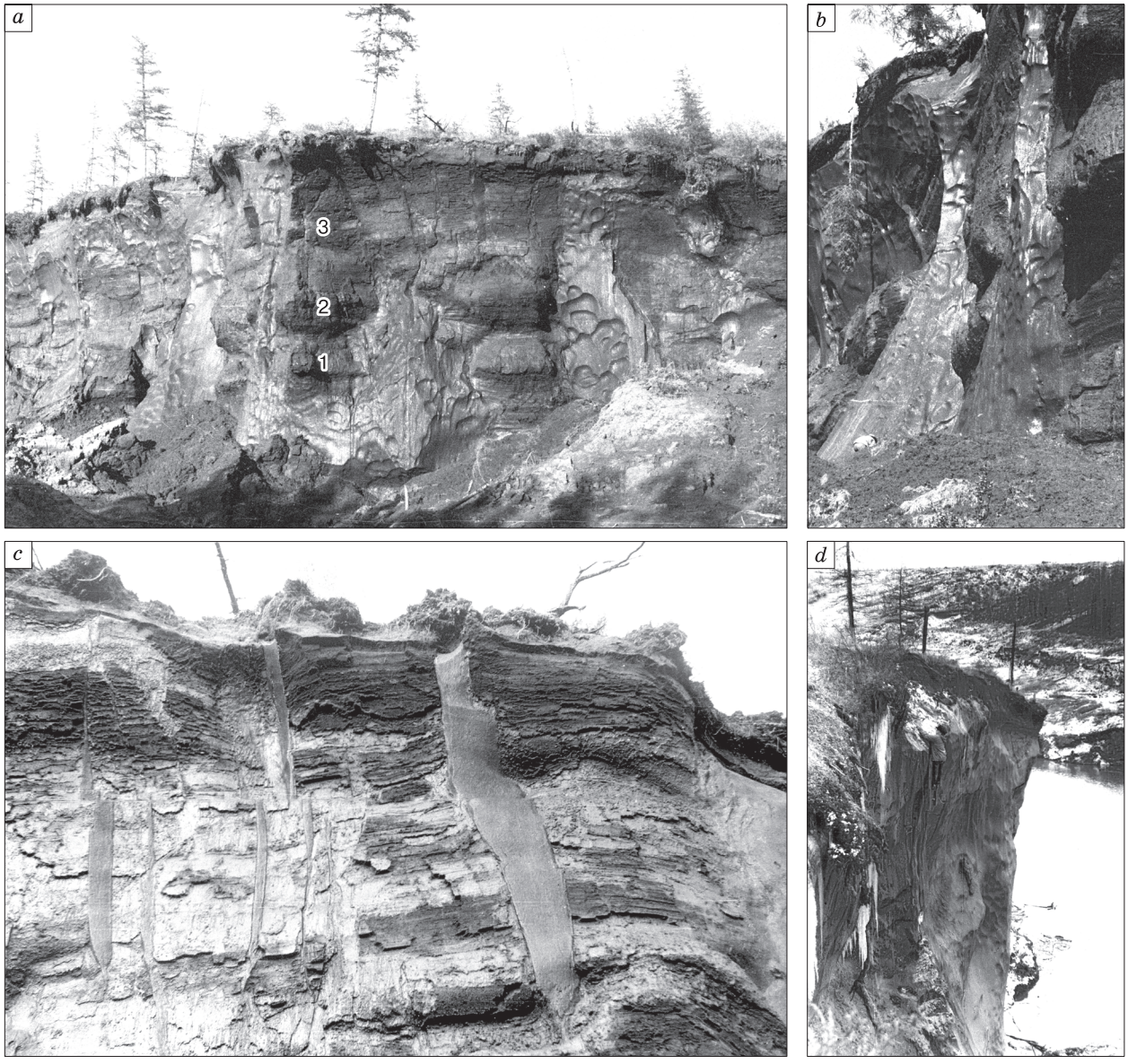

Fig. 2. Syngenetic Late Pleistocene ice wedges of Zelyony Mys on the right bank in the lower reaches of the Kolyma River.

a – general view, *b*–*d* – fragments. 1–3 – organic layers. Photo by Yu.K. Vasil'chuk.

Such a cryogenic structure is associated with the process of accumulation of the strata in the subaquatic environment and its freezing during the draining stage, i.e., during the formation of the peat horizon [*Vasil'chuk, 1999*].

Ice wedges dissect the entire yedoma deposits. In the lower part, the width of the ice wedges reaches 2.0–2.5 m in the frontal section, while in the upper part they are much narrower. Their width in the frontal section does not exceed 0.5–1.0 m, the distance between them is 2–5 m (Fig. 2). At the level of peat horizons "transit" ice wedges have pronounced shoulders.

The ice of wedges is gray, vertically banded; the banding is caused by elongated inclusions of sandy loam.

METHODS OF FIELD AND LABORATORY STUDIES

Organic matter for radiocarbon dating was sampled from the frozen wall of the outcrop. The roots for the dating were sampled immediately after the sampling of the frozen soil monolith. The water obtained during the melting of ice wedges was used for washing them. Samples of ice wedges were taken from the axi-

al part of ice wedges with a volume of 0.5–1.0 dm^3, according to the method developed by Yu.K. Vasilchuk [*Vasil'chuk, 1991, 1992*].

Radiocarbon age of ice wedges and host sediments. Radiocarbon dating of organic macrofossils (mainly grass roots and shrub twigs) out of the yedoma deposits has been carried out at the Geological Institute of the Russian Academy of Sciences, with the participation of L.D. Sulerzhitsky, the sample preparation has been performed by the authors within a month after the sampling.

The AMS dating of microinclusions of the organic matter directly extracted out of ice has been carried out at the accelerator mass spectrometer at laboratory of the Seoul National University with the assistance of professor J.-Ch. Kim. The samples for dating were stored in a laboratory refrigerator at a temperature of –10 °C. To calibrate ^{14}C dating, we used the OxCal calibration program [*Ramsey, 2009*], version 4.3, based on the IntCal13 calibration data set [*Reimer et al., 2013*].

Hydrogeochemistry of ice wedges and host sediments. Determination of the content of water-soluble salts in ice wedges has been performed by titration in the laboratory of PNIIIS within a month after sampling.

Isotopic analysis of ice wedges has been performed in the laboratory of the Water Problems Institute of the Russian Academy of Sciences (senior researcher A.D. Esikov) on a Varian Mat 250 mass spectrometer, sample preparation was carried out by the authors within a month after sampling.

RESULTS OF LABORATORY STUDIES

Radiocarbon dating of host sediments and directly of ice wedges. Four dates, which were the ba-

Table 1. **Radiocarbon dating of organic material of Late Pleistocene yedoma sediments in Zelyony Mys section, right bank in the lower reaches of the Kolyma River**

Sample ID / source	Depth, m	^{14}C age, BP	Lab. ID	Material	Calibrated ^{14}C ages, 99.7 % (cal BP)	Median calendar age (cal BP)
[*Gubin, Lupachev 2008*]	3.2	13 140 ± 140	EP-941615	Soil	16 350–15 145	15 761
308-YuV/46	12.0	28 600 ± 1500	GIN-3574	Roots	40 105–28 927	32 936
315-YuV/5	12.0	33 800 ± 900	GIN-3850	Roots	41 558–35 410	38 177
[*Zanina, 2005*]	12.0	30 500 ± 1400	IEMAE-1179	Ground squirrel burrow, seeds, P-917	41 070–31 105	34 833
[*Zanina, 2005*]	12.0	32 800 ± 1400	IEMAE-1178	Ground squirrel burrow, seeds, P-923	42 616–33 675	37 278
315-YuV/4b	12.0	43 700 ± 800	GIN-3849	Mammoth tibia	49 905–45 100**	47 043
315-YuV/4d	12.0	>50 000	GIN-3848	Mammoth jaw	–	–
308-YuV/27	16.4	27 900 ± 1200	GIN-3575	Roots	37 024–28 776	32 220
308-YuV/27	16.4	>39 000	GIN-3575	Roots	–	–
308-YuV/28	23.7	37 600 ± 800	GIN-3576	Roots	44 202–39 986	41 977
308-YuV/28	23.7	>40 000	GIN-3576	Roots	–	–
352-YuV/1	20.0	42 800 ± 700	GIN-5710	Bison horn	48 824–44 381	44 381
[*Gubin, Zanina, 2013*]	The lower part of the yedoma	43 600 ± 1000*	GIN-8014	Large branches	49 857–44 998**	46 943
[*Gubin, Zanina, 2013*]	The lower part of the yedoma	43 400 ± 1000*	GIN-8013	Large branches	49 752–44 796**	46 743
[*Gubin, Zanina, 2013*]	The lower part of the yedoma	> 48 000*	GIN-8011	Large branches	–	–
[*Gubin, Zanina, 2013*]	The lower part of the yedoma	> 48 000*	GIN-8012	Large branches	–	–
[*Lozhkin, 1977*]	The lower part of the yedoma (8 m above river level)	35 200 ± 800	MAG-295	Roots	42 250–37 103	39 829
		28 240 ± 330	MAG-294	Roots	33 529–31 187	32 162
		27 200 ± 200	MAG-298	Roots	31 574–30 763	31 155
[*Veksler, Prede, 1985*]	The lower part of the yedoma	33 900 ± 500	RI-111	Poorly decomposed peat	40 153–36 366	38 312
[*Veksler, Prede, 1985*]	The lower part of the yedoma	38 700 ± 700	RI-115	Poorly decomposed peat	44 741–41 383	42 736

Note: ^{14}C dates were calibrated using OxCal 4.3 [*Ramsey, 2009*] based on the Intcal13 calibration data [*Reimer et al., 2013*].

* The sampling has been carried out in the lower part of the ravine at residual yedoma outcrop. Upper part has been demolished by slope processes [*Gubin, Zanina, 2013*].

** Based on the results of calibration in the OxCal 4.3, the dating may be beyond the limit of ^{14}C method.

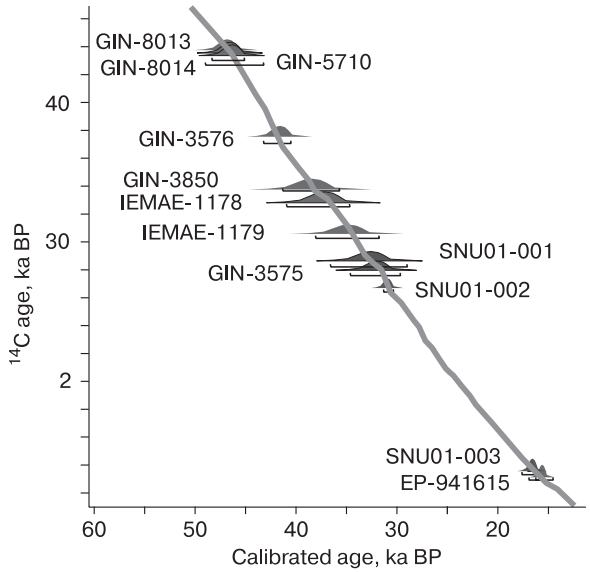

Fig. 3. Calibrated radiocarbon ages of Zelyony Mys yedoma sediments and ice wedges.

sis for the initial referencing of the wedges in time, have been obtained based on the roots, i.e. on organic residues occurring *in situ*. In the upper peaty layer, those dates are 32.2 and 32.9 cal ka BP, in the middle layer it is 38.1 cal ka BP, and in the lower one the date is 41.9 cal ka BP (Table 1, Fig. 3).

Due to the low content of organic matter in the upper part of the yedoma, the time of the end of its accumulation was first determined to be approximately 13 ka BP [*Vasil'chuk, 1992, p. 384*]. Thus, the time interval for the formation of wedges was approximately estimated from 45 to 13 ka BP, which corresponds to the time interval from 48 to 15 cal ka BP. Later the upper time limit of the yedoma formation has been confirmed by the ^{14}C dating of a buried soil horizon near the day surface (which was 15.7 cal ka BP). Later on, ground squirrel burrows (34.8 and 37.2 cal ka BP, Table 1) [*Zanina, 2005*] and large branches from the base of the yedoma (46.9 and 46.7 cal ka BP) [*Gubin, Zanina, 2013*] were dated in the same interval of the middle layer. Those dates (from 48 to 15 cal ka BP) have fully confirmed the reliability of the Zelyony Mys yedoma chronology proposed in [*Vasil'chuk et al., 1985*].

The uppermost date obtained by the authors out of a sample taken directly from the ice, has confirmed the time of the end of the wedge formation – 15.7 cal ka BP (Fig. 3, Table 2).

Out of the axial part of the ice wedge, the dates of 16.4, 30.8 and 32.7 cal ka BP have been obtained at the depths of 3, 6.5 and 8 m correspondingly (Table 2). On the whole, those dates fit well into the gene-

Table 2. **The AMS radiocarbon dating of organic microinclusions in syngenetic Late Pleistocene ice wedges in Zelyony Mys section, right bank in the lower reaches of the Kolyma River**

Sample ID	Depth, m	^{14}C age, BP	Lab. ID	δ^{13}C of organics, ‰	Calibrated ^{14}C ages, 99.7 % (cal BP)	Median calendar age (cal BP)
315-YuV/16	3.0	13 600 ± 200	SNU01-003	–32.5	17 386–15 591	16 422
315-YuV/11	6.5	26 700 ± 300	SNU01-002	–25.4	31 457–29 868	30 879
315-YuV/8	8.0	28 700 ± 500	SNU01-001	–30.2	34 261–31 208	32 728

Table 3. **Composition and content of water-soluble salts in Late Pleistocene syngenetic ice wedges**

Sample ID	Depth, m	Solids content, mg/L	Major ions, mg/L						pH
			HCO_3^-	Cl^-	SO_4^{2-}	Ca^{2+}	Mg^{2+}	$Na^+ + K^+$	
308-YuV/52	3.0	78.0	72.0	5.7	7.4	16.0	6.1	4.4	7.15
315-YuV/11	6.5	94.0	68.3	8.5	13.2	16.8	6.8	5.3	7.00
315-YuV/9	7.5	84.0	68.3	6.4	9.9	16.0	6.3	4.4	7.07
308-YuV/55	8.0	74.0	56.1	5.7	10.7	11.6	6.1	5.1	7.13
308-YuV/56	8.5	60.0	41.5	5.7	8.2	8.0	4.4	5.8	6.97
315-YuV/6	9.0	86.0	74.4	6.4	9.1	16.8	7.5	3.0	7.13
308-YuV/40	9.5	120.0	85.4	6.0	**21.4**	12.2	7.8	18.4	7.30
308-YuV/43	11.6	104.0	85.4	5.3	18.1	13.4	**8.1**	13.6	7.65
315-YuV/21	13.1	**134.0**	**102.5**	6.3	4.1	**25.3**	7.8	1.2	6.83
315-YuV/22f	13.1	82.0	58.6	**9.8**	11.5	9.2	2.7	18.4	7.05
315-YuV/23f	13.1	88.0	79.3	7.7	6.6	12.8	5.1	13.8	7.10
308-YuV/48	15.5	100.0	70.8	6.0	**21.4**	10.0	7.0	9.9	**7.70**
308-YuV/5	15.6	100.0	73.2	7.8	18.1	7.6	5.2	**22.8**	7.50
308-YuV/8	17.0	104.0	75.6	6.0	19.7	15.4	2.8	18.9	**7.70**

N o t e: the maximum values are shown in bold.

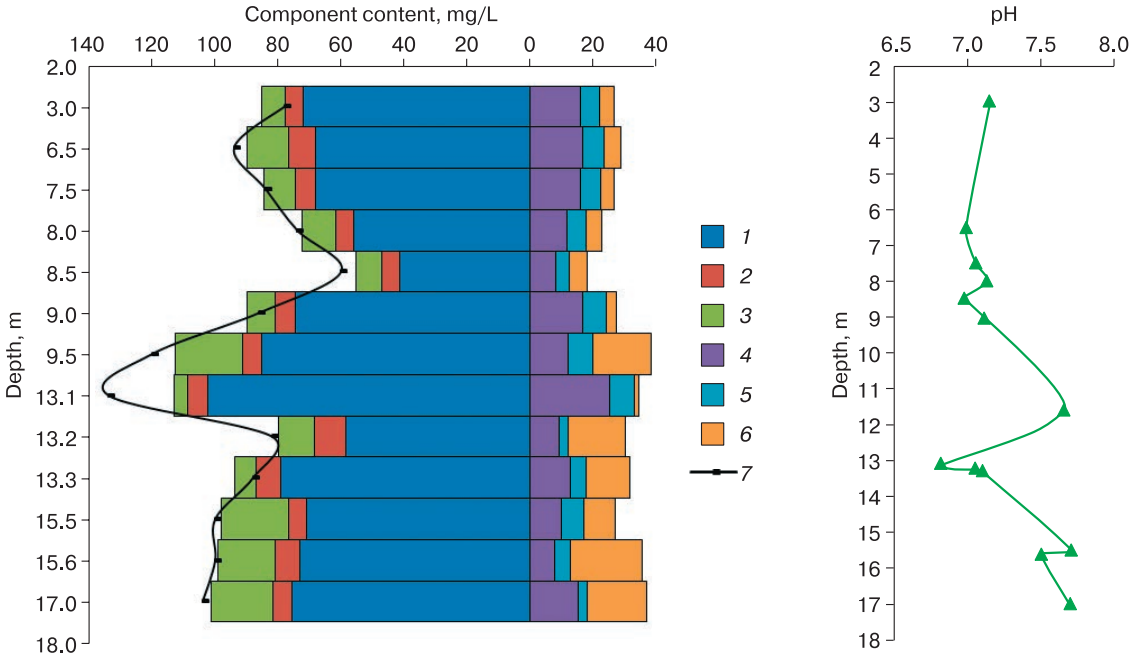

Fig. 4. Composition of water-soluble salts in syngenetic ice wedges in the Zelyony Mys yedoma:

1 – HCO_3^-; *2* – Cl^-; *3* – SO_4^{2-}; *4* – Mg^{2+}; *5* – Ca^{2+}; *6* – $Na^+ + K^+$; *7* – solids content.

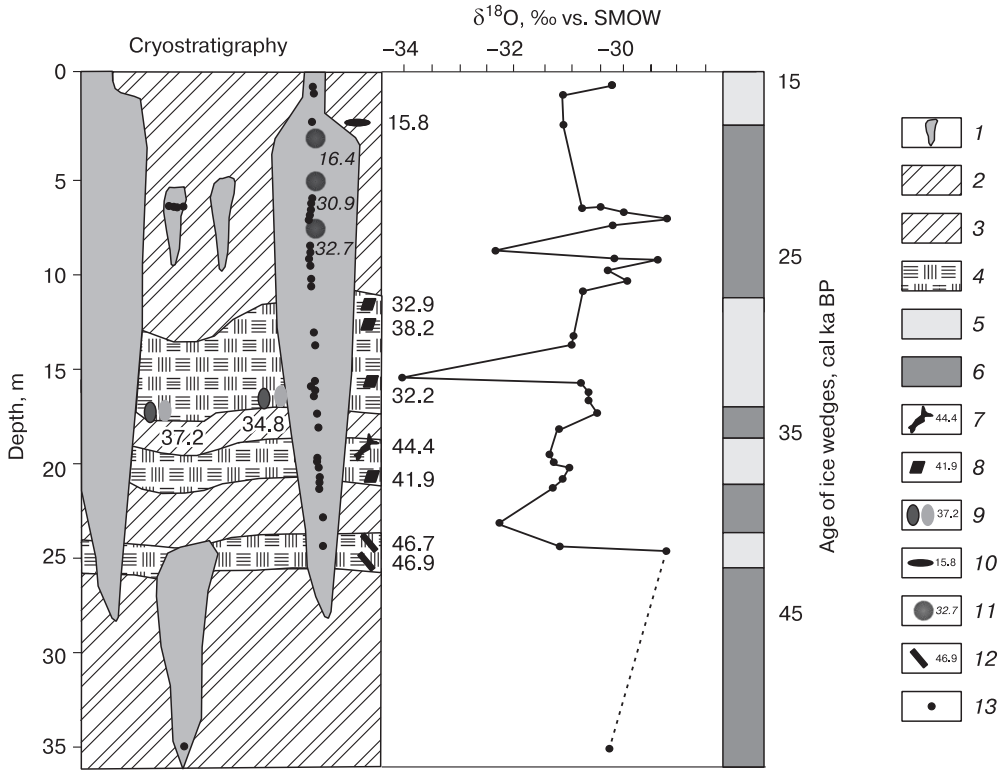

Fig. 5. $\delta^{18}O$ values in ice wedges of Zelyony Mys yedoma.

1 – ice-wedge ice; *2* – frozen gray sandy loam with layered and reticulate cryostructure (thin to medium layers); *3* – frozen brownish-gray sandy loam with layered cryostructure thin to medium layers); *4* – frozen peat of cross-layered, reticulate cryostructure; *5* – sediments of the subaerial stage of yedoma accumulation; *6* – sediments of the subaqueous stage of yedoma accumulation; calibrated ^{14}C age of: *7* – bones, *8* – peat, *9* – seeds from burrows, *10* – soils, *11* – ice wedge, *12* – branches; *13* – sampling sites of ice wedges for isotope analysis. (Sampling sites for ^{14}C dates on seeds from buried burrows, soils and large branches are shown conditionally, since the sampling was carried out in different seasons or not from the main wall of the outcrop.)

ral time range of the formation of the upper part of that ice-wedge complex. Based on direct dating, it can be assumed that the rate of accumulation of ice wedges varied from 0.2 to 1 m per thousand years.

Older dates obtained from a mammoth's bones indicate redeposition of the latter. There is reason to believe that the 47 cal ka BP date of the mammoth bone refers to the initial stage of yedoma accumulation, especially since the horn of a bison dated of about 46 cal ka BP (42 800 ± 700 – GIN-5710) found at the footslope showed similar date. Since those bones lie apart from the skeleton, they are certainly redeposited.

Hydrochemical features of wedge ice. The mineralization of ice wedges is not high (60–134 mg/L); bicarbonates (up to 102 mg/L) dominate in the composition of the salts. The mesocyclicity is clearly visible – in the lower parts of the cycles the ice is more mineralized (100 mg/L and more), further upward mineralization decreases (to 60–80 mg/L), then it increases again (to 94 mg/L), and above it decreases to 78 mg/L (Table 3, Fig. 4).

The authors believe that most important is that the low mineralization of ice is quite consistent with the predominant formation of ice wedges out of melted snow. The maximum mineralization at a depth of 13.1 m is due to the maximum content of carbonate ion (102.5 mg/L) and calcium ion (25.3 mg/L). In the lower part of the wedges, the maximum content of $Na^+ + K^+$ cations is noted (22.8 mg/L). We also note three rhythms that stand out in the distribution of sulfate ion, potassium and sodium ions content. The relatively high content of sulfate ion comparing to chloride ion indicates a high degree of the climate continentality during the period of ice wedges formation.

Oxygen isotope composition of ice wedges. On the oxygen isotope diagrams for thick wedges (Fig. 5) the range of the $\delta^{18}O$ values (from –34.1 to –29.4 ‰) is comparatively large. The data on the buried wedges located at a depth of 7 m lie within the range of –30.5 to –29.1 ‰ (Table 4, point 341-YuV).

In isotopic terms, ground ice in the host sediments is slightly heavier than wedge ice; the $\delta^{18}O$ values in it vary from –30.6 to –27.0 ‰ [*Vasil'chuk, 1992*]. That ratio of isotopic characteristics does not contradict the hypothesis of the lacustrine origin of yedoma on the slope of the Kolyma River valley.

In veinlets at the Kolyma River floodplain near Zelyony Mys the $\delta^{18}O$ values vary from –26.1 to –23.0 ‰, while in segregated and pore ice of the floodplain alluvium the $\delta^{18}O$ values range from –23.0 to –19.1 ‰; i.e., the Pleistocene wedges are almost by 8 ‰ lighter than modern ones, and the segregated and pore ice, as a rule, is by 4–5 ‰ lighter them.

Table 4. **$\delta^{18}O$ values in the Late Pleistocene ice wedges (IW), segregated and pore ice (I) in the Zelyony Mys section, right bank in the lower reaches of the Kolyma River and in veinlets (V) on the floodplain**

Sample ID	Depth, m	$\delta^{18}O$, ‰	Ice type	Sample ID	Depth, m	$\delta^{18}O$, ‰	Ice type
Syngenetic Late Pleistocene ice wedges in Zelyony Mys yedoma							
308-YuV/49	0.5	–30.3	IW	308-YuV/48	15.5	–34.1	IW
308-YuV/50	1.0	–31.3	IW	308-YuV/5	15.6	–30.9	IW
308-YuV/51	2.0	–31.3	IW	308-YuV/6	15.7	–30.7	IW
308-YuV/54	7.0	–30.9	IW	308-YuV/7	16.3	–30.7	IW
341-YuV/51	7.0	–30.5	IW	308-YuV/8	17.0	–30.6	IW
341-YuV/52	7.0	–30.0	IW	308-YuV/9	17.6	–31.2	IW
341-YuV/53	7.0	–29.1	IW	308-YuV/10	18.3	–31.5	IW
341-YuV/54	7.0	–30.2	IW	308-YuV/37	18.7	–31.4	IW
308-YuV/55	8.0	–32.8	IW	308-YuV/12	19.7	–31.1	IW
308-YuV/56	8.5	–30.3	IW	308-YuV/13	20.6	–31.4	IW
308-YuV/40	9.5	–29.4	IW	308-YuV/14	21.5	–31.6	IW
308-YuV/41	9.8	–30.4	IW	308-YuV/16	23.5	–32.4	IW
308-YuV/42	10.2	–29.9	IW	308-YuV/17	24.3	–31.3	IW
308-YuV/43	11.6	–30.7	IW	308-YuV/18	24.9	–29.2	IW
308-YuV/44	13.4	–31.0	IW	341-YuV/40	35.0	–30.2	IW
308-YuV/45	14.0	–31.1	IW				
Syngenetic segregated and pore ice in Zelyony Mys yedoma							
341-YuV/8	10.0	–30.6	I	341-YuV/1	10.9	–27.0	I
341-YuV/4	10.7	–27.6	I	341-YuV/36	33.2	–29.6	I
Veinlet penetrating into Holocene ice wedges at Kolyma floodplain near Zelyony Mys							
15-TYa/2	0.7	–25.6	V	15-TYa/3	0.8	–25.4	V
Veinlets penetrating into Holocene ice wedges at the floodplain on Ambolikha channel near Chersky							
9-TYa/1	0.4	–23.0	V	7-TYa/1a	0.5	–24.0	V
7-TYa/1	0.5	–24.1	V	8-TYa/1	0.5	–26.1	V

DISCUSSION

Radiocarbon age of the yedoma sediments and ice wedges. Based on a set of ^{14}C dates, the period of the Zelyony Mys yedoma formation lasted about 33 ka, i.e., between 48 and 15 cal ka BP. The lower limit of the yedoma strata formation has been recorded by three dates of large branches and vertebrate bones (mammoth, bison; Table 1); and the upper limit has been determined by the ^{14}C dating out of the buried soil sampled by A. Pfeffer close to the permafrost top – 15.7 cal ka BP (Table 1), and by the AMS dating of material obtained directly out of ice wedge – 16.4 cal ka BP (Table 2).

The dates of 35.2, 28.2, and 27.2 ka BP (39.8, 32.1, and 31.1 cal ka BP), – obtained for peaty layers of the yedoma exposed 8 m above the water level on the right bank of the Kolyma River, in Chersky area [*Lozhkin, 1977*], – are in good agreement with the chronology proposed by the authors.

For correct dating, the data on seed in buried burrows of ground squirrels are also important, since these dates have been obtained from obviously synchronous organic material. Such findings testify the cyclic variable subaqual-subaerial genesis of the syngenetic ice-wedge complexes. The dates from the Zelyony Mys yedoma burrows (37.2 and 38.4 cal ka BP [*Zanina, 2005*]) indicate the subaerial phase of the terrain development when the ice wedges were actively growing in width.

Based on the model of the cyclical process of the syngenetic formation of thick ice wedges [*Vasil'chuk, 1999*], it is possible to estimate the ratio of the time duration of the subaqueous and subaerial conditions, i.e., the periods when the layers of almost organic-free sandy loam were accumulated and the periods of peat accumulation or the formation of soil horizons (Fig. 5). At the same time, under subaerial conditions, the wedges increased in width, and at the stage of subaqueous sedimentation, the growth of the wedges slowed down or stopped, as evidenced by small buried veins. Heads of veins lie at the level of the lower peat layer at 25 m depth and similar small wedges are found on the level of the soil horizon with heads at a depth of 3 m. Evaluating the series of the ^{14}C dates, we note that at the yedoma section base, the branches of large shrubs, dated 49–45 cal ka BP are often found, as well as plant remains and bones with dates beyond the limit of radiocarbon method. The overlying peat layer fix the time of subaerial phase and is dated to 44.4–41.9 cal ka BP.

It is obvious that a layer of gray-brown sandy loam has been accumulated rather quickly, which is typical of the subaquatic phase. The next subaerial phase can be distinguished not only by the dates of the roots washed up from a layer with a high concentration of organic matter (38.2 cal ka BP), but also by the dates of seeds from ground squirrel burrows (34.8 and 37.3 cal ka BP). The third pronounced organic layer (fixing the next subaerial phase) is dated by the roots 32.2 and 32.9 cal ka BP. Those data are in good agreement with dating of Stanchikovskiy Yar yedoma [*Gubin, Zanina, 2013*], which is also located on the right bank of the Kolyma River near the Zelyony Mys section. There are three layers with a high content of plant residues. The lowest layer and the middle one are dated from 49.9 to 41.8 and from 41.7 to 38.3 cal ka BP, respectively. The upper layer with a high organic content is dated at 32.2–31.5 cal ka BP.

During the period yedoma accumulation at Zelyony Mys and Stanchikovsky Yar there were at least three subaerial phases lasted 2–3 ka. The sediments of subaquatic phases clearly predominate, but that is not due to the duration of sedimentation, but owing to its greater intensity. During the subaqueous phase the same amount of sediment accumulates 2–3 times faster than in the subaerial phase.

Variations of $\delta^{18}O$ values in ice wedges for the period of yedoma formation. A characteristic feature of the isotope diagram of ice wedges of Zelyony Mys is extremely low $\delta^{18}O$ values, especially in the lower parts of ice wedges (Fig. 5). This probably indicate extremely severe (even for cold winters of the Late Pleistocene) winter conditions in that region.

The isotopic composition of ice wedges at the level of the lower peat layer is characterized by the $\delta^{18}O$ values of –31.3 to –29.2 ‰. The $\delta^{18}O$ values in ice wedges at a depth of 16–17 m at the level of the middle layer vary slightly from –31.2 to –30.7 ‰. The minimum $\delta^{18}O$ values for the section (–34.1 ‰) have been obtained at a depth of 15.5 m. A local minimum of the $\delta^{18}O$ values (–32.8 ‰) has also been obtained at a depth of 8 m. Thus, three cycles can be distinguished in the isotopic composition of ice wedges. After an increase of $\delta^{18}O$ values (up to –29 and –30 ‰), a sharp drop is noted (up to –32 or even up to –34 ‰), indicating a significant winter cooling 46–41 cal ka BP and 38–32 cal ka BP. The time of the third cycle can be determined only indirectly, approximately as 24–22 cal ka BP.

In 2005 D.V. Mikhalev et al. [*2012*] had sampled the remaining unexposed upper eight-meter part of Zelyony Mys yedoma and had obtained the $\delta^{18}O$ values of –32.5 to –31.2 ‰ (close to those obtained by us in the upper part), and the $\delta^{2}H$ values of – 248.5 to –240.2 ‰.

At Chersky settlement on the right bank in the lower reaches of the Kolyma River (68.7592° N, 161.3325° E) Yu.K. Vasilchuk and N.A. Budantseva [*2018*] have investigated residual yedoma outcrop preserved within the settlement 300 m downstream the pier. Here the yedoma inset into pre-Pleistocene rocks. The deposits are dark-gray sandy loam with a low organic content. The outcrop is 20–25 m high. Ice wedges are exposed at the depth of 1.0–1.5 m. The age of the ice wedge can be approximately estimated

Table 5. **Mean January air temperature (t_J) in the northwest of Yakutia for the period between 47 and 12 cal ka BP reconstructed based on oxygen isotope composition of ice wedges ($\delta^{18}O_{IW}$)**

The name of reference section	Coordinates	$\delta^{18}O_{IW}$, ‰		t_J, °C		Source
		Paleo	Current	Paleo	Current	
1	2	3	4	5	6	7
47–42 cal ka BP						
Zelyony Mys	68.7875° N, 161.3806° E	–30.2	–25.5	–45	–36	This article
Duvanny Yar	68.6000° N, 159.1000° E	–31.9	–25.1	**–48**	–35	[*Vasil'chuk et al., 2001*]
Kotelny Island	74.2778° N, 147.6059° E	–29.5	–18.0	–44	–29	[*Vasil'chuk et al., 2019*]
Oyogos Yar	72.6775° N, 143.5550° E	–29.5	–24.4	–44	–30.4	[*Opel et al., 2017*]
Bolshoy Lyakhovsky Island	73.3333° N, 141.6667° E	–30.0	–20.4	–45	–31	[*Meyer et al., 2002*]
Mamontova Khayata	71.7695° N, 129.4547° E	–30.2	–23.0	–45	–31	[*Meyer et al., 2002; Wetterich et al., 2011*]
Kurungnakh Island	72.3282° N, 126.2843° E	–31.8	–24.6	**–48**	–34.3	[*Schirrmeister et al., 2003*]
Kular	70.6333° N, 131.8833° E	–31.0	–25.0	–46	–37	[*Vasil'chuk, Vasil'chuk, 2020*]
37–32 cal ka BP						
Zelyony Mys	68.7875° N, 161.3806° E	–33.0	–25.5	**–49**	–36	This article
Duvanny Yar	68.6000° N, 159.1000° E	–32.0	–25.1	–48	–35	[*Vasil'chuk et al., 2001*]
Bison	68.6250° N, 159.2894° E	–32.0	–26.0	–48	–35	[*Vasil'chuk et al., 2003*]
Kotelny Island	74.2778° N, 147.6059° E	–29.0	–18.0	–43	–29	[*Vasil'chuk et al., 2019*]
Mamontova Khayata	71.7695° N, 129.4547° E	–31.0	–23.0	–46	–33	[*Meyer et al., 2002*]
30–25 cal ka BP						
Zelyony Mys	68.7875° N, 161.3806° E	–30.2	–25.5	–45	–36	This article
Duvanny Yar	68.6000° N, 159.1000° E	–31.9	–25.1	–48	–35	[*Vasil'chuk et al., 2001*]
Bison	68.6250° N, 159.2894° E	–33.0	–26.0	–49	–35	[*Vasil'chuk et al., 2003*]
Plakhinskii Yar	68.6788° N, 160.2852° E	–34.8	–25.8	**–51**	–35	[*Vasil'chuk, Vasil'chuk, 2018*]
Kotelny Island	74.2778° N, 147.6059° E	–29.0	–18.0	–43	–29	[*Vasil'chuk et al., 2019*]
Mamontov Klyk	73.6072° N, 117.1250° E	–30.0	–21.3	–45	–33	[*Schirrmeister et al., 2008*]
Mamontova Khayata	71.7695° N, 129.4547° E	–31.0	–23.0	–46	–33	[*Meyer et al., 2002*]
Buor-Khaya	72.3333° N, 126.2833° E	–31.0	–23.0	–45	–34	[*Schirrmeister et al., 2003*]
Kular	70.6333° N, 131.8833° E	–32.0	–26.0	–47	–37	[*Vasil'chuk, Vasil'chuk, 2020*]
24–22 cal ka BP						
Zelyony Mys	68.7875° N, 161.3806° E	–30.4	–25.5	–45	–36	This article
Duvanny Yar	68.6000° N, 159.1000° E	–32.2	–25.1	**–48**	–35	[*Vasil'chuk et al., 2001*]

Table 5, continued

1	2	3	4	5	6	7
Plakhinskii Yar	68.6788° N, 160.2852° E	–31.6	–25.8	–47	–35	[*Vasil'chuk, Vasil'chuk, 2018*]
Kotelny Island	74.2778° N, 147.6059° E	–25.0	–18.0	–37	–29	[*Vasil'chuk et al., 2019*]
Mamontova Khayata	71.7695° N, 129.4547° E	–29.5	–23.0	–44	–33	[*Meyer et al., 2002*]
20–18 cal ka BP						
Zelyony Mys	68.7875° N, 161.3806° E	–31.6	–25.5	–47	–36	This article
Duvanny Yar	68.6000° N, 159.1000° E	–30.5	–25.1	–46	–35	[*Vasil'chuk et al., 2001*]
Plakhinskii Yar	68.6788° N, 160.2852° E	–32.0	–25.8	**–48**	–35	[*Vasil'chuk, Vasil'chuk, 2018*]
Kotelny Island	74.2778° N, 147.6059° E	–25.0	–18.0	–37	–29	[*Vasil'chuk et al., 2019*]
16–12 cal ka BP						
Zelyony Mys	68.7875° N, 161.3806° E	–30.7	–25.5	–45	–36	This article
Duvanny Yar	68.6000° N, 159.1000° E	–31.0	–25.1	**–46**	–35	[*Vasil'chuk et al., 2001*]
Plakhinskii Yar	68.6788° N, 160.2852° E	–31.0	–25.8	**–46**	–35	[*Vasil'chuk, Vasil'chuk, 2018*]

N o t e: extremely low values for each period are shown in bold.

based on radiocarbon dates obtained by B.G. Miller (as he describes 'out of a 10–15 m terrace on the right bank of the Kolyma River'). Two dates have been obtained here: 33 900 ± 500 years (RI-111) for poorly decomposed peat with herbaceous inclusions and, down the section, 38 700 ± 700 years (RI-115) for poorly decomposed peat [*Veksler, Prede, 1985*]. Ice wedges are relatively narrow, not more than 1 m wide. For the best-exposed ice wedge at a depth of 1.5 to 4 m, the $\delta^{18}O$ values variations have been analyzed. The calculation using the formula of Yu.K. Vasil'chuk, allows us to say that at Chersky area at the end of the Pleistocene the mean air temperature of the coldest winter month (January or February) varied from –47 to –49 °C (Table 5).

Mean January air temperature during yedoma formation. The authors have reconstructed the mean January air temperature (t°_{J}) by the sections of the lower reaches of the Kolyma River. The reconstruction was based on a comparison of the isotopic composition of veinlets ($\delta^{18}O_{IV}$) and the modern mean January air temperature for the period of ice wedge formation, i.e., the for the last 60–100 years [*Vasil'chuk, 1991, 1992*]. As a result, the equation has been obtained:

$$t^{\circ}_{J} = 1.5 \cdot \delta^{18}O_{IV} \left(\pm 3\,^{\circ}C\right).$$

A range of ±3 °C indicates the average range of variations in the reconstructed temperature within the analyzed time interval.

According to the above-given equation, the mean January air temperature of the Late Pleistocene (48–15 cal ka BP) has been calculated for certain periods for key sections in the lower reaches of the Kolyma River (Table 5).

For the period of 47–42 cal ka BP, the lowest air January temperature is noted for the region of Duvanny Yar (–48 °C). Equally low temperatures were at the Kurungnah Island during that period. At Zelyony Mys section of the Kolyma valley the mean January air temperature was lower than –45 °C (Table 5). Later, 37–32 cal ka BP, the mean January air temperature dropped to –49 °C in the Zelyony Mys area. Further to the north, for example, on the Kotelny Island, the mean January air temperature during that period did not exceed –43 °C. Between 30 and 25 cal ka BP the mean January air temperature in Zelyony Mys area was –45 °C, and in Plakhinskii Yar area decreased to –51 °C. In the period of 24–22 cal ka BP, the mean January air temperature in the Kolyma valley did not change compared to the previous interval: in the Zelyony Mys region it was –45 °C, and in the Duvanny Yar region it was –48 °C (Table 5). For the period between 20 and 18 cal ka BP the lowest mean January air temperatures in the Kolyma River valley have been recorded for Plakhinskii Yar, Duvanny Yar, and Zelyony Mys areas: –48 °C, slightly above –46 and –47 °C, correspondingly. I.e., these temperatures are not the coldest. For Kotelny Island, the reconstructed mean January air temperature is

noticeably higher than –37 °C. In the period of 16–12 cal ka BP the mean January air temperature in the Kolyma River valley remained low in the areas of Zelyony Mys (–45 °C), Duvanny Yar and Plakhinskii Yar (–46 °C).

Isotope data demonstrate that mean January air temperatures in the coldest epochs were by 12–15 °C lower than current ones and ranged from –48 to –51 °C, and in periods with less severe conditions varied from –40 to –45 °C.

CONCLUSIONS

The cyclical structure of the Zelyony Mys yedoma and the cyclic change in the conditions of ice wedges formation have been confirmed; subaquatic and subaerial stages of accumulation of yedoma sediments and ice wedges have been identified.

Zelyony Mys outcrop in the lower reaches of the Kolyma River represents three or two levels of wide Late Pleistocene ice wedges and buried narrow ice veins fixing the stages of yedoma formation.

The age of Zelyony Mys yedoma has been established: the beginning and completion of the yedoma accumulation date back correspondingly to 48 and 15 cal ka BP.

In Zelyony Mys section, three cycles of the change in the isotopic composition of ice wedges have been identified: 46–41 cal ka BP, 37–32 cal ka BP, and approximately 24–22 cal ka BP.

Comparison with isotopic composition of ice wedges in the yedoma reference sections of Plakhinskii Yar, Duvanny Yar, Stanchikovsky Yar, Chersky and others allow us to conclude that the winters in the lower reaches of the Kolyma River at the end of the Late Pleistocene cryochron, were significantly more severe than modern ones.

The lowest mean January air temperature (by 15 °C lower than modern ones) in the lower reaches of the Kolyma River has been obtained by the authors for the period of 37 to 25 cal ka BP, which corresponds to a decrease in temperature on a global scale.

The work has been carried out with the financial support of the Russian Foundation for Basic Research (grant 18-05-60272-Arctic, isotope measurements and analysis of isotope and radiocarbon data), the Russian Science Foundation (grant 19-17-00126, generalization of the results).

References

Davydov, S.P., Fyodorov-Davydov, D.G., Neff, J.C., et al., 2008. Changes in Active Layer Thickness and Seasonal Fluxes of Dissolved Organic Carbon as a Possible Baseline for Permafrost Monitoring. In: Proceedings of Ninth International Conference on Permafrost, vol. 2, pp. 333–336.

Fyodorov-Davydov, D.G., Sorokovikov, V.A.,Ostroumov, V.E., et al., 2004. Spatial and temporal observations of seasonal thaw in the Northern Kolyma Lowland. Polar Geography 28 (4), 308–325.

Gubin, S.V., Lupachev, A.V., 2008. Soil formation and the underlying permafrost. Eurasian Soil Science 41, 574–585.

Gubin, S.V., Zanina, O.G, 2013. Variation of soil cover during the Ice Complex deposit formation, Kolyma Lowland (Part 1). Kriosfera Zemli (Earth's Cryosphere), XVII (4), 48–56.

Kozhevnikov, Yu.P., 1981. Botanical-geographical observations in the Kolyma in areas of the middle Berezovka River and Chersky. In: Biology and ecology of plants in the Kolyma basin. Far East Scientific Center of the Academy of Sciences of the USSR, Vladivostok, pp. 99–117 (in Russian).

Lozhkin, A.V., 1977. Radiocarbon dates of the Upper Pleistocene deposits on the New Siberian Islands and the age of the yedoma suite of the North-Eastern USSR. Reports of the USSR Academy of Sciences (Doklady Academii Nauk SSSR), 235, 435–437.

Meyer, H., Derevyagin, A.Yu., Siegert, C., Hubberten, H.-W., 2002. Palaeoclimate studies on Bykovsky Peninsula, North Siberia – hydrogen and oxygen isotopes in ground ice. Polarforschung 70, 37–51.

Mikhalev, D.V., Nikolayev, V.I., Romanenko, F.A., 2012. Reconstruction of the conditions of underground ice formation within the Kolyma Lowland during the Late Pleistocene-Holocene using the results of isotope investigations. Vestnik Moskovskogo Universiteta. Seria 5, Geografia (Moscow University Bulletin. Series 5, Geography), No. 5, 35–42.

Murzin, Yu.A., Torgovkin, Ya.I., 1984. New outcrop of the Ice Complex in the lower Kolyma River valley. In: Cryogenic processes and phenomena in Siberia. Permafrost Institute Publishing House, Yakutsk, pp. 119–127 (in Russian).

Opel, T., Wetterich, S., Meyer, H., et al., 2017. Ground-ice stable isotopes and cryostratigraphy reflect late Quaternary palaeoclimate in the Northeast Siberian Arctic (Oyogos Yar coast, Dmitry Laptev Strait). Climate of the Past 13, 587–611.

Ramsey, C., 2009. Bayesian Analysis of Radiocarbon Dates. Radiocarbon 51 (1), 337–360.

Reimer, P.J., Bard, E., Bayliss, A., et al., 2013. IntCal13 and marine13 radiocarbon age calibration curves 0–50 000 years cal BP. Radiocarbon 55, 1869–1887.

Romanovsky, V.E., Drozdov, D.S., Oberman, N.G., et al., 2010. Thermal state of permafrost in Russia. Permafrost and Periglacial Processes 21, 136–155.

Schirrmeister, L., Grosse, G., Schwamborn, G., et al., 2003. Late Quaternary history of the accumulation plain north of the Chekanovsky Ridge (Lena Delta, Russia): a multidisciplinary approach. Polar Geography 27 (4), 277–319.

Schirrmeister, L., Grosse, G., Kunitsky, V., et al., 2008. Periglacial landscape evolution and environmental changes of Arctic lowland areas for the last 60 000 years (western Laptev Sea coast, Cape Mamontov Klyk). Polar Research 27, 249–272, DOI: 10.1111/j.1751-8369.2008.00067.x.

Vasil'chuk, Yu.K., 1991. Reconstruction of the palaeoclimate of the Late Pleistocene and Holocene of the basis of isotope studies of subsurface ice and waters of the permafrost zone. Water Resources 17 (6), 640–647.

Vasil'chuk, Yu.K., 1992. Oxygen Isotope Composition of Ground Ice (Application to Paleogeocryological Reconstructions). Department of Theoretical Problems of the RAS, Moscow University, Research Institute of Engineering for Construction (PNIIIS), Moscow, Book 1, 420 pp., Book 2, 264 pp. (in Russian).

Vasil'chuk, Yu.K., 1999. The model of cyclic-pulsing formation of syngenetic permafrost with large ice wedges. Kriosfera Zemli (Earth's Cryosphere), III (2), 50–61.

Vasil'chuk, Yu.K., Budantseva, N.A., 2018. Stable oxygen isotopes in new sections of the yedoma and Holocene sediments of Chersky, the lower Kolyma River. Arktika i Antarktika (Arctic and Antarctic), No. 3, 95–106, DOIi: 10.7256/2453-8922.2018.3.27600.

Vasil'chuk, Yu.K., Makeev, V.M., Maslakov, A.A., et al., 2019. Late Pleistocene and Early Holocene winter air temperatures in Kotelny Island: reconstructions using stable isotopes of ice wedges. Earth's Cryosphere (Kriosfera Zemli), XXIII (2), 12–24.

Vasil'chuk, Yu.K., Vasil'chuk, A.C., 2018. Winter air paleotemperatures at 30–12 ka BP in the lower Kolyma River, Plakhinskii Yar yedoma: evidence from stable isotopes. Kriosfera Zemli (Earth's Cryosphere), XXII (5), 3–16, DOI: 10.21782/EC2541-9994-2018-5(3-16).

Vasil'chuk, Yu.K., Vasil'chuk, A.C., 2020. Isotope-geochemical composition of the ice wedges in the slope yedoma on the Kular Ridge and reconstruction of the mean January air paleotemperature during 47,000–25,000 BP. Earth's Cryosphere (Kriosfera Zemli), XXIV (3), 22–33.

Vasil'chuk, Yu.K., Vasil'chuk, A.C., Kim, J.C., 2003. The AMS radiocarbon dating of pollen concentrate from the Late Pleistocene ice wedges of the Bison section, Kolyma Region. Bulletin of Earth Sciences 393 (8), 1141–1145.

Vasil'chuk, Yu.K., Vasil'chuk, A.C., van der Plicht, J., et al., 2001. Radiocarbon dating of the Late Pleistocene ice wedges in the Bison section in the lower reaches of the Kolyma River. Bulletin of Earth Sciences 379 (5), 589–593.

Vasil'chuk, Yu.K., Yesikov, A.D., Oprunenko, Yu.F., et al., 1985. New data of stable oxygen isotopes composition in syngenetic Late Pleistocene ice wedge of the lower Kolyma River. Transactions (Doklady) of the USSR Academy of Sciences. Earth Science Sections. Published by Scripta Technica, Inc. A Wiley Company. New York, vol. 281 (2), pp. 91–94.

Veksler, V.S., Prede, E.I., 1985. Radiocarbon datings made at the laboratory of marine soil analytical studies of VMNPO "Soyuzmorinzhgeologiya", report IV. Commission for Study of the Quaternary Bulletin. Nauka, Moscow, pp. 131–133 (in Russian).

Wetterich, S., Rudaya, N., Tumskoy, V., et al., 2011. Last Glacial Maximum records in permafrost of the East Siberian Arctic. Quaternary Science Reviews, vol. 30, 3139–3151. – https://doi.org/10.1016/j.quascirev.2011.07.020.

Zanina, O.G., 2005. Fossil rodent burrows in frozen Late Pleistocene beds of the Kolyma Lowland. Entomological Review, 85 (1), S133–S140.

Zanina O.G., Lopatina, D.A., 2017. The possibilities of reconstructing the composition of vegetation communities on the basis of conjugated palynological, phytolith and carpological analyses for Kolyma River lower course area. Earth's Cryosphere (Kriosfera Zemli), XXI (3), 12–22.

URL: www.pogoda.klimat.ru, 2020 (last visited: 28.06.2020).

Received May 27, 2020
Revised version received November 30, 2020
Accepted December 23, 2020

Kriosfera Zemli, 2021, vol. XXV, No. 2, pp. 56–67

ABOUT THE INCORRECTNESS OF YU.K. VASIL'CHUK'S METHOD FOR THE RECONSTRUCTION OF PALEOTEMPERATURES USING ISOTOPE COMPOSITION OF WEDGE ICE

Review of the article by Yu.K. Vasil'chuk, A.C. Vasil'chuk "Air January paleotemperature reconstruction 48–15 calibrated ka BP using oxygen isotope ratios from Zelyony Mys Yedoma"

A.A. Galanin

Melnikov Permafrost Institute, Siberian Branch of the Russian Academy of Sciences, Merzlotnaya str. 36, Yakutsk, 677010, Russia; agalanin@gmail.com

It has been revealed that methodological techniques and formulas developed and widely used by Yu.K. Vasil'chuk for the reconstruction of average January air temperatures ($t_J = 1.5 \cdot \delta^{18}O$), the sum of winter negative air temperatures ($\Sigma t_w = 250 \cdot \delta^{18}O$), as well as average winter air temperatures ($t_w = \delta^{18}O$) based on the oxygen isotope composition of ice wedges are incorrect, and the paleoclimatic reconstructions obtained from these formulas are unreliable.

Key words: *stable isotopes* ^{18}O *and* D, *ice wedges, reconstruction of paleotemperatures, Pleistocene, Holocene, permafrost.*

INTRODUCTION

The first attempts to use water isotope composition of wedge ice for the assessment of paleotemperatures had been making since the 1970s. Initially, they generated a lot of interest and lively discussion. However, in 1980–1990 many researchers had come to the conclusion that the use of ice wedges as a source of paleotemperature information has many limitations [*Arkhangelov et al., 1987; Konyakhin, 1988; Vasil'chuk, 1990, 1991; Golubev et al., 2001*]. The formation of the isotope composition of wedge ice depends not only on climatic factors, but also on local growth conditions, which are currently not possible to take into account. Therefore, in most modern publications, the isotope composition of ice wedges is interpreted primarily on a qualitative rather than quantitative level [*Meyer et al., 2002, 2015; Schirrmeister et al., 2003; Derevyagin et al., 2010; Wetterich et al., 2011; Boereboom et al., 2013*].

Yu.K. Vasil'chuk is a renowned expert in the study of the isotope composition of various types of natural ice, and since the 1990s to the present, has published many works in that area. In the article reviewed here, the issues of using the oxygen isotope composition of ice wedges for quantitative paleoclimatic reconstructions of the second half of the Late Pleistocene in the lower Kolyma basin are considered. In it, the author uses several previously derived formulas [*Vasil'chuk, 1990, 1991; Vasil'chuk, Vasi'lchuk, 2017, 2018; and many others*], which, in his opinion, functionally relate the $\delta^{18}O$ values (‰) in ice wedges and air paleotemperature. For the mean January air temperatures that dependence has the form of

$$t_J = 1.5 \cdot \delta^{18}O, \quad (1)$$

for the sum of negative winter air temperatures it looks like

$$\Sigma t_w = 250 \cdot \delta^{18}O, \quad (2)$$

and for the mean winter air temperature it is

$$t_w = \delta^{18}O. \quad (3)$$

As follows from the formulas (1)–(3), the mean winter air temperature is numerically equal to $\delta^{18}O$ value, the January air temperature is one and a half times higher than $\delta^{18}O$ value, and the sum of winter negative air temperatures is 250 times higher than it. It is not only the simplicity of the dependences used by the author to describe a very complex multifactorial system for the formation of isotope compositions of ice wedges that raises doubts, but also the fact that all reconstructed temperatures are interconnected by simple linear equations and can be easily derived from each other. So, with a simple substitution of the formula (3) into the formula (1), it turns out that $t_J = 1.5 \cdot t_w$. According to the formulas of Yu.K. Vasil'chuk, the mean January air temperature is one and a half times lower than the mean winter air temperature. The same applies to the sum of negative winter air temperatures, which can be deduced from the mean winter air temperature or January air temperature. The reviewer believes that such consequences, which directly follow from formulas (1)–(3), completely contradict the results of current meteorological observations and the basic principles of climatology, they call into question the correctness of that method.

The aim of this article is to discuss the validity of of Yu.K. Vasil'chuk's methodology used in peer-re-

viewed articles and many other publications of the author [*Vasil'chuk, 1990, 1991; Vasil'chuk, Vasil'chuk, 2017; Vasil'chuk et al., 2019a,b*]. For this, initial data from methodological publications of Yu.K. Vasil'chuk, as well as key results of Russian and international research in that area, have been analyzed.

Some theoretical aspects of using ice wedge isotopic composition as paleoclimatic indicator

To assess the applicability of the methodology used by Yu.K. Vasil'chuk [*Vasil'chuk, 1990, 1991, 1992*], several basing theoretical assumptions of the use of ice wedges isotope composition as paleotemperature indicator should be highlighted. The first assumption is that the isotopic composition of ice wedges is formed out of the melted snow cover waters, which flow and refreeze in frost cracks. The second assumption is that the isotope composition of the snow cover is initially related to air temperature and reconstructed paleoclimatic characteristics; this relationship is reliably established for the study area. The third assumption is that the isotopic composition of atmospheric precipitation has not undergone significant fractionation (change) during the formation of the snow cover, its thawing and refreezing in frost cracks.

It is obvious that the correct use of wedge ice isotope compositions as paleoclimatic indicators provides for a continuous discussion of the results obtained within these assumptions when interpreting reconstructed paleotemperatures. Otherwise, the reliability of these results is highly questionable.

The first assumption concerns the hypothesis of the origin of syngenetic Late Pleistocene ice wedges widespread in the loess-ice (yedoma) sediments of the Arctic and Subarctic. According to this hypothesis, ice wedges grow due to systematic opening of the frost cracks in winter. During the warm period, melted snow water flows into vertical frost cracks and quickly refreezes there. That process is repeated from year to year and leads to an increase in ice wedges in width and height. The hypothesis is supported by most of modern researchers [*Meyer et al., 2002; Schirrmeister et al., 2003*], including Yu.K. Vasil'chuk [*1992*], and is not criticized here either. This formation mechanism is clearly confirmed by thin vertical banding and a very light isotopic composition. In general, it follows that ice wedges belong to the congelation type of ice formed by the freezing of snow meltwater. The elementary (annual) ice veins that make up ice wedges have different ages and different isotope compositions, which is associated with the short-period and long-period variations in the atmospheric air temperature during snowfall.

The vertical 'stratification' of ice wedges and the inability to predict where the next ice vein will form represent the most serious and almost unsolvable problems of using wedge ice for detailed paleoclimatic reconstructions [*Meyer et al., 2002*]. The available data on the absolute age of ice wedges and host sediments demonstrates that their formation took place over thousands and tens of thousands years under conditions of significant climatic fluctuations. In addition, in many cases, ice is significantly younger than the host sediments at the same elevation level, which is reflected in a wider variation in wedge ice isotopic composition in horizontal transects than in the vertical transects. At the same time, the age and isotopic composition of ice in the upper and lower parts of the wedge may turn out to be the same, which is why it is recommended to sample ice across the wedges.

All well-known specialists in this field point out to crucial importance of the sampling strategy in studying the isotope composition of ice wedges [*Meyer et al., 2002, 2015; Schirrmeister et al., 2003; Derevyagin et al., 2010; Wetterich et al., 2011; Boereboom et al., 2013*]. Thus, in the article by H. Meyer and colleagues [*Meyer et al., 2002*] devoted to the study of the isotope composition of ice wedges of the Bykovsky Peninsula, there is a special paragraph 'Sampling strategy', where the authors state: 'Stable isotopes of vertical transects of ice wedges show up to four times lower standard deviations than horizontal transects, because vertical sampling is carried out along the cracking direction (following one vein). Therefore, a randomly sampled vertical profile does not necessarily reflect climatic trends'. This article is cited in the peer-reviewed manuscript by Yu.K. Vasil'chuk, but the author does not comment on the conclusion of his colleagues on wedge ice sampling strategy.

Indeed, as further concludes H. Meyer and colleagues [*Meyer et al., 2002*], the variation in the isotopic composition of wedges in horizontal transect is much more significant (Fig. 1). The absence of a vertical plane of symmetry in the $\delta^{18}O$ variation graph (Fig. 1, *b*) indicates that ice wedge did not grow symmetrically, but by adding new ice veins, predominantly on the left side. As the wedge grew, the oxygen isotopic composition of ice changed almost one and a half times, from 32 to 24 ‰. That indicates significant changes in climatic conditions and the isotopic composition of the snow cover during the formation of ice wedges.

In the manuscript under review, Yu.K. Vasil'chuk, as in many of his publications, sampling has been performed along a vertical transect (see p. 49 of this issue, Fig. 5 of reviewed article). According to the concepts of wedge ice structure and formation mechanism considered above, these samples may represent some group of ice veins of a similar age. That assumption is fully confirmed by the absence of any regular changes in the oxygen isotopic composition in the vertical profile of the wedge. Single deviations are statistically insignificant and cannot be considered as

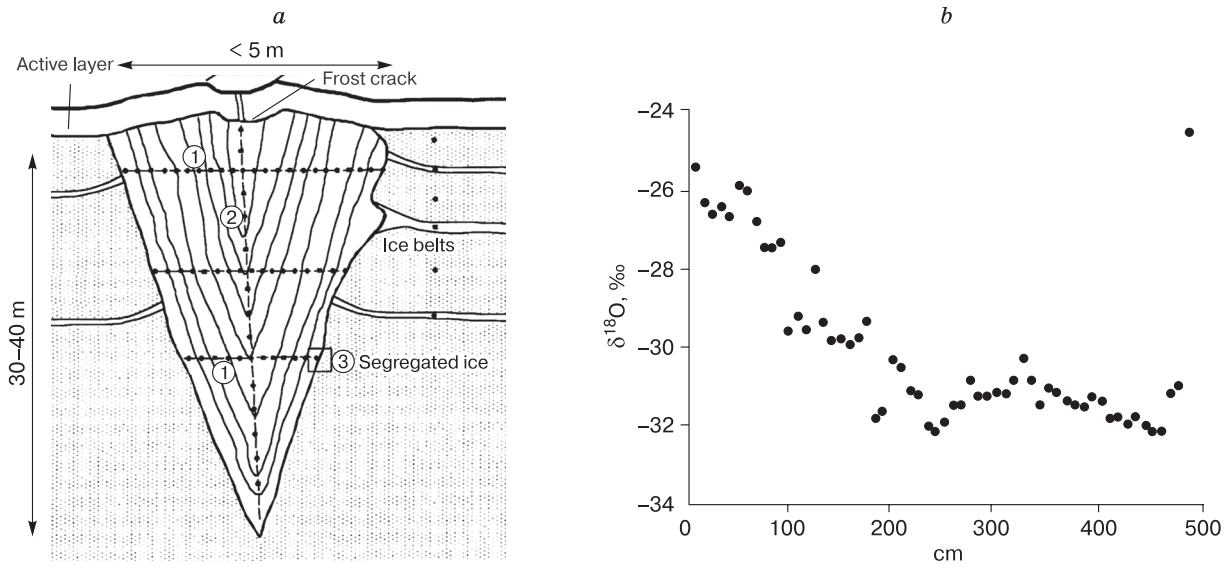

Fig. 1. Recommended sampling strategy for studying ice wedge isotope composition (*a*) and variation of $\delta^{18}O$ value across an ice wedge about 5 m wide along transect 1 (*b*), Bykovsky Peninsula, according to [*Meyer et al., 2002*].

a: black dots are sampling points; the numbers in circles: 1 – horizontal transect; 2 – vertical transect; 3 – exchange processes between ice wedge and segregated ice.

climatic events; moreover, they are very small and can be caused by changes in local conditions.

With this sampling method most of the samples fall into a narrow set of ice veins of a similar age, while the composition of the lateral and possibly more ancient parts of ice wedges remains unknown. Insignificant variation within the range of 30–32 ‰ and single deviations of the $\delta^{18}O$ values are rather random and cannot be considered as climatic events. In general, direct assessment of climate trends can't be made based on the vertical variation of the $\delta^{18}O$ values.

The second assumption, lying in the base of the use of ^{18}O and D as temperature indicators, is the fundamental dependence of the isotopic composition of atmospheric precipitation on its condensation temperature [*Craig, 1961; Dansgaard, 1964; Clark, Fritz, 1997*]. This dependence is substantiated by W. Dansgaard [*1964*] using a large amount of data. During condensation of atmospheric water vapor into ice (snow) in the temperature range of $-30\ ^\circ C < t < 0\ ^\circ C$, the isotopic composition of the condensate (ice, snow) is approximately described by the equations $\delta^{18}O = 0.68t - 13.6$ and $\delta D = 5.6t - 100$. The $\delta^{18}O$ and δD values are here expressed in permille (‰), and the temperature t is expressed in centigrade (°C). In very cold regions with low condensation temperatures of atmospheric vapor (−20 to −40 °C) the slopes of the equations for $\delta^{18}O$ and δD decrease to 0.58 and 4.5, respectively [*Dansgaard, 1964*].

Thus, the isotopic composition of the snow falling in winter depends on the air temperature at the time of its falling. The lower that temperature, the lighter the isotopic composition of the falling snow. Snow, snowpatches, glaciers and some other types of natural ice belong to the sedimentary-metamorphic type of natural ice. Their isotopic composition is directly related to the temperature conditions at the moment of condensation and can be used as a temperature indicator.

It is surprising that neither in the article reviewed here, nor in the methodological publications of Yu.K. Vasil'chuk [*Vasil'chuk, 1990, 1991; Vasil'chuk, Vasil'chuk, 2017; Vasil'chuk et al., 2019a,b*] the fundamental relationship established by W. Dansgaard [*1964*] and the formulas for the relationship between the $\delta^{18}O$ and D values of atmospheric precipitation and air temperature at the time of precipitation are not discussed in any way.

Since the air temperature changes significantly during winter, the isotopic composition of the falling snow changes along with it. For example, in Yakutsk, snow with the lightest isotopic composition usually falls during January, the coldest month of the year [*Kurita et al., 2005; Papina et al., 2017*]. During the observation period of 2013 to 2015, individual extremely low values of $\delta^{18}O$ and D (−45.0 and −350.1 ‰) have been observed in the January precipitation [*Papina et al., 2017*]. In general, the relationship between the isotopic composition of atmospheric precipitation in the cold period and the mean

air temperature during it fallout is described by the equations

$$\delta^{18}O = 0.59t^{\circ} - 19.7 \ (R^2 = 0.88),$$

$$\delta D = 4.16t^{\circ} - 149.38 \ (R^2 = 0.89),$$

where t° – mean air temperature. The slopes of those equations (0.59 and 4.16) are close to the values of the coefficients (0.58 and 4.5) of Dansgaard's equations [*Dansgaard, 1964*] established for the conditions of condensation of the atmospheric water vapor into snow within the surface air temperatures range of –20 to –40 °C.

The above equations [*Papina et al., 2017*] have been obtained using data on snow precipitation isotopic composition and air temperature during precipitation. However, they in no way correlate with the equations of Yu.K. Vasil'chuk (for the mean January air temperature and for the mean air temperature of the cold period) [*Vasil'chuk, 1990, 1991; Vasil'chuk, Vasil'chuk, 2017*], which, for the convenience of comparison, can be written in the form of

$$\delta^{18}O = 0.67t_J,$$

$$\delta^{18}O = t_w.$$

It should be noted that the lowest temperatures during winter are associated with clear anticyclonic weather, in which there is practically no precipitation. Therefore, in the ultra-continental regions, the share of January snow in the total winter snow supply is small. At the same time, the maximum amount of snowfall is associated with the penetration of cyclones, strong thaws and higher condensation temperatures of the falling snow.

Meteorological data indicate that January is the coldest month of the year only in continental regions, while in maritime arctic climate the coldest month is February. Therefore, February (not January) snowfall will have the lightest isotopic composition. The areas of maritime Arctic climate, where the coldest month is February, include a significant part of the Chukotka Peninsula and some part of the Arctic coast of the northeastern Asia (see meteorological data of the Provideniya, Pevek, Bilibino, Mys Shmidta, Tiksi weather stations). So it is not clear what paleotemperatures Yu.K. Vasilchuk reconstructs using the formula (1) for those areas? Is that dependence also valid for the mean February air temperature? If so, in what cases?

In general, normalized values of the isotopic compositions of the snow cover demonstrate a strong relationship with the air temperature during its fallout. Therefore, they can be used to estimate the air temperature based on the formulas of W. Dansgaard [*1964*] after their calibration for specific climatic regions, as has been done in [*Papina et al., 2017*]. Those formulas can also be used to assess the temperature conditions of the formation of all sedimentary-metamorphic ice types since their isotopic composition is directly related to air temperature during condensation.

The third assumption of using the ice wedges as temperature indicators is that their composition is close to the initial snow cover and did not undergo significant fractionation at the stages of its thawing and refreezing in frost cracks. Fractionation of water isotope composition occurs continuously during its evaporation from the ocean, movement inland, and precipitation [*Craig, 1961; Dansgaard, 1964; Rozanski et al., 1993; Clark, Fritz, 1997; Kurita et al., 2005*]. The isotopic composition becomes much lighter away from the ocean.

It is known that the ratio between $\delta^{18}O$ and δD in atmospheric vapor near the dew point is very stable, it persists at different temperatures and is described by the equation $\delta D = 8 \cdot \delta^{18}O + 10$, called Global Meteoric Water Line (GMWL)', 'Craig's line', 'the equilibrium line of the isotopic composition' and others [*Rozanski et al., 1993; Clark, Fritz, 1997*]. As a result of complex fractionation processes during the water cycle, isotopic compositions can deviate above or below GMWL. The magnitude and nature of that deviation is usually measured in the form of deuterium excess (d_{exc}) calculated by the formula [*Dansgaard, 1964*]

$$d_{exc} = \delta D - 8 \cdot \delta^{18}O.$$

In arid regions partial evaporation occurs even at the stage of liquid atmospheric precipitation movement to the earth surface. In that case, lighter water (H_2O) returns to the vapor state, and heavy-water molecules ($H_2{}^{18}O$, $D_2{}^{16}O$) is accumulated in the liquid phase. However, the rate of evaporation of the $H_2{}^{18}O$ molecules is higher than that of the $D_2{}^{16}O$ molecules; therefore, the liquid phase is relatively depleted in heavy oxygen and enriched in deuterium. That process is called evaporative fractionation. In a graphical form, in $\delta^{18}O/\delta D$ coordinates, the isotopic compositions with pronounced evaporative fractionation lie significantly below the GMWL, and their deuterium excesses are often negative.

In winter, with the progressive cooling of air masses, the amount of water vapor is significantly reduced and its isotopic composition becomes increasingly lighter. That is due to the depletion of water vapor with heavy water molecules, which condense first. Under such conditions, isotopic equilibrium $\delta D = 8 \cdot \delta^{18}O + 10$ is not maintained due to the difficulty of isotopic exchange in the ice – vapor system [*Dansgaard, 1964*]. Therefore, the isotopic composition of the atmospheric vapor shifts above GMWL, and the deuterium excess acquires high positive values (>10).

In winter snow cover isotopic composition also does not remain constant even before the beginning of snow melting. This is associated with intense snow sublimation (bypassing the liquid phase). It has been instrumentally established that in Central Yakutia in winter up to 30 % of the snowfall and more evaporate [*Are, 1972; Golubev et al., 2001*]. During sublimation, mainly the light water molecules evaporate, and the snow residue is enriched in heavy isotopes. An increase in the concentration of ^{18}O and D (1.5–3 times) in the snow cover as a result of its sublimation is evidenced by the research results of V.N. Golubev with colleagues [*2001*].

In the Central Yakutia 10 generalized snow cover samples (for its entire thickness) were taken during one winter period. The $\delta^{18}O$ and δD variations reached about 10 and 75 ‰, respectively, and the average values were $\delta^{18}O = -32.0 \pm 5.1$ ‰ and $\delta D = -248.4 \pm 35.4$ ‰, $d_{exc} = 7.5 \pm 6.5$ ‰ [*Galanin et al., 2019*]. The studied composition is described by the equation $\delta D = 6.8 \cdot \delta^{18}O - 31.9$ [*Galanin et al., 2019*] and poled apart from the composition of winter snowfall described by the equation $\delta D = 8.2 \cdot \delta^{18}O + 21.9$ [*Papina et al., 2017*]. A significant decrease in deuterium excess and slope in the snow cover indicates a powerful evaporative fractionation both before the beginning of the spring snowmelt and throughout it. The heaviest isotopic compositions ($\delta^{18}O = -19.3$ ‰, $\delta D = -160.9$ ‰, $d_{exc} = -6.7$ ‰) differ by almost 2 times and are typical for the samples taken from the last snowpatches in June [*Galanin et al., 2019*].

It follows from the above that when calculating paleotemperatures based in isotope composition of wedge or other ice types, first of all it is necessary to assess fractionation degree, deuterium excess, and to compare values relative to the GMWL. Otherwise, it is impossible to establish the real genesis of the studied water or ice, as well as reconstruct temperature conditions of their formation.

For example, during the coldest and dry winters the role of sublimation of the snow cover inevitably increases, which will be reflected in a significant increase in the isotopic composition of the snow cover and ice wedges. While at methodology of Yu.K. Vasil'chuk heavier isotopic composition of ice wedges is always compared with climate warming.

Unfortunately, the issues of snow cover isotope composition formation and fractionation mechanisms at the stage of transformation into ice wedges are not considered at all in the reviewed article by Yu.K. Vasil'chuk. Many important and well-known works in that area [*Golubev et al., 2001; and many others*] are not cited or commented by the author. In most of his studies Yu.K. Vasil'chuk operates only oxygen isotope composition and does not take into account deuterium in any way. The reviewer believes that using only the $\delta^{18}O$ values it is impossible to assess the fractionation degree of the studied water and ice, as well as to establish the real origin of their isotopic composition.

Analysis of methodology of Yu.K. Vasil'chuk for the reconstruction of paleotemperatures based on isotope composition of ice wedges

A critical aspect of the reviewed article by Yu.K. Vasil'chuk, A.C. Vasil'chuk is not only the incorrect sampling strategy and the lack of data on the isotopic fractionation of ice wedges studied by the authors. The lack of explanations in methodological publications of the author [*Vasil'chuk, 1990, 1991, 1992; Vasil'chuk, Vasil'chuk, 2017, 2020; Vasil'chuk et al., 2019a,b; and many others*] of how the author's formulas (1)–(3), see Introduction, were mathematically derived and on what data they are based, causes skepticism. While studying the works of Yu.K. Vasil'chuk, the reviewer was surprised to find that those formulas were first used by the author in 1990 [*Vasil'chuk, 1990*], but initial data lying in their base had been published only in 1992 [*Vasil'chuk, 1992*].

It is paradoxical that none of the author's work over the past 30 years, where these formulas were used, considered the primary data and the method of their approximation, did not indicate the accuracy, reliability and reproducibility of the obtained results. The author only reports that according to the formula (1) ($t_J = 1.5 \cdot \delta^{18}O$), the mean January air temperatures are reconstructed with an accuracy of ±3 °C [*Vasil'chuk, 1990, 1991, 1992; Vasil'chuk, Vasil'chuk, 2017*].

In the peer-reviewed article and in his other publications the author reports that the method for obtaining this formula was first elaborated by him and published in the English version of the Russian journal *Water Resources* [*Vasil'chuk, 1991*]. If that formula is so important for paleoclimatic reconstructions, then why, for almost 30 years after its publication, the author did not carry out additional methodological studies on its refinement, calibration, verification on a more representative sample of primary data? It is strange that the author has no later publications on the development and the improvement of methods for the reconstructing paleotemperatures based on wedge ice isotope composition.

The publication of Yu.K. Vasil'chuk's methodology [*Vasil'chuk, 1991*] in the English version of the journal had been remaining inaccessible to most researchers for a long time. More than 15 years ago, the reviewer tried to find that publication and analyze the methodology used by the author. However, attempts to get acquainted with that most self-cited work of the author [*Vasil'chuk, 1991*] was unsuccessful at that time due to remoteness from large libraries, as well as poor development of domestic and international scientific electronic resources, lack of access to international citation databases. The reviewer assumes that for most other researchers access to the

primary data of the Yu.K. Vasil'chuk's methodology was limited and practically impossible for a long time.

While reviewing the article, the reviewer has found that both Russian [*Vasil'chuk, 1990*] and English [*Vasil'chuk, 1991*] versions of that article have become available on the scientific electronic library eLibrary.Ru. The comparison of both versions has revealed that they are completely identical. The reviewer is quite surprised that the author never refers to the Russian-language version [*Vasil'chuk, 1990*] of his methodological publication, which would undoubtedly be more accessible to a wide range of readers.

To his next surprise, examining the main most self-cited methodological publications of Yu.K. Vasil'chuk [*Vasil'chuk, 1990, 1991*], the reviewer has not found the formula (1) ($t_J = 1.5 \cdot \delta^{18}O$) for the mean January air temperature as well as the method of its elaboration in their text. After careful study of this publication, the formula has nevertheless been found in the title of one of the column headings of the table, along with the mean January air temperatures reconstructed on its basis. But any indications about the initial data and the method of obtaining the formulas (1)–(3) in publications [*Vasil'chuk, 1990, 1991*] has not been found by the reviewer.

In the same publication, the reviewer has found the formula (2) ($\Sigma t_w = 250 \cdot \delta^{18}O$), elaborated by Yu.K. Vasil'chuk for the reconstruction of the sum of negative winter air temperatures. But there are no algorithms or methodological techniques for elaborating the formula (2) in the publications of Yu.K. Vasil'chuk [*Vasil'chuk, 1990, 1991*]. However, it is in those publications that all the formulas appear for the first time without any references to the previous methodological works. That is also confirmed by earlier publications, in which the author has not yet applied any formulas for reconstructing paleotemperatures.

In Annotation of articles [*Vasil'chuk, 1990, 1991*], Yu.K. Vasil'chuk also does not report anything about the formulas he has elaborated, but declare that he has compared the maps of the $\delta^{18}O$ value distribution in recent ice veins (ice veinlets) and the maps of isotherms of the sums of negative winter air temperatures within the USSR regions with low-temperature permafrost. Indeed, those publications contain the highly generalized small-scale climatic maps from the USSR climate handbook [*USSR climate..., 1966a,b, 1967*], which demonstrate the mean January air and mean winter air temperatures of the northeast Asia in the form of isotherms. On the same maps, the author has placed the locations and oxygen isotopic compositions of the ice wedges tested by him. Moreover, the latter are located mostly hundreds of km away from the nearest weather station. Nothing is said about how exactly functional dependencies (1) and (2) were obtained based on the analysis of the map data. It is also misleading that in all his subsequent publications the author points out that the formulas (1)–(3) have been obtained using precisely the data from

Table 1. **The $\delta^{18}O$ values in modern ice veins of syngenetic ice wedges on Ayon Island, in the north of Chukotka and the nearby islands of the Eastern Russian Arctic, after [*Vasil'chuk, 1992*] with additions after [*Vasil'chuk Yu.K., Vasil'chuk A.C., 2017*]**

Location of recent wedges	Coordinates	$\delta^{18}O_{IW}$, ‰ in recent ice wedges	Climatic data from weather stations			
			Σt_w	t_w	t_J	t_s
Ayon Island	69°47′ N, 168°39′ E	–20.0	–5047	–20	–29	–12
Mouth of the Rauchua River	69°30′ N, 166°43′ E	–22.0	–5436	–21	–32	–13
Kuvet River	69°16′ N, 175°02′ E	–21.0	–4700	–18	–27	–11
Wrangel Island	71°14′ N, 179°24′ W	–20.0	–4272	–17	–25	–11
Amguema River	67°03′ N, 178°53′ W	–19.0	–4992	–19	–29	–11
Lake Koolen	65°59′ N, 170°58′ W	–16.0	–3400	–14	–22	–7
Lake Elgygytgyn	67°30′ N, 172°00′ E	–20.4	–4598	–18	–27	–10
Henrietta Island	77°06′ N, 156°30′ E	–15.3	–5330	–17	–27	–12
Zhokhov Island	76°09′ N, 152°43′ E	–20.0	–5363	–18	–29	–13
Kotelny Island	75°27′ N, 140°50′ E	–18.1	–5408	–19	–29	–14
Bunge Land Island	75°24′ N, 141°16′ E	–17.6	–5989	–21	–28	–14
Maly Lyakhovsky Island	74°07′ N, 140°40′ E	–18.0	–5408	–20	–31	–14
Bolshoy Lyakhovsky Island, south	74°07′ N, 140°40′ E	–20.4	–5400	–20	–31	–14
New Siberia Island	75°03′ N, 148°28′ E	–18.0	–5500	–20	–30	–14
Chetyrekhstolbovy Island	70°47′ N, 161°36′ E	–20.0	–5143	–19	–30	–13
Plakhinskii Yar	70°47′ N, 161°36′ E	–25.0	–5733	–23	–35	–13

Note: $\delta^{18}O_{IW}$ is the $\delta^{18}O$ values in ice wedges, ‰ vs. SMOW; Σt_w is the sum of winter air temperatures, degree-days; t_w is the mean winter air temperature, °C; t_J is the mean January air temperature, °C; t_s is mean annual ground temperature (°C) without snow and vegetation. (The title of the table and notes are preserved in the author's version [*Vasil'chuk, Vasil'chuk, 2017*].)

weather stations, and not the generalized small-scale maps compiled on their basis!

At the same time, as one gets acquainted with other publications of Yu.K. Vasil'chuk, it becomes obvious that these maps [*Vasil'chuk, 1990, 1991*] were used for deriving formulas (1)–(3). It is obvious that the climatic characteristics for all sampling points of the recent ice wedges (ice veinlets) have been established by Yu.K. Vasil'chuk by extrapolating the isotherms of small-scale climatic maps out of the handbook [*USSR climate..., 1966a,b, 1967*] into a table, probably obtained by the author after the derivation of the formulas, since it is absent in his most cited methodological works [*Vasil'chuk, 1990, 1991*], and appears 2 years later in another inaccessible publication [*Vasil'chuk, 1992*]. Finally, in 2017, original table and the formulas based on it were published in a widely available publication [*Vasil'chuk, Vasil'chuk, 2017*] and are now available for analysis. For convenience of consideration, the table with initial data for the formulas (1)–(3) is given below (Table 1).

Analysis of the correctness and reliability of the initial data for formulas (1)–(3)

Initial data (the $\delta^{18}O_{IW}$ value, Table 1) of the oxygen isotopic composition of the recent ice veins (ice veinlets) of different regions of the permafrost zone of the northern Eurasia, used by the author to elaborate formulas (1)–(3) [*Vasil'chuk, 1990, 1991, 1992; Vasil'chuk, Vasil'chuk, 2017*] arises many questions. What does the author mean by *the recent age* and how has it been established?

According to the statement of the author, one standard 10 × 10 cm wedge ice sample includes many ice veins and covers the interval of 100 to 300 years [*Vasil'chuk, 1990, 1991*]. In that case, the 'recent' ice veins10–20 cm thick studied by the author could have been forming starting from the Little Ice Age up to the present time. During that time, both the global and regional climates have undergone significant changes, as evidenced by the data of meteorological observations. The mean winter and mean annual air temperatures during this period have increased by several degrees. This warming has been reflected in a significant retreat of glaciers. Since older veins preserved in permafrost for several thousand years could also have been included in the author's initial sample, the reviewer believes that their oxygen isotope composition can characterize not current climatic conditions, but averaged ones over the entire Late Holocene, since no absolute dating of these veins is available.

Variations in the oxygen isotope composition of recent ice veins reach significant values even in one region. Thus, in the area of Oyogoss Yar (Dmitry Laptev Strait), in 38 samples of recent ice veins, the $\delta^{18}O_{IW}$ value varies from –18.24 to –25.27 ‰ [*Opel et al., 2011*], and on the Bykovsky Peninsula (22 samples) it does the same from –22.38 to –29.02 ‰ [*Meyer, 2001*] and others. When trying to determine the modern mean January air temperature (t_J) for those areas according to the formula (1) of Yu.K. Vasil'chuk ($t_J = 1.5 \cdot \delta^{18}O$) by substituting the $\delta^{18}O_{IW}$ values, it turns out that in the Oyogoss Yar it varies from –27 to –38 °C, and on the Bykovsky Peninsula it fluctuates from –34 to –44 °C, respectively. However, when using the formula (1) to interpret the isotopic compositions of ancient ice wedges, much smaller deviations of the $\delta^{18}O$ value of 2–5 ‰, obtained from 1–2 samples, are interpreted by Yu.K. Vasil'chuk as changes in the mean January air temperature by 5–7 °C or more. That approach seems to be absolutely unacceptable and contradicting the real data.

Another controversial aspect of using the composition of Holocene ice wedges to reconstruct the temperatures during formation of the Late Pleistocene ice wedges is the possibility of a fundamental difference in their genesis and formation conditions. The Late Pleistocene ice wedges in loess-ice (yedoma) deposits were formed syngenetically. Many researchers believe that loess-ice sediments, together with syngenetic ice wedges, are Pleistocene relics. During the Holocene and at present they practically did not form, but only degraded, forming vast thermokarst alas plains [*Katasonov, 1979; Ershov, 1989*]. The landscape and climatic conditions of their formation are classified as 'extinct' [*Katasonov, 1979; Tomirdiaro, Chernenky, 1987*].

On the contrary, the Holocene ice veins investigated by Yu.K. Vasilchuk can be epigenetic ice wedges formed during freezing of the recent and Holocene floodplains. Relic ice wedges of the Late Pleistocene age can also undergo secondary (epigenetic) freezing and frost cracking. However, the ice that composes recent ice wedges may turn out to be an isotopic derivative of not only melted snow water, but also the supra-permafrost and flood river waters flowing into frost cracks.

Thus, the analysis of 22 isotopic determinations for icings congelation ice in the Central Yakutia [*Galanin et al., 2019*] reveals that their averaged composition ($\delta^{18}O = -21.1 \pm 1.2$ ‰, $\delta D = -172.2 \pm 9.5$ ‰, $d_{exc} = -2.5 \pm 2.5$ ‰) is even lighter than the averaged composition ($\delta^{18}O = -19.4 \pm 2.3$ ‰) of recent Arctic ice wedges from the publications of Yu.K. Vasil'chuk [*1990, 1991*].

However, the icings are of hydrogenic origin and are formed by freezing of the river water. The isotopic composition of river water is always much heavier than of melt snow water, as for snow cover is formed of the atmospheric precipitation in the cold season.

The fundamental difference in the genesis of relict syngenetic ice wedges from the recent epigene-

tic veins is indicated by the cardinal difference in their deuterium excess. That should be known to Yu.K. Vasil'chuk by the publication [*Budantseva, Vasil'chuk, 2019*], in which he is a co-author.

It is possible to distinguish between different genetic types of ices of close oxygen isotope composition by the value of d_{exc}. Sedimentary-metamorphic ice (snow cover, glaciers) and their close derivatives have $d_{exc} > 5$ ‰, which indicates their close relationship with atmospheric precipitation.

That relationship is usually observed in the isotopic composition of the Late Pleistocene ice wedges (5 ‰ $< d_{exc} < 10$ ‰) [*Galanin et al., 2019*]. Lower deuterium excess in ice wedges and heavier values of isotope composition are characteristic of the coldest and driest intervals, in particular, the last cold stage of MIS 2. A low deuterium excess $d_{exc} < 5$ ‰ may indicate a significant fractionation and a very indirect relationship between the isotope composition of ice wedges and the composition of the initial snow cover and air temperatures at the time of its formation.

As it follows out of Table 1 [*Vasil'chuk, Vasil'chuk, 2017*], as well as from other data [*Meyer, 2001; Opel et al., 2011*], the oxygen isotope composition of recent ice wedges in the northern Eurasia is completely different from the isotopic composition of the modern snow cover that falls in those areas at temperatures below –20...–40 °C [*Kurita et al., 2005; Papina et al., 2017; Galanin et al., 2019*]. Unfortunately, the author does not provide any convincing descriptions of the structure of the studied ice veins, the isotopic composition of which he used to elaborate the formulas (1)–(3). The lack of information on the δD value makes it impossible to estimate the value of d_{exc} and draw the conclusions about the nature of fractionation and the ice origin. All that leads to a decrease in the reliability of methodological constructions, the formulas (1)–(3) based on this data, as well as the author's paleotemperature reconstructions made on their basis.

Weather stations records used by Yu.K. Vasil'chuk [*Vasil'chuk, Vasil'chuk, 2017*] for the elaboration of formulas and (given in Table 1) causes most serious skepticism. It is not clear what weather station the author has in mind and for what observation period. Most readers obviously do not dwell on that question. At the same time, in all publications of the author there are no references to the source of these data.

Most of the locations of recent ice wedges investigated by Yu.K. Vasil'chuk are extremely remote from any weather stations, however, the author also provides detailed climatic characteristics for them (Table 1). The author confidently manipulates the climatic data of long-term observations of such distant objects as the Henrietta Island, Kotelny, Zhokhova, Maly Lyakhovsky, Bunge Land islands, citing not only the mean winter and mean January air temperatures, but also the mean annual air temperatures of the earth surface. That issue can only be dealt with by analyzing the first publications [*Vasil'chuk, 1990, 1991*], in which the formulas (1)–(3) appear.

However, even in those publications there are no any initial tables with a list of weather stations and data on meteorological observations, but small-scale climatic maps from the USSR climate handbook for 1966–1967 are given [*USSR climate..., 1966a,b, 1967*]. The author does not explain exactly how those small-scale maps have been transformed into the quantitative temperature characteristics and converted from the graphical form to the digital format. However, the author reports that he used data from 250 weather stations for his analysis! The reviewer considers that information to be speculative and unreliable.

In the context of those publications and the illustrations presented in them, it is easy to understand that all meteorological data have been taken by the author by graphical extrapolation of isotherms. Such method of obtaining the initial climatic characteristics for approximating the isotope compositions of recent ice wedges and deriving the formulas (1)–(3), according to the reviewer, is categorically unacceptable. That is due to both a very sparse network of weather stations in the region and the significant distortions associated with the generalization of meteorological data when plotting isotherms. The maps also do not take into account changes in climatic parameters due to altitudinal zonality and local climatic features.

It causes great skepticism that up to the present time the author continues to use the formulas built on the basis of climatic data derived more than half a century ago, without thinking about the need to recheck and adjust them in accordance with ongoing climatic changes, with an increase in the duration of time series of observations at weather stations, etc.

Analysis of the mathematical reliability of formulas (1)–(3) and the connection with the initial data

The list of critical uncertainties and the possible sources of errors identified above is so large and extremely critical that further proof of the ineligibility of Yu.K. Vasilchuk's methodology [*Vasil'chuk, 1990, 1991*], it would seem, is no longer required. At the same time, since the author is silent about the algorithms and methods on the basis of which his formulas have been derived, the reviewer tried to do it on his own.

For that, an analysis of the statistical relationship (correlation) between the $\delta^{18}O_{IW}$ values and the instrumental data (Σt_w, t_w, t_J) taken from the publication [*Vasil'chuk, Vasil'chuk, 2017*] has been carried out (Table 1, Fig. 2). To assess the nature and magnitude of the correlation of those parameters and to construct graphs, standard Microsoft Excel tools have been used.

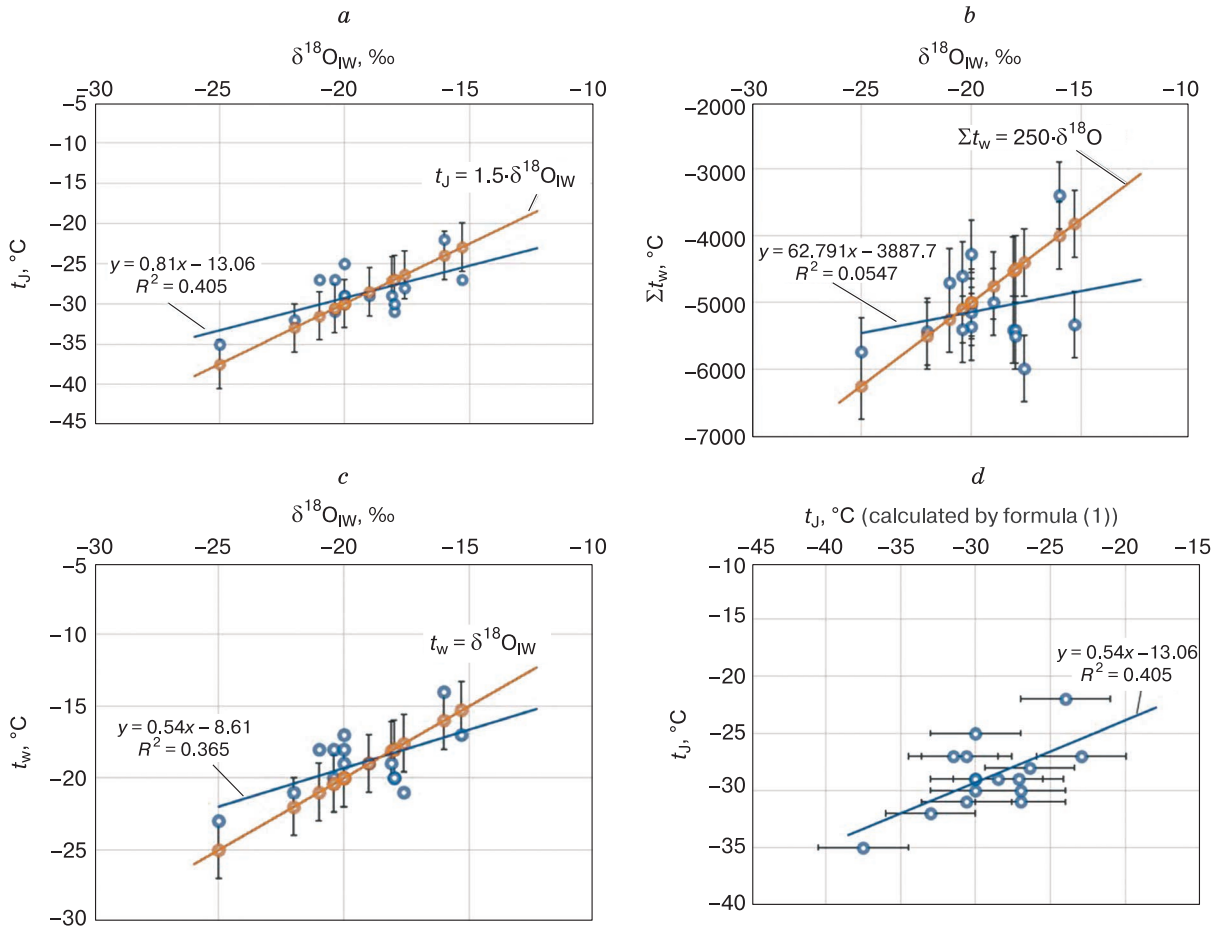

Fig. 2. Linear regressions (blue dots and lines) between climatic parameters and the $\delta^{18}O_{IW}$ values in recent ice veins (ice veinlets) in different regions of the northern Eurasia and their approximation by Yu.K. Vasil'chuk's formulas (orange dots and lines).

a – linear regression between $\delta^{18}O_{IW}$ and the mean January air temperature and approximation by the formula $t_J = 1.5 \cdot \delta^{18}O$; *b* – linear regression between the $\delta^{18}O_{IW}$ values and the sum of winter negative air temperatures and approximation by the formula $\Sigma t_w = 250 \cdot \delta^{18}O$; *c* – linear regression between the $\delta^{18}O_{IW}$ values and mean winter air temperature and approximation by the formula $t_w = \delta^{18}O$; *d* – linear regression between the mean January air temperatures according to weather stations data and the same temperatures calculated by the formula $t_J = 1.5 \cdot \delta^{18}O$ based on the oxygen isotope composition of recent ice veins . The initial data and error values are taken from the publication [*Vasil'chuk, Vasil'chuk, 2017*] and are shown in Table 1.

Analysis of Fig. 2 indicates the nature of the statistical relationship between the content of the ^{18}O isotope in the recent ice wedges from different regions and the climatic characteristics for those regions, extrapolated to sampling points by overlay. It is fair to assume that the lines and regression equations demonstrated in Fig. 2 reflect the correlation not with the data of instrumental observations at weather stations, but with the contours of the isotherms of those parameters on the climatic maps of 1965–1966 [*USSR climate..., 1966a,b, 1967*]. For comparison, the graphs reflect both real correlations (blue dots and lines) obtained by the reviewer and the results of approximating those parameters (orange dots and lines) by Yu.K. Vasil'chuk [*Vasil'chuk, 1990, 1991*]. The reviewer has suggested that if the equations (1)–(3) have been derived by the author precisely on the basis of the data in the table and according to the formulas (1)–(3) they have a linear form, then the linear regression equations derived by the reviewer will have the same form. To his surprise, the reviewer has found (Fig. 2) that the obtained regression lines and the equations approximating them are fundamentally different from the equations (1)–(3) of Yu.K. Vasil'chuk. So, the relationship between the $\delta^{18}O$ value and the mean January air temperature according to the data in Table 1 is approximated by the equation $t_J = 0.81 \cdot \delta^{18}O - 13.06$ with large deviations ($R^2 = 0.405$), while on the basis of the same data Yu.K. Vasil'chuk has deduced the dependence $t_J = 1.5 \cdot \delta^{18}O$.

There is no relationship ($R^2 = 0.055$) between the $\delta^{18}O$ value and the sum of negative winter air temperatures (Σt_w) and it is described by random regression with the equation $\Sigma t_w = 62.79 \cdot \delta^{18}O - 3887.7$, while Yu.K. Vasil'chuk has derived the dependence $\Sigma t_w = 250 \cdot \delta^{18}O$ from the same data. The same applies to the relationship between the $\delta^{18}O$ value and the mean winter air temperature (t_w), which is statistically insignificant ($R^2 = 0.365$) and is described by the regression equation $t_w = 0.54 \cdot \delta^{18}O$, while Yu.K. Vasil'chuk has derived the formula $t_w = \delta^{18}O$.

The result of the analysis of the formulas (1)–(3) is the graph in Fig. 2, *d*, which demonstrates the regression equation ($y = 0.54x - 13.06$) between the observed mean January air temperatures at weather stations and the same temperatures reconstructed based on the $\delta^{18}O$ values according to the formula (1) of Yu.K. Vasil'chuk. Note that it is one and the same climatic characteristic, therefore, it should be approximated with high significance ($R^2 > 0.9$) by an equation in the form of $y = x$ and pass through the point (0; 0). But there is no correlation between the measured and calculated values ($R^2 = 0.405$). The magnitude of the systematic discrepancy between the measured and calculated values can be easily estimated by substituting the zero value for x or y. As a result, we obtain the value of the systematic discrepancy between the calculated and observed mean January air temperature equal to 13.06 °C.

Thus, based on the reviewer's analysis of the formulas (1)–(3) of Yu.K. Vasil'chuk, originally published by him in [*Vasil'chuk, 1990, 1991, 1992*] and repeatedly used in all subsequent publications, it has been found that those formulas are not substantiated by facts and do not follow from the primary data on the isotope composition of recent ice veins and meteorological data given in [*Vasil'chuk, 1992; Vasil'chuk, Vasil'chuk, 2017*]. Data given by Yu.K. Vasil'chuk is approximated by completely different dependencies (Fig. 2). The real primary data lying in the base of the formulas (1)–(3), as well as the way they have been derived, remain unknown.

At the end of the review of the article by Yu.K. Vasil'chuk and his method for reconstructing paleotemperatures based on the oxygen isotope composition of ice wedges, it is necessary to state the following. Many present-day researchers studying the isotopic composition of ice wedges [*Meyer et al., 2002*] restrict themselves to very modest qualitative conclusions about the paleotemperatures of their formation. Interpreting the vertical and horizontal variations in the isotope composition of ice wedges, those authors indicate that winter air temperatures were colder or warmer at one time or another, but they do not translate them into specific absolute values, as Yu.K. Vasil'chuk does in most of his reconstructions and in the article reviewed here. Despite the incorrectness of the methodology of Yu.K. Vasil'chuk and the unreliability of the paleoclimatic reconstructions obtained on its basis, the author continues to use the formulas derived in 1990 [*Vasil'chuk, 1990*] and actively publish his results in many journals.

The recent statement of Yu.K. Vasil'chuk that his formulas were officially criticized back in 1991 by Professor J. Ross McKay and Professor A. Washbourne in the responses sent to the abstract of his doctoral dissertation [*Budantseva, Vasil'chuk, 2019*] – is extremely perplexing. They tested Yu.K. Vasil'chuk's formulas on the isotopic compositions of ice wedges in North America and have come to the conclusion that they are completely inapplicable. However, Yu.K. Vasil'chuk writes that for a long time after the elaboration of formulas, he was engaged in their examination and verification, and now has come to the conclusion that they are good for the entire northern Eurasia [*Budantseva, Vasil'chuk, 2019*]. All that reminds of a pun, since neither the formulas, their coefficients, nor errors have been changed in any way since the time of their publication [*Vasil'chuk, 1990*], and the methods of their development remain unknown until now.

CONCLUSIONS

Yu.K. Vasil'chuk is a well-known specialist in the study of the isotopic composition of fossil ice, the reviewer is familiar with many of his works, including some generalizations. Over the past 25–30 years, Yu.K. Vasil'chuk has published a lot of factual data, including borrowed ones, characterizing the isotopic compositions of underground and surface ice from different regions of Russia. The works of Yu.K. Vasil'chuk is often cited, and the actual data is used for comparative analysis.

At the same time, the method for reconstructing of the air January paleotemperatures, mean winter air temperatures, and the sum of negative winter air temperatures, proposed by the author in 1990, causes great skepticism from foreign and Russian researchers. Sampling method along vertical transect predominantly used by Yu.K. Vasil'chuk, is incorrect, contradicts the general regularities of the structure and origin of ice wedges and does not allow to estimate reliably the real variation of their isotope composition. That method contradicts the sampling strategy recommended by the leading present-day experts in the field of ice wedge research.

The formulas for recalculating the oxygen isotopic composition into air paleotemperatures, elaborated by Yu.K. Vasil'chuk, have no physical justification, they have been derived in an incorrect way, contradict the data of meteorological observations, including those cited by the author himself in his publications, as well as those obtained by other authors. The reconstructions of air paleotemperatures in the Pleistocene and Holocene, obtained on the basis of these formulas, are unreliable.

In their paleotemperature reconstructions, Yu.K. Vasil'chuk and his co-authors do not use the concentration of deuterium and the value of deuterium excess at all, do not pay attention to the analysis of the fractionation degree of the studied ice wedges, their genetic relationship with the Global Meteoric Water Line [*Craig, 1961*] and atmospheric precipitation. Most of the publications do not take into account the key foreign works [*Dansgaard, 1964*] in the field of studying the relationship between the isotope composition of natural water and ice and the temperature conditions of their formation.

After these critical remarks all other shortcomings of the reviewed article do not deserve special comments. In general, the reviewer believes that the further continuation of the publication of the results of applying the methodology of Yu.K. Vasil'chuk in scientific publications will negatively affect not only the image of the author himself. To a greater extent, this will discredit the journals themselves, causing great skepticism on the part of foreign and Russian researchers not only in the field of geochemistry of stable isotopes, but also in geocryology, paleogeography and paleoclimatology.

High scientific status of Yu.K. Vasil'chuk demands from his publications the highest possible level of elaboration, adherence to the principles of statistics, scientific ethics and common sense, since those publications will be considered by some researchers, especially the young ones, as methods for further research. The continued use of the Yu.K. Vasil'chuk's methodology by his students and followers will lead to an exacerbation of the theoretical crisis in the study of the isotope compositions of ice wedges and geocryology in general.

References

Are, A.L., 1972. Evaporation and evolution of snow cover in the vicinity of Yakutsk. In: Experimental studies of heat exchange processes in frozen rocks. Nauka, Moscow, pp. 160–167 (in Russian).

Arkhangelov, A.A., Konyakhin, M.A., Mikhalev, D.V., et al., 1987. Oxygen isotope composition of underground ice. In: Problems of Geocryology. Nauka, Moscow, pp. 136–143 (in Russian).

Boereboom, T., Samyn, D., Meyer, H., Tison, J.-L., 2013. Stable isotope and gas properties of two climatically contrasting (Pleistocene and Holocene) ice wedges from Cape Mamontov Klyk, Laptev Sea, northern Siberia. The Cryosphere 7, 31–46, DOI: 10.5194/tc-7-31-2013.

Budantseva, N.A., Vasil'chuk, Yu.K., 2019. Hydrogen isotopes and deuterium excess in the shoots of ice veins in northern Eurasia. Arktika i Antarktika (Arctic and Antarctic), No. 4, 16–32, DOI: 10.7256 / 2453-8922.2019.4.31391.

Clark, I.D., Fritz, P., 1997. Environmental isotopes in hydrogeology. Lewis Publishers, Boca Raton, New York, 328 pp.

Craig, H., 1961. Isotopic variations in meteoric waters. Science 133, 1702–1703.

Dansgaard, W., 1964. Stable isotope in precipitation. Tellus XVI (4), 436–468.

Derevyagin, A.Yu., Chizhov, A.B., Meyer, H., 2010. Winter temperature conditions of Laptev Sea region during the last 50 thousand years in the isotopic record of ice wedges. Kriosfera Zemli (Earth's Cryosphere), XIV (1), 32–40.

Ershov, E.D. (Ed.), 1989. Geocryology of USSR. Middle Siberia. Nedra, Moscow, 414 pp. (in Russian).

Galanin, A.A., Pavlova, M.R., Papina, T.S., et al., 2019. Stable isotopes of O^{18} and D in key components of water flows and the permafrost zone of Central Yakutia (Eastern Siberia). Led i sneg (Ice and Snow), 59 (3), 333–354.

Golubev, V.N., Konischev, V.N., Sokratov, S.A., et al., 2001. Influence of sublimation in a seasonal snow cover on formation of an isotopic content of wedge ice. Kriosfera Zemli (Earth's Cryosphere), V (3), 71–76.

Katasonov, E.M. (Ed.), 1979. Structure and absolute geochronology of the alass deposits of Central Yakutia. Nauka, Novosibirsk, 95 pp. (in Russian).

Konyakhin, M.A., 1988. Oxygen isotope composition of polygonal wedge ice as an indicator of the conditions of their formation and genesis. Author's abstract of PhD thesis. Moscow, 26 pp. (in Russian).

Kurita, N., Sugimoto, A., Fujii, Y., et al., 2005. Isotopic composition and origin of snow over Siberia. J. Geophys. Res., vol. 110, D13102, DOI: 10.1029/2004JD005053.

Meyer, H., 2001. Late Quaternary climate history of Northern Siberia – evidence from ground ice. PhD Dissertation. Alfred Wegener Institute. Polar- und Meeresforschung Forschungsstelle, Potsdam, 112 pp.

Meyer, H., Derevyagin, A.Yu., Siegert, C., Hubberten, H.W., 2002. Palaeoclimate studies on Bykovsky Peninsula, North Siberia – hydrogen and oxygen isotopes in ground ice. Polarforschung, No. 70, 37–51.

Meyer, H., Opel, T., Laepple, T., et al., 2015. Long-term winter warming trend in the Siberian Arctic during the mid-to late Holocene. Nature Geoscience 8 (2), 122–125.

Opel, T., Derevyagin, A.Yu., Meyer, H., et al., 2011. Palaeoclimatic Information from Stable Water Isotopes of Holocene Ice Wedges on the Dmitrii Laptev Strait, Northeast Siberia, Russia. Permafrost and Periglacial Processes 22, 84–100.

Papina, T.S., Malygina, N.S., Eirikh, A.N., et al., 2017. Isotopic composition and sources of atmospheric precipitation in Central Yakutia. Earth's Cryosphere (Kriosfera Zemli), XXI (2), 52–61.

Rozanski, K., Aragufis-Aragufis, L., Gonfiantini, R., 1993. Isotopic patterns in modem global precipitation. Climate Change in Continental Isotopic Records, Geophys. Monogr., vol. 78, 1–36.

Schirrmeister, L., Grosse, G., Schwamborn, G., Andreev, A.A., et al., 2003. Late Quaternary history of the accumulation plain north of the Chekanovsky Ridge (Lena Delta, Russia): a multidisciplinary 1 approach. Polar Geography 27 (4), 277–319.

Tomirdiaro, S.V., Chernenky, B.I., 1987. Cryogenic-aeolian deposits of the Eastern Arctic and Subarctic. Nauka, Moscow, 198 pp. (in Russian).

Vasil'chuk, Yu.K., 1990. Reconstruction of the palaeoclimate of the Late Pleistocene and Holocene of the basis of isotope studies of subsurface ice and waters of the permafrost zone. Vodnye Resursy (Water Resources), 17 (6), 162–170.

Vasil'chuk, Yu.K., 1991. Reconstruction of the palaeoclimate of the Late Pleistocene and Holocene of the basis of isotope studies of subsurface ice and waters of the permafrost zone. Water Resources 17 (6), 640–647.

Vasil'chuk, Yu.K., 1992. Oxygen isotope composition of recurrent-veined ice (experience of paleogeocryological reconstructions): In 2 volumes. Department of Theoretical Problems of the Russian Academy of Sciences, Moscow State University, PNIIIS, Moscow, vol. 1. 420 pp.; vol. 2, 264 pp. (in Russian).

Vasil'chuk, Yu.K., Makeev, V.M., Maslakov, A.A., et al., 2019a. Late Pleistocene and Early Holocene winter air temperature reconstructions of the Kotelny Island using stable isotopes of ice wedges. Earth's Cryosphere (Kriosfera Zemli), XXIII (2), 12–24.

Vasil'chuk, Yu.K., Shmelev, D.G., Cherbunina, M.Y., et al., 2019b. New oxygen isotope diagrams of late pleistocene and holocene ice wedges of Mamontova Gora and Syrdah Lake, Central Yakutia. Doklady Akademii nauk (Reports of Academy of Sciences), 486 (3), 365–370.

Vasil'chuk, Yu.K., Vasil'chuk, A.C., 2017. Oxygen isotope composition of the ice wedges of Ayon island and Late Pleistocene and Holocene palaeotemperature reconstruction of the northern Chukotka. Vestnik Moskovskogo Universiteta. Seriya 4. Geologiya (Moscow University Bulletin. Series 4. Geology), No. 6, 92–104.

Vasil'chuk, Yu.K., Vasil'chuk, A.C., 2018. Winter air paleotemperatures at 30–12 ka BP in the lower Kolyma River, Plakhinskii Yar yedoma: evidence from stable isotopes. Earth's Cryosphere (Kriosfera Zemli), XX (5), 3–16.

Vasil'chuk, Yu.K., Vasil'chuk, A.C., 2020. Isotope-geochemical composition of the ice wedges in the slope yedoma on the Kular Ridge and reconstruction of the mean January air paleotemperature during 47,000–25,000 BP. Earth's Cryosphere (Kriosfera Zemli), XXIV (3), 22–33.

Wetterich, S., Rudaya, N., Tumskoy, V., et al., 2011. Last Glacial Maximum records in permafrost of the East Siberian Arctic. Quaternary Science Reviews, vol. 30, 3139–3151. – https://doi.org/10.1016/j.quascirev.2011.07.020

USSR climate handbook, 1966a. Part II. Air and soil temperature. Issue 24, Yakut ASSR. Gidrometeoizdat, Leningrad, 403 pp. (in Russian).

USSR climate handbook, 1966b. Part II. Air and soil temperature. Issue 33, Chukotka National District and Magadan Region. Gidrometeoizdat, Leningrad, 288 p. (in Russian).

USSR climate handbook, 1967. Part II. Air and soil temperature. Issue 21, Krasnoyarsk Territory and Tuva ASSR. Gidrometeoizdat, Leningrad, 504 pp. (in Russian).

Received December 7, 2020
Revised version received December 20, 2020
Accepted December 24, 2020

EARTH'S CRYOSPHERE
SCIENTIFIC JOURNAL

Kriosfera Zemli, 2021, vol. XXV, No. 2, pp. 68–72

CHRONICLE

TO THE ANNIVERSARY OF THE EARTH CRYOSPHERE INSTITUTE, TYUMEN SCIENTIFIC CENTRE SB RAS

V.P. Melnikov, M.R. Sadurtdinov, A.N. Nesterov, R.Yu. Fedorov, E.V. Ustinova

Earth Cryosphere Institute, Tyumen Scientific Centre, Siberian Branch of the Russian Academy of Sciences, Malygina str. 86, Tyumen, 625026, Russia; mr_sadurtdinov@mail.ru

The main milestones of the history of the Earth Cryosphere Institute, Tyumen Scientific Centre SB RAS are reflected in the light of its thirtieth anniversary, celebrated in 2021.

Key words: *Earth Cryosphere Institute, Tyumen Scientific Centre SB RAS, history of creation, anniversary.*

In May 2021, the Earth Cryosphere Institute, Siberian Branch of the Russian Academy of Sciences (ECI SB RAS) commemorates 30th anniversary. Creation of this institute in Tyumen back in 1991 was an event marking an important stage in the development of cryology as a science studying the world of cold. Building of the research team has effectively enabled interdisciplinarity covering most aspects of the object of study. Apart from scientists studying permafrost, the developing institute called for other experts in physics, chemistry, mechanics, system theory, etc. In this collaborative effort, the created pool of researchers aimed high to work out a holistic scientific view of the world of cold. This allowed an enlargement perspective for the object of cryological research (cryolithosphere and glaciosphere), with the increment of almost a 100 km-high column of the Earth's atmosphere, and areas of low positive temperatures combined with high pressures where gas hydrate may form (lithosphere and hydrosphere). The uniqueness of the research team created at ECI SB RAS is further accentuated by the implementation of the developed by them comprehensive approach to the study of the Earth's cryosphere in its integrity, encompassing cryogenic objects and processes in the lithosphere, hydrosphere, atmosphere and biosphere.

The Earth Cryosphere Institute SB RAS was breaking new ground in the years when the crisis of the 1990s led to the drastic reduction of state support for science, which entailed curtailment of most field works and experimental studies, while many long-established scientific teams working in research institution depleted of funding were literally trying to make ends meet. However, owing to its founder, academician Vladimir P. Melnikov, the Institute managed not only to deservingly pull through all the adversities of that time, but in a short time gained wide international recognition of the results of its scientific and research activities (Fig. 1).

The year of the birth of the Earth Cryosphere Institute was marked by an unprecedented historical decision made by Yuri K. Shafranik, the head of administration (Governor) of the Tyumen region after the events of August 19, 1991, to transfer the property in the headquarters of the Tyumen Regional Committee of the Communist Party to the academic community.

In the mid 1990s, a group of the country's leading geocryologists from All-Russian Scientific Research Institute for Hydrogeology and Engineering Geology (VSEGINGEO), Moscow, joined the Institute, thereby forming the Moscow branch of the Earth Cryosphere Institute.

The traditional Pushchino annual international permafrost conferences, whose successful organization was both the responsibility and merit of David A. Gilichinsky, Elizaveta M. Rivkina and their team, provided an impetus towards stronger networking and creative benefits thereof.

A series of the Yamal international conferences, with the first one held in Yamburg (1989), left an indelible impression on Russian and foreign scientists. Given that these events were sponsored by the government of the Yamal-Nenets Autonomous District, as well as Gazprom and Neftegazstroy companies, the level of their organization was unanimously estimated as superb by the conference participants. Thus, after the 1989 Yamburg Conference American Professor T. Peve, the president of the International Permafrost Association (IPA), said in the telegram sent to V.P. Melnikov: "Vladimir, we have never had such conferences and never will". Also worth noting is that six helicopters were in service to daily take all 140 attendees to study the frozen rock sections prepared in

Fig. 1. Academician Vladimir P. Melnikov, the founder of the Earth Cryosphere Institute, SB RAS and its director from 1991 to 2014, the organizer and permanent editor-in-chief of the "Earth's Cryosphere" journal.

advance for observations on Yamal and Gydan, and to get a bird's eye view of all the elements of tundra landscapes typical of permafrost regions (cryolithozone).

The Earth Cryosphere Institute has hosted a number of international conferences in Tyumen. Among them, the 2004 international conference "Cryosphere of Oil and Gas Provinces" to commemorate 60th anniversary of the Tyumen region. Its opening ceremony was marked by two welcoming speeches: by Sergey Sobyanin, Governor of the Tyumen Region, and by Dr. Jerry Brown, IPA President.

In 2012, the Institute was actively involved in organizing and conducting the 10th Jubilee International Conference on Permafrost (The Tenth International Conference on Permafrost, TICOP). With over 500 scientists from more than 25 countries gathered in the city of Salekhard, the meeting ranked as largest scientific conference on permafrost in Russia in the past three decades.

For more than thirty years, scientists from the Earth Cryosphere Institute have been conducting field research at geocryological research stations in Russia: Vaskiny Dachi and Marre-Sale (Yamal Peninsula), Nadym and Urengoy (Western Siberia), Shapkino, Bolvansky and Kashin (North of European Russia).

In 2017, the Earth Cryosphere Institute entered into the Federal Scientific Centre SB RAS (Tyumen).

Of the 54 researchers currently employed with Institute, more than 60 % are under the age of 39, thus enabling amalgamation of mature scientific ex-

Fig. 2. The ECI research staff, Tyumen.

pertise and youth vigor (Fig. 2). The breadth of the institute's research lines is remarkably expressed in its structure, which includes four laboratories titled "Cryogenic processes", "Cartographic modeling and forecast of the state of natural cryogenic geosystems", "Natural gas hydrates", "Heat and mass transfer phenomena", and a scientific project "The methodological framework of cryospheric sciences" (Fig. 3).

The Earth Cryosphere Institute actively cooperates with scientific and educational organizations: Lomonosov Moscow State University, Tomsk State University (TSU), Tyumen State University (TyumSU), Melnikov Permafrost Institute (MPI SB RAS), Sergeev Institute of Environmental Geoscience, Russian Academy of Sciences (IGE RAS), etc. In recent years, the Institute has been involved in a number of international programs (e.g., Circumpolar Active Layer Monitoring (CALM), Thermal State of Permafrost (TSP)) and its researchers have participated in leading international and Russian conferences.

For almost 25 years now, the Earth Cryosphere Institute has been the main co-founder of the "Earth's Cryosphere" journal, the only national edition covering all aspects of cryology published since 1997.

We should not forget about another important fact as we reflect on this jubilee year: in two years' time, we will mark the centenary of the term "cryosphere" coined in 1923 by A.B. Dobrovolsky. Not only does this upcoming anniversary make us look back and analyze the path the science of cold has accomplished over the past century, it also enjoins on us a forward-looking commitment to deepen and widen our knowledge of the Earth's cold envelope. The novel approaches and cutting edge remote sensing technologies which became available in the 20th century and applicable to the cryosphere dynamics

Fig. 3. Present-day activities of the Earth Cryosphere Institute.

a – the Pechora field team of the ECI Tyumen Scientific Center SB RAS with the Nenets State Nature Reserve staff; *b* – the 2019 field works at the Vaskiny Dachi research station, Yamal Peninsula (the Cryogenic Processes Laboratory employees with colleagues); *c* – young scientists, the future of the Natural Gas Hydrate Laboratory (*from left to right*): V.A. Vlasov, PhD (Phys.-Math.); A.M. Reshetnikov, PhD (Tech.), laureate of the Academician P.I. Melnikov Prize, Siberian Branch of the Russian Academy of Sciences; N.S. Molokitina, PhD (Phys.-Math.), winner of the competition for the scholarship of the President of the Russian Federation for young scientists and postgraduates; A.O. Drachuk, PhD (Phys.-Math.); M.Sh. Madygulov, junior research scientist; *d* – V.V. Nakladnov, postgraduate student from the Heat and Mass Transfer Phenomena Laboratory – fitting a laboratory model of frozen soil cooling system; *e* – V.S. Sheinkman, leading researcher, and the students on geological hiking trail along the Kodar Ridge; *f* – editorial group of the "Earth's Cryosphere" journal.

a

b

c

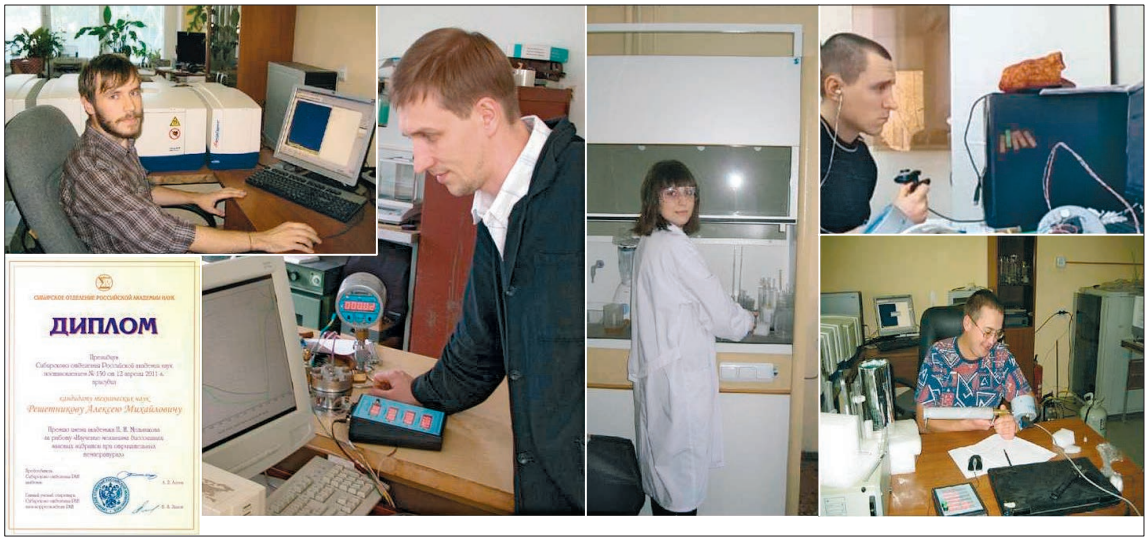

d

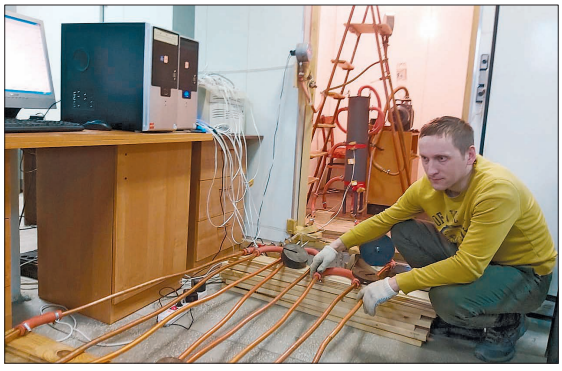

e

f

monitoring, as well as increasing opportunities to improve our understanding of the complex physical, chemical and biological processes occurring in it, have enabled an unparalleled extension of the scope of knowledge about the object of research. Against this backdrop, global society is increasingly becoming aware of the key role of the cryosphere as one of the most important resource ensuring stability of mankind's existence and its sustainable development. These tendencies impose even greater responsibility on the Earth Cryosphere Institute, to further promote the knowledge integrating concept within a holistic scientific view of the cryosphere and look for answers to both current and future climate changes and environmental challenges.

In the year of this remarkable anniversary, we sincerely wish the ECI staff to preserve their creative longevity in the future, and increase their research potential, in a continuous effort to expand the horizons of knowledge of the world of cold.

Received March 20, 2021